NRL Report 7486

An Experimental Study of the Acoustic Field of a Line Source Coincident with the Focal Line of a Parabolic-Cylinder Reflector

J. A. SINSKY, PETER H. ROGERS, AND A. V. BOZZI

Transducer Branch
Acoustics Division

December 20, 1972

NAVAL RESEARCH LABORATORY
Washington, D.C.

CONTENTS

ABSTRACT

The acoustic radiation patterns from acoustically soft parabolic reflectors driven by a line source coincident with the focal lines of the reflectors were measured in the NRL Acoustic Research Tank Facility to verify a mathematical model of an ideal parabolic-cylinder reflector. Data taken in the near and far fields of the reflectors at various frequencies between 10 kHz and 40 kHz were plotted together with the theoretically predicted radiation patterns. Agreement is good between theory and experiment. The experiment was performed with a shallow reflector (4.0-inch focal length and 28.3-inch aperture) and with a deep reflector (2.0-inch focal length and 28.4-inch aperture), and all measurements were made in the median planes of the reflectors. Emphasis was placed on careful construction of the parabolic reflectors and precision alignment of the line source. Error analyses were performed to determine the parabolicness of the reflectors and the effect on the radiation pattern of a slight misalignment of the line source. To illustrate the use of the mathematical model as a design tool, curves were plotted showing the reflector performance characteristics as a function of the reflector parameters.

PROBLEM STATUS

This is an interim report on a continuing NRL problem.

AUTHORIZATION

NRL Problem S02-19
Project RF 05-121-402-6200

Manuscript submitted September 6, 1972.

AN EXPERIMENTAL STUDY OF THE ACOUSTIC FIELD OF A LINE SOURCE COINCIDENT WITH THE FOCAL LINE OF A PARABOLIC-CYLINDER REFLECTOR

INTRODUCTION

In a recent paper one of the authors [1] developed a mathematical model for the acoustic radiation from an ideal parabolic-cylinder reflector driven by a line source coincident with its focal line. The model is two-dimensional in that the reflector is assumed to be infinite in length but of finite width. The major features of the radiation are determined as a function of the focal length and aperture of the parabola, the frequency of the line source, and the type of reflector (rigid or pressure release). A precision experiment to test the accuracy of this model was performed in the NRL Acoustic Research Tank Facility using two soft parabolic reflectors with the same aperture but different focal lengths and a USRD type F36 hydrophone [2] as the line source. The mathematical model was employed to compute theoretical radiation patterns for the same test distances and axis of rotation used in the experiment, and good agreement is documented in this report between theory and experiment for the near-field and the far-field radiation in the median plane of the reflector. The careful construction of the parabolic reflectors, the alignment of the line source in the reflector, and the performance of the experiment will be discussed, and a detailed analysis will be made of the experimental tolerances and the validity of the stated theoretical assumptions.

APPARATUS

Construction of the Reflectors

The two reflectors that were used in this experiment are illustrated in Figs. 1a and 1b. In water the shallow reflector had a 3.98-inch focal length and an aperture width of 28.3 inches and the deep reflector had a 2.03-inch focal length and an aperture width of 28.4 inches. The aperture height, the dimension parallel to the axis of the line source, was 16 inches for both reflectors. The reflecting surfaces consisted of neoprene closed-cell rubber bonded to copper sheet and supported in a wooden frame. Transducer mounts were employed which allowed precision alignment of the axis of the transducer along the focal lines of the reflectors. The reflectors were suspended and rotated in the water by a vertical support shaft bolted to the back plate of each reflector. The reflectors were buoyant in the water; therefore ballast was required to keep the reflector axes vertical during the experiment.

The details of constructing the two reflectors were identical. The desired parabola specified by the aperture width and focal length was plotted on graph paper. A second curve was drawn parallel to the parabola but offset to compensate for the thickness of the closed-cell rubber and its copper backing plate. In this way the curvature of the exposed surface of the closed-cell rubber in the finished reflector closely approximated the desired

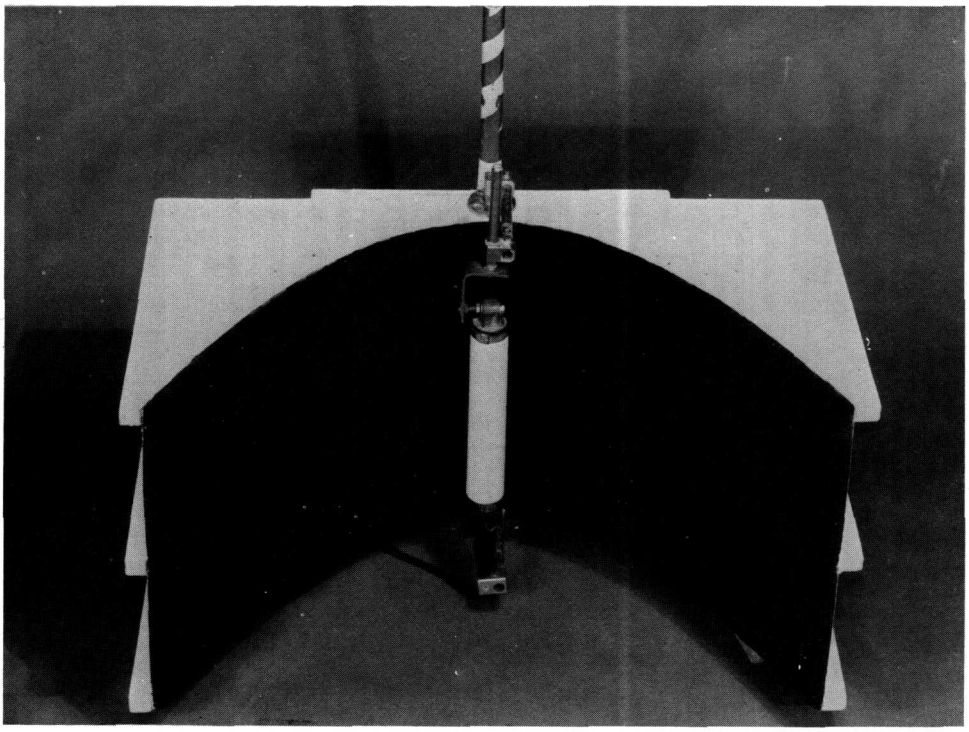

Fig. 1a—Shallow reflector

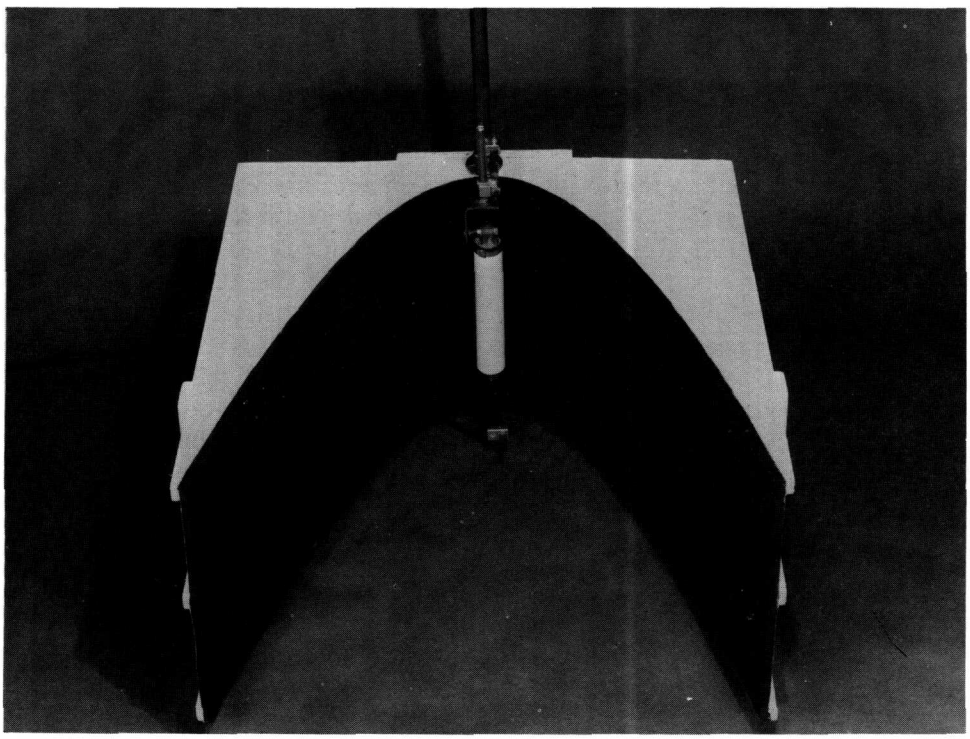

Fig. 1b—Deep reflector

parabola. Three horizontal ribs cut from 3/4-inch-thick exterior grade plywood sheets insured the integrity and rigidity of the parabolic reflector surface along its height. Initially the three sheets of plywood were fastened in a stack and cut simultaneously to the pattern, which was transcribed on the top sheet. The rough-cut edges of the wood were filed and then sanded. The plywood sheets were separated and secured parallel to each other at the extremes and middle of the reflector height with vertical struts and a rectangular wooden backplate. Levels and squares were used to align the ribs parallel and equidistant. The cut parabolic edges of the ribs provided a housing for the reflector material such that the reflector surface was a section of a right parabolic cylinder. A malleable 1/32-inch-thick copper sheet was cut oversize, bent by hand to the contour of the parabolic edges of the ribs, and temporarily tacked into place; then the perimeter corresponding to the proposed reflector area was marked. The copper was removed, cut to shape, bright dipped in an acid solution to remove oxidation and impurities, and remounted permanently to the ribs with wood screws and tacks. The 1/2-inch-thick layer of closed-cell rubber was bonded to the cleaned copper surface with Formica 140 brushable contact cement. The bonding required two installments, because the adhesive bonds on contact and it was too difficult to instantaneously set the entire reflector surface in place. Pressure was applied with a roller over the entire surface to insure uniform contact and prevent trapped air between the rubber and the copper. Finally the rubber was trimmed flush with the perimeter of the reflector and the exposed plywood surfaces were painted with four coats of waterproof oil-based paint.

The finished dimensions of the reflectors' surfaces were determined by several measurements in air, but for the dimensions in water the compression of the closed-cell rubber layer by water pressure at the depth of the experiment had to be considered. The thickness correction due to compression and an error analysis of the measurements on the reflectors are described in Appendix A. Both reflectors were found to be parabolic cylinders within the limits of measurement error, and their focal lengths underwater were 3.98 $\pm$ 0.011 inches for the deep reflector and 2.03 $\pm$ 0.005 inches for the shallow reflector. Figure 2 summarizes the underwater dimensions of the reflectors that were used in the mathematical model to generate theoretical radiation patterns and includes the errors in these dimensions.

Line Source and Its Alignment in the Reflector

The line source was a USRD type F36 transducer whose active element consists of seven capped lead zirconate-titanate cylinders mounted in a line 8 inches long. The elements are housed in an oil-filled butyl-rubber boot that fits over a framework of six steel rods. Electrical power is supplied to the transducer through 40 feet of two-conductor, shielded, neoprene-sheathed cable. Overall the F36 cylindrical molded rubber boot is 10 inches long by 1-3/4 inches in diameter, and the acoustic center of the transducer is assumed to be at the physical center of the boot. The F36 was designed to be suspended by two metal eyes near the electrical cable input, but during the performance of the experiment it was suspended by a bored metal fitting at the opposite end of the transducer. A tapered rubber sleeve at the cable end of the transducer was restrained in a metal ring whose spatial position was universally adjustable. The F36 was designed to be used at high audio frequencies, and its acoustic radiation pattern is omnidirectional within $\pm$ 0.5 dB in the median plane of the transducer.

The successful performance of the experiment required not only a truly parabolic cylindrical section as the reflecting surface but also accurate alignment of the axis of the

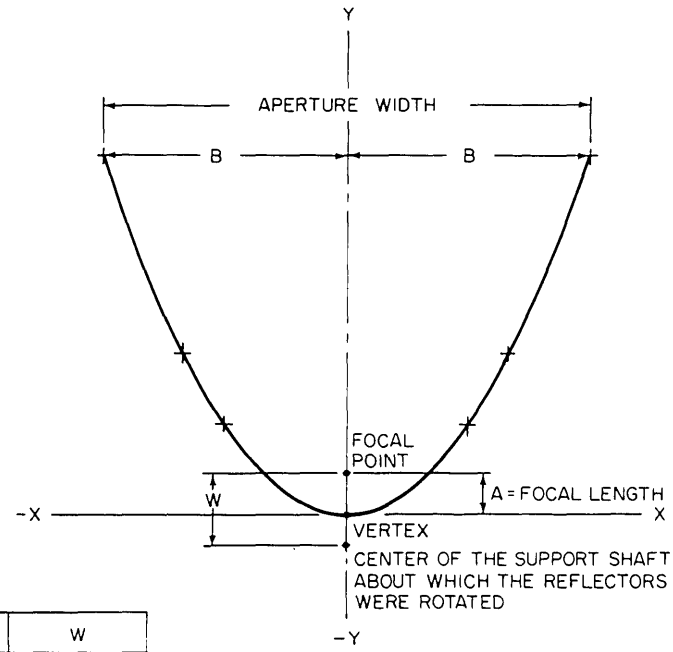

REFLECTOR	2B (in)	A (in)	W
SHALLOW	28 3 ± 0 1	398 ± 0.011	723 ± 0 04
DEEP	28 4 ± 0.1	2.03±0.005	5.32 ± 0.03

Fig. 2—Dimensions of the reflectors

line source along the focal line. The alignment was accomplished in two stages: the transducer was placed approximately at the focal line and fixed in the plane determined by the vertex of the parabola and the focal line by optical methods, and in this plane the axis of the transducer was adjusted to coincide with the focal line by the use of a metal spacer. The support rods and Fisher Scientific Flexaframe connectors enabled the fine adjustment of the transducer's spatial orientation.

The optical part of the alignment procedure is illustrated in Fig. 3. Strips of masking tape graduated at equal intervals by thin dark lines were wrapped around the shaft of the transducer near the ends. The transducer was then placed at a position P estimated to be the focal line. A plumb line was dropped in front of the transducer from a point on the Y axis at the top of the reflector. The line through the vertex CC', was drawn on the black reflector surface as a thin white line. A surveyor's transit, 10 feet from the reflector on a flat mounting plate made horizontal by leveling screws, was moved laterally until the reticle in the transit eyepiece, the plumb line, and the white vertex line were sighted in coincidence. The transducer was delicately adjusted at its ends so that the same number of graduated marks appeared on the right and left of the transit reticle. This procedure established the axis of the transducer in the $X = 0$ plane of the reflector. A small rectangular spacer of 1/16-inch-thick brass stock was cut to a length equal to the focal length minus the radius of the transducer. The transducer's orientation in the $X = 0$ plane was then adjusted by sliding the spacer along the vertex line (CC') of the reflector and simultaneously touching the back surface of the transducer boot. The line source was centered with respect to the height dimension of the reflector. The total uncertainty in alignment in the Y coordinate axis direction was ± 1/16 inch and in the X coordinate axis direction was $\pm \sqrt{2}/32$ inch. The overall success of the alignment procedure is manifest in the

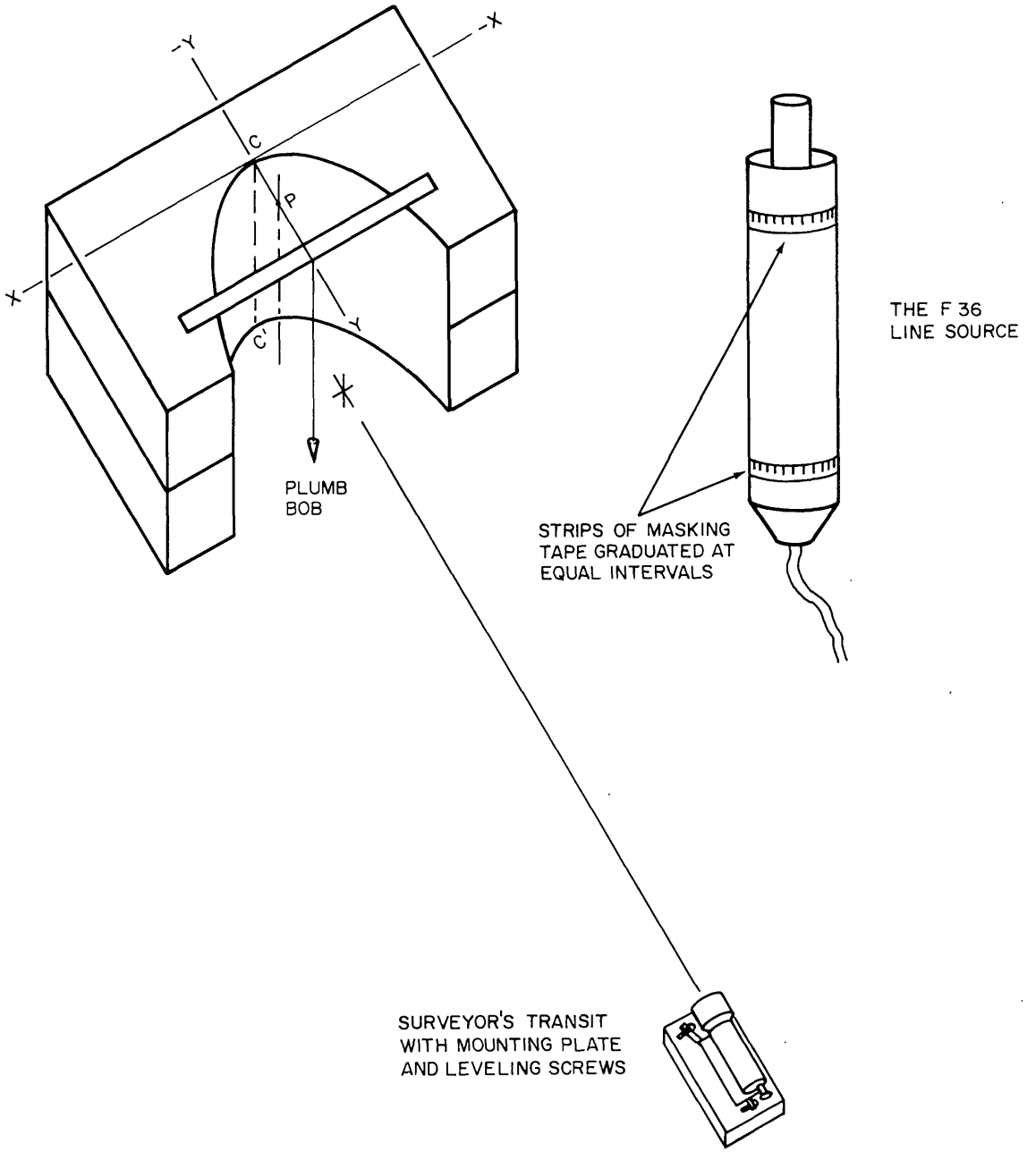

Fig. 3—Optical alignment procedure

agreement between theory and experiment, because the theory assumes the line array was coincident with the focal line of the reflector.

Block Circuit Diagrams and the Test Tank

The reflector was supported in the water by a rotatable vertical shaft rigidly mounted to a Scientific Atlanta Series 5115C-3 rotating head [3]. Horizontal beam patterns were obtained by fixing the hydrophone at a point in the acoustic field of the reflector and rotating the shaft that supported the reflector and transducer. The distance between the focal line of the reflector and the center of the support shaft about which the reflectors were rotated is shown as W in Fig. 2. Remote control of the direction of rotation, speed, and angular position of a transducer during beam pattern measurements was provided by the Scientific Atlanta Series 4100 positioner control unit.

The block circuit diagrams of the transducer driving system and the receiving system are shown in Figs. 4a and 4b. The pulse-modulated driving signal and gated measuring system allowed determination of free-field steady-state data in the confined space of the calibration tank [3]. The hydrophone used in the experiment was an Atlantic Research Model LC-10. The active element in the LC-10 is a ceramic cylindrical shell plated on the inside and outside surfaces which is approximately 1/2 inch long, 1/4 inch in diameter, and 0.04 inch thick.

EXPERIMENTAL DATA

Numerous radiation patterns recorded in the median planes of the reflectors are shown in Figs. 5 and 6. All of the recorded patterns are shown as solid lines, and the corresponding theoretically predicted patterns of the mathematical model are shown as dashed lines. The theoretical patterns are normalized to match the experimental patterns at 0 degrees. Figures 5 are patterns of the 4.0-inch-focal-length reflector and Figs. 6 are patterns of the 2.0-inch-focal-length reflector. Each pattern is identified by R, the separation distance between hydrophone and reflector support shaft, and f, the frequency. The separation distance was 20 feet for patterns 5a through 5m and 6a through 6k, 10 feet 8 inches for patterns 5n through 5q and 6l through 6m, and 40 inches for patterns 5r through 5u. Figures 5 and 6 represent only a sample of the total number of patterns corresponding to different experimental parameters recorded during the experiment.

The mathematical model requires the acoustic radiation of the line source to be axially symmetric in a plane perpendicular to its axis over the frequency range of interest. Consequently the radiation patterns of the F36 transducer freely suspended in the medium in the absence of the reflector should be circles. Far-field patterns were taken every 5 kHz from 10 kHz to 40 kHz, and they were all circles centered at the axis of the F36 to within ± 0.5 dB. The very-near-field radiation of the F36 line source was measured between 10 kHz and 40 kHz and found to be omnidirectional to within the accuracy of the measuring apparatus; this result and its associated experiment are described in Appendix B. The transmitting voltage response of the F36 measured in a plane perpendicular to the axis increases 13 dB per octave between 10 kHz and 23 kHz and varies by 15 dB between 23 kHz and 40 kHz; but the amplitude variation was unimportant to the goals of the experiment, provided the transducer behaved as a line source. The finite diameter of the line source was judged to have little effect on the reflector radiation because it was small compared both to the wavelength of sound at most of the frequencies of interest

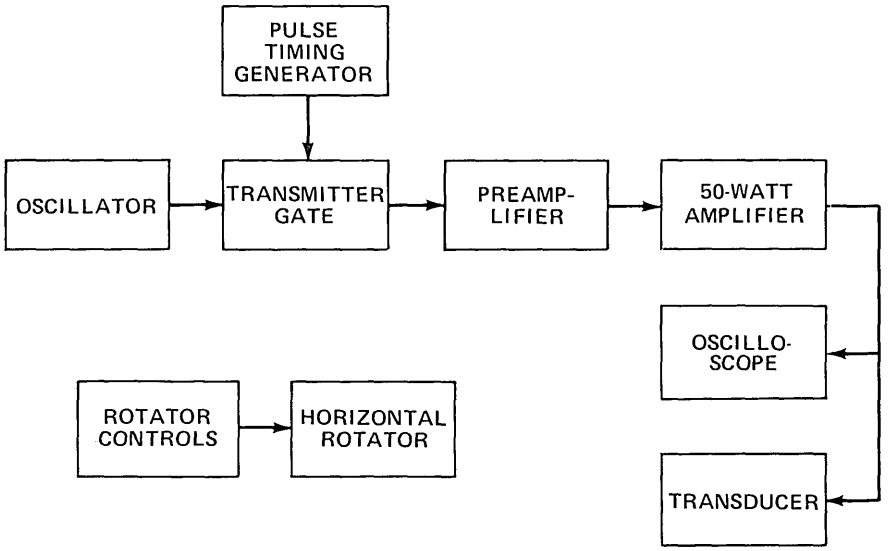

Fig. 4a—Transducer driving system

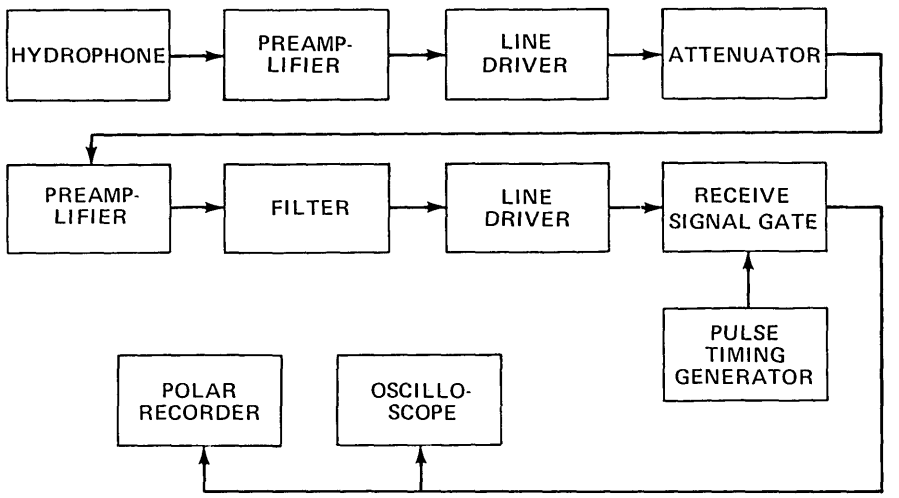

Fig. 4b—Receiving system

and to the aperture width of the reflector. The mathematical model also assumes that 100% of the acoustic power incident on the reflector surface is reflected. The power efficiency of the finished reflector is estimated in Appendix C from measurements to be 96%, which implies nearly total reflection of sound at the reflector surface and very little energy loss in the reflector material.

Additional experimental data were taken to determine how closely the reflecting surface conformed to a parabolic cylinder and to investigate the effect of a misalignment of the line source on the radiation patterns. These studies constitute an error analysis which examines some possible causes of the differences between the measured and calculated radiation patterns. In Appendix A measurements in air on the finished reflectors are tabulated and corrected for the compression of the closed-cell rubber due to the static

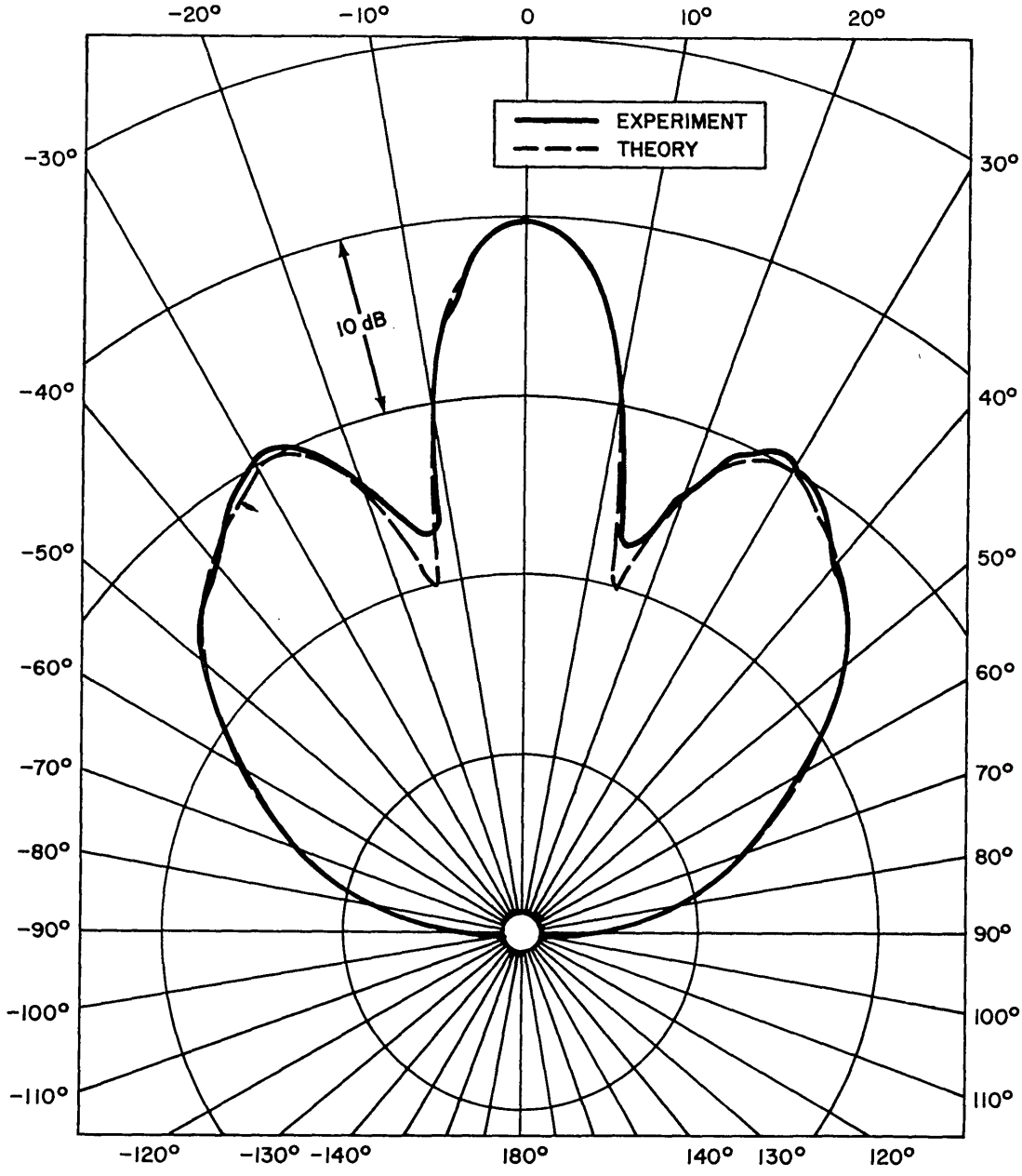

Fig. 5a—Radiation patterns in the median plane of the shallow (4.0-inch-focal-length) reflector for R = 20 feet and f = 10 kHz

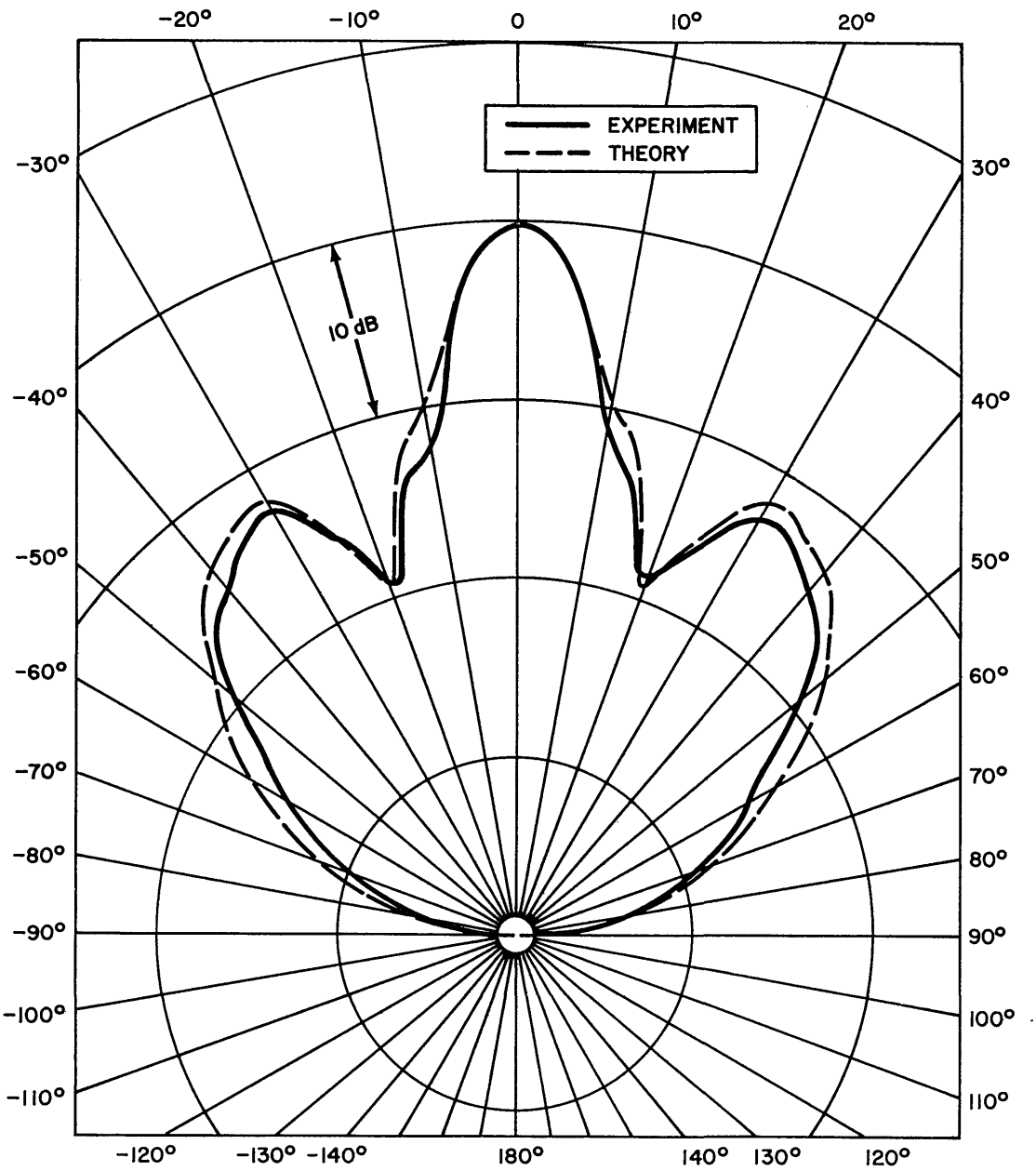

Fig. 5b—Radiation patterns in the median plane of the shallow (4.0-inch-focal-length) reflector for R = 20 feet and f = 13 kHz

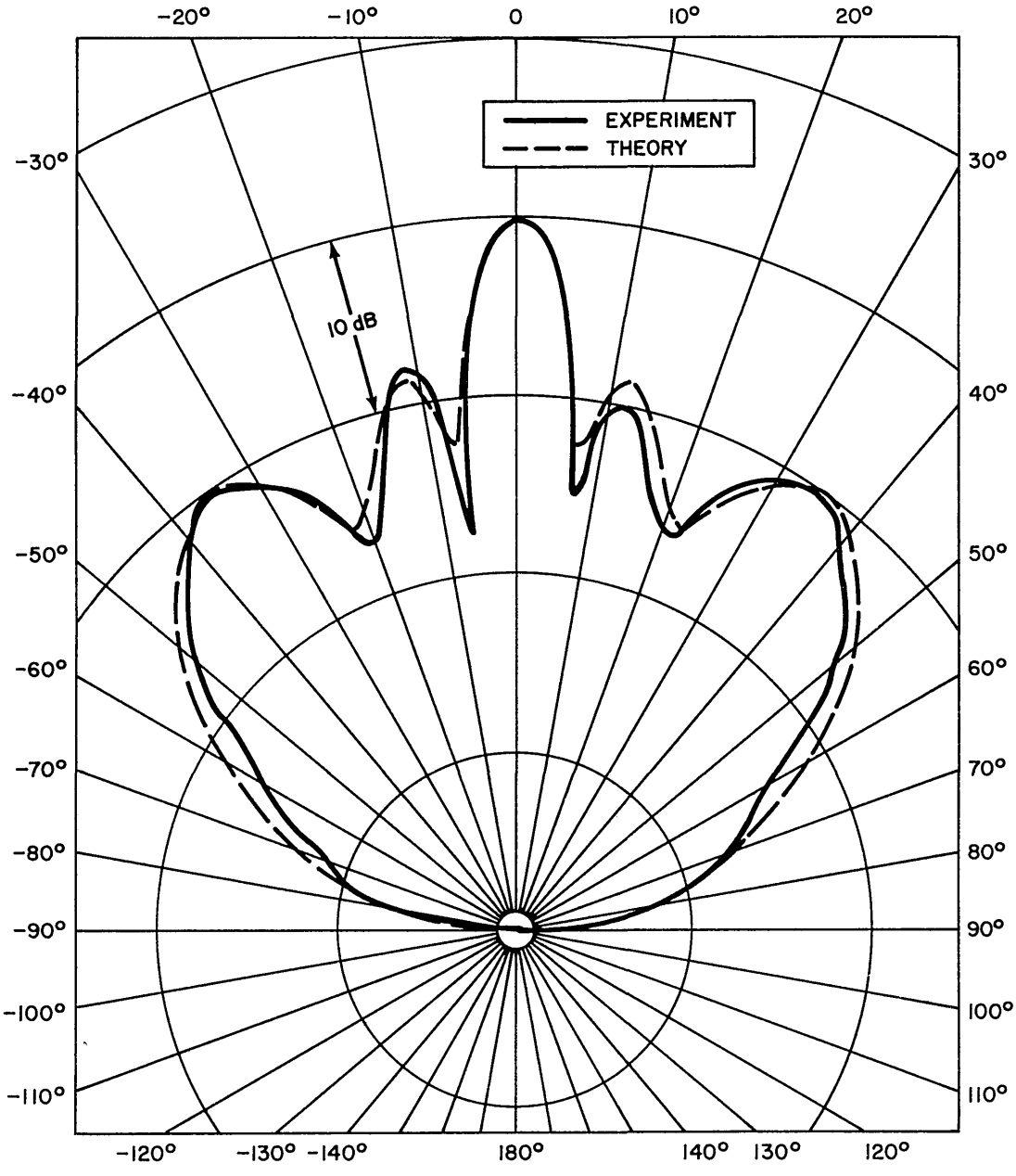

Fig. 5c—Radiation patterns in the median plane of the shallow (4.0-inch-focal-length) reflector for R = 20 feet and f = 15 kHz

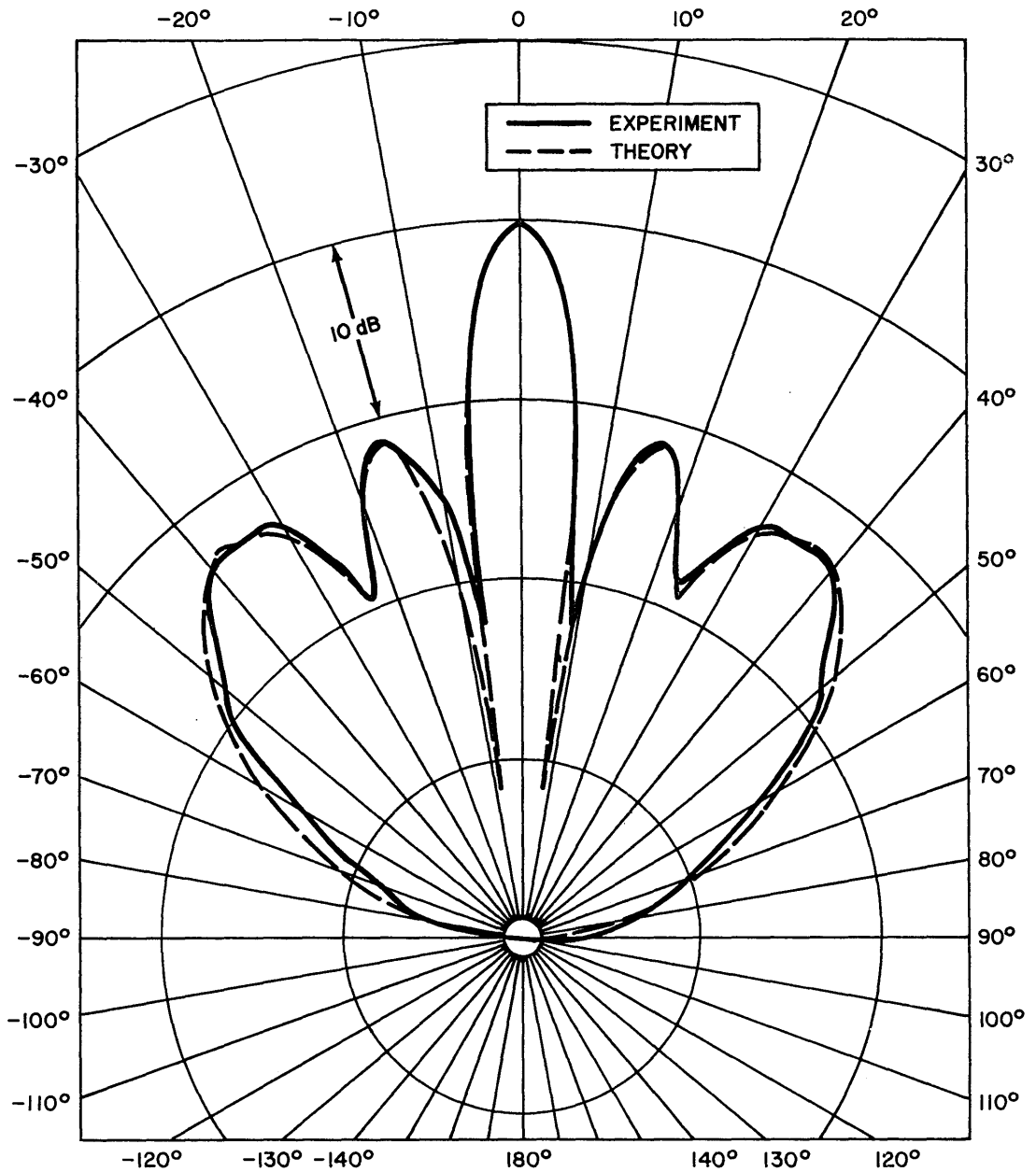

Fig. 5d—Radiation patterns in the median plane of the shallow (4.0-inch-focal-length) reflector for R = 20 feet and f = 17 kHz

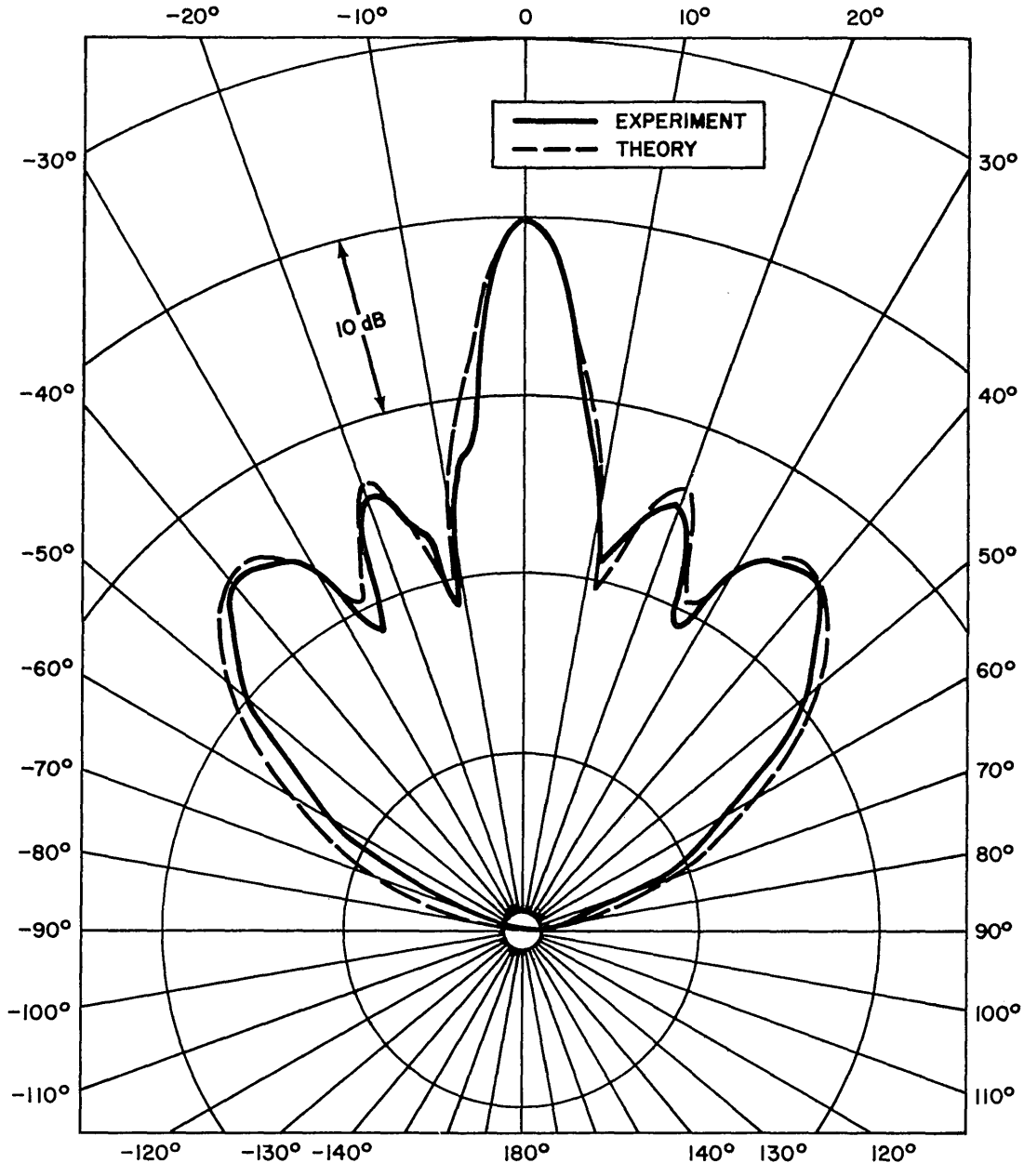

Fig. 5e—Radiation patterns in the median plane of the shallow (4.0-inch-focal-length) reflector for R = 20 feet and f = 20 kHz

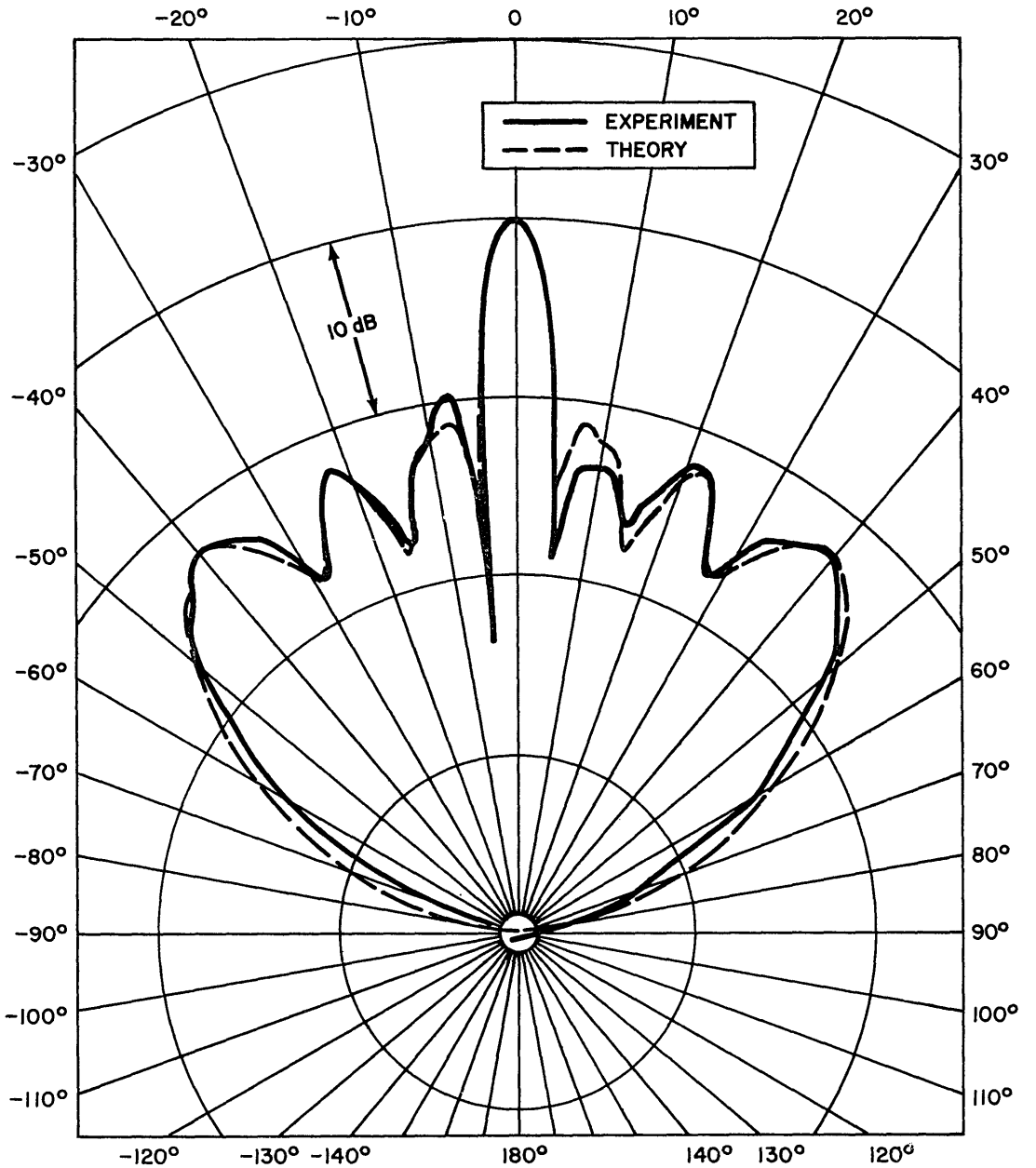

Fig. 5f—Radiation patterns in the median plane of the shallow (4.0-inch-focal-length) reflector for R = 20 feet and f = 23 kHz

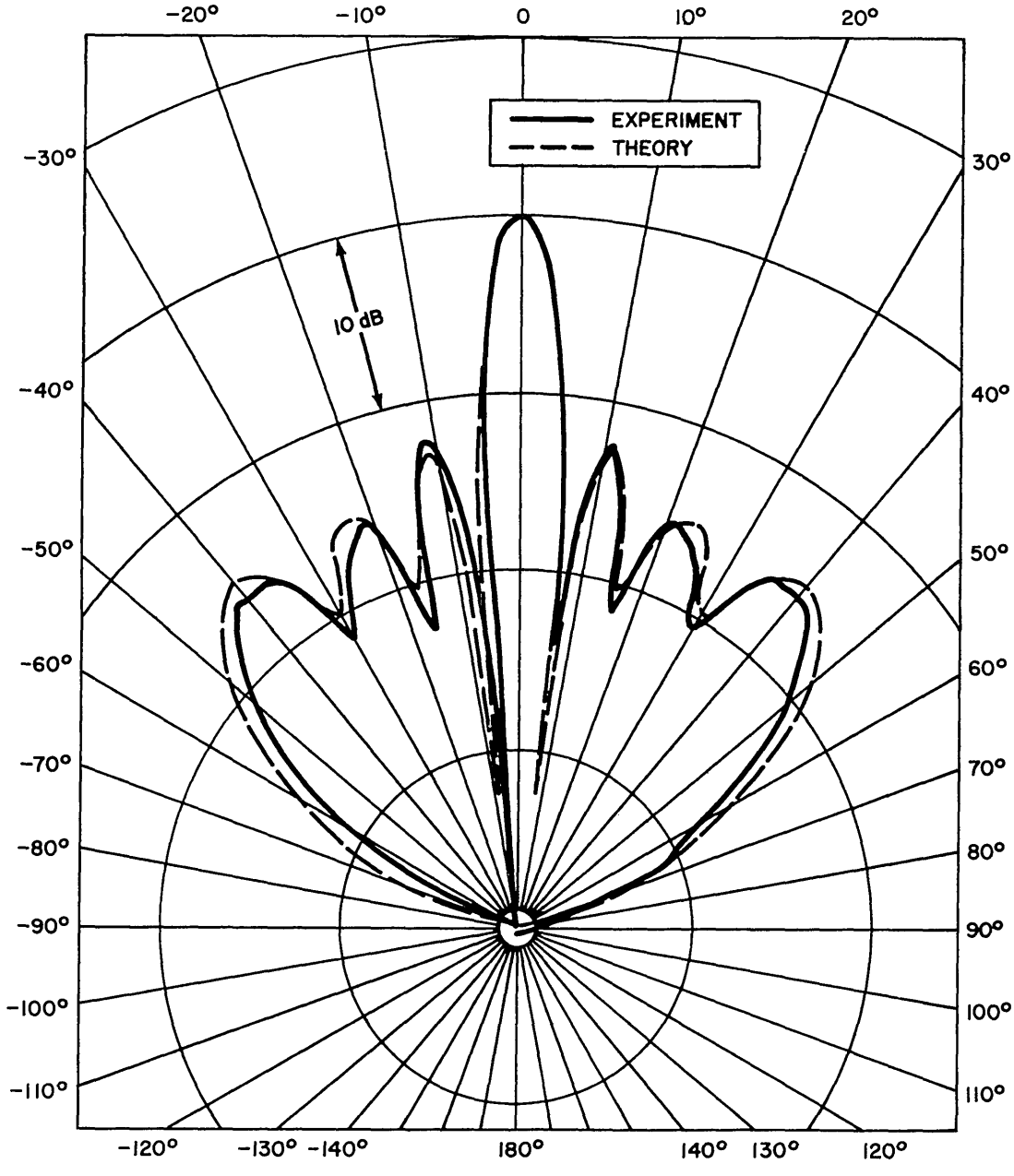

Fig. 5g—Radiation patterns in the median plane of the shallow (4.0-inch-focal-length) reflector for R = 20 feet and f = 25 kHz

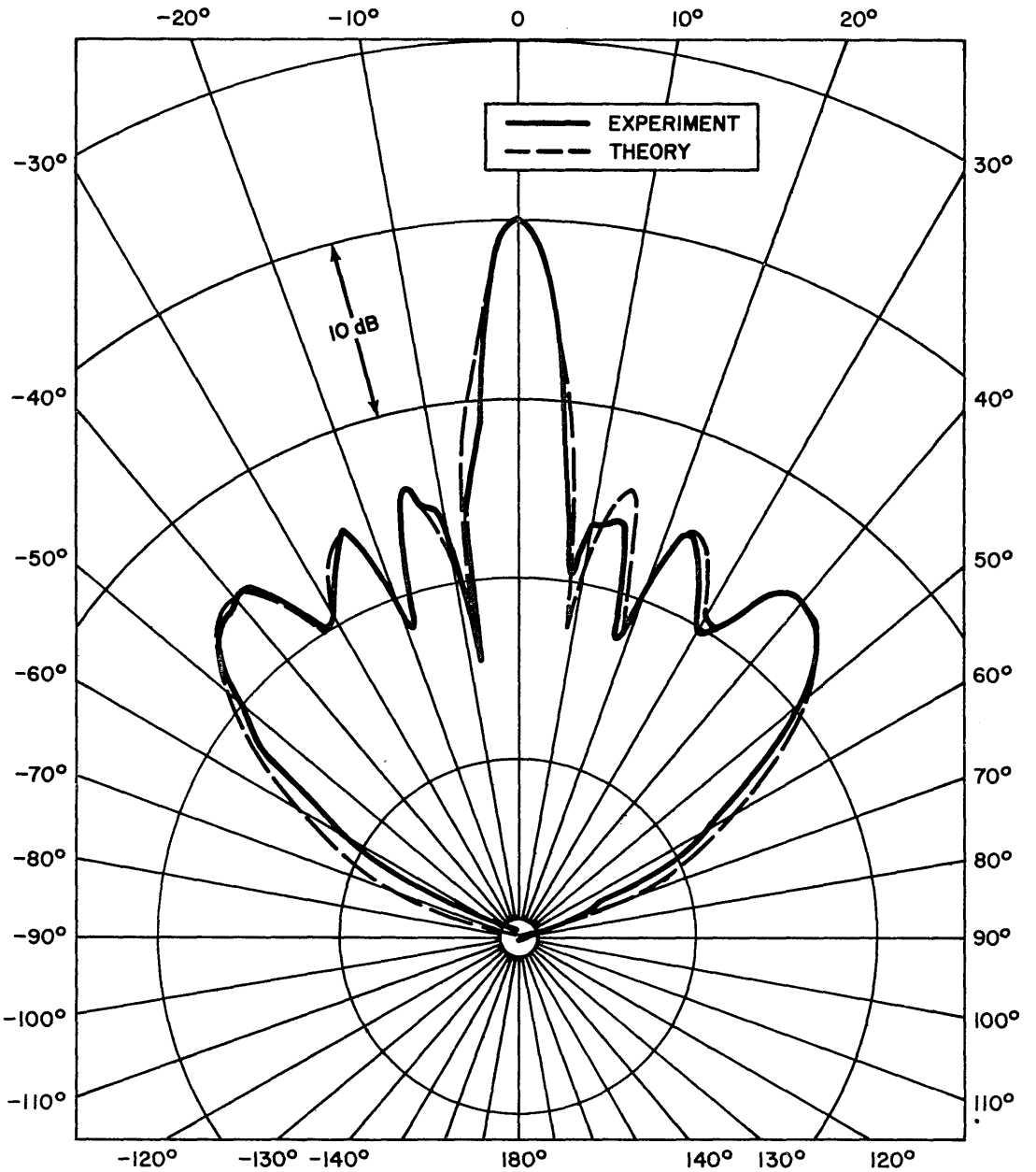

Fig. 5h—Radiation patterns in the median plane of the shallow (4.0-inch-focal-length) reflector for R = 20 feet and f = 27 kHz

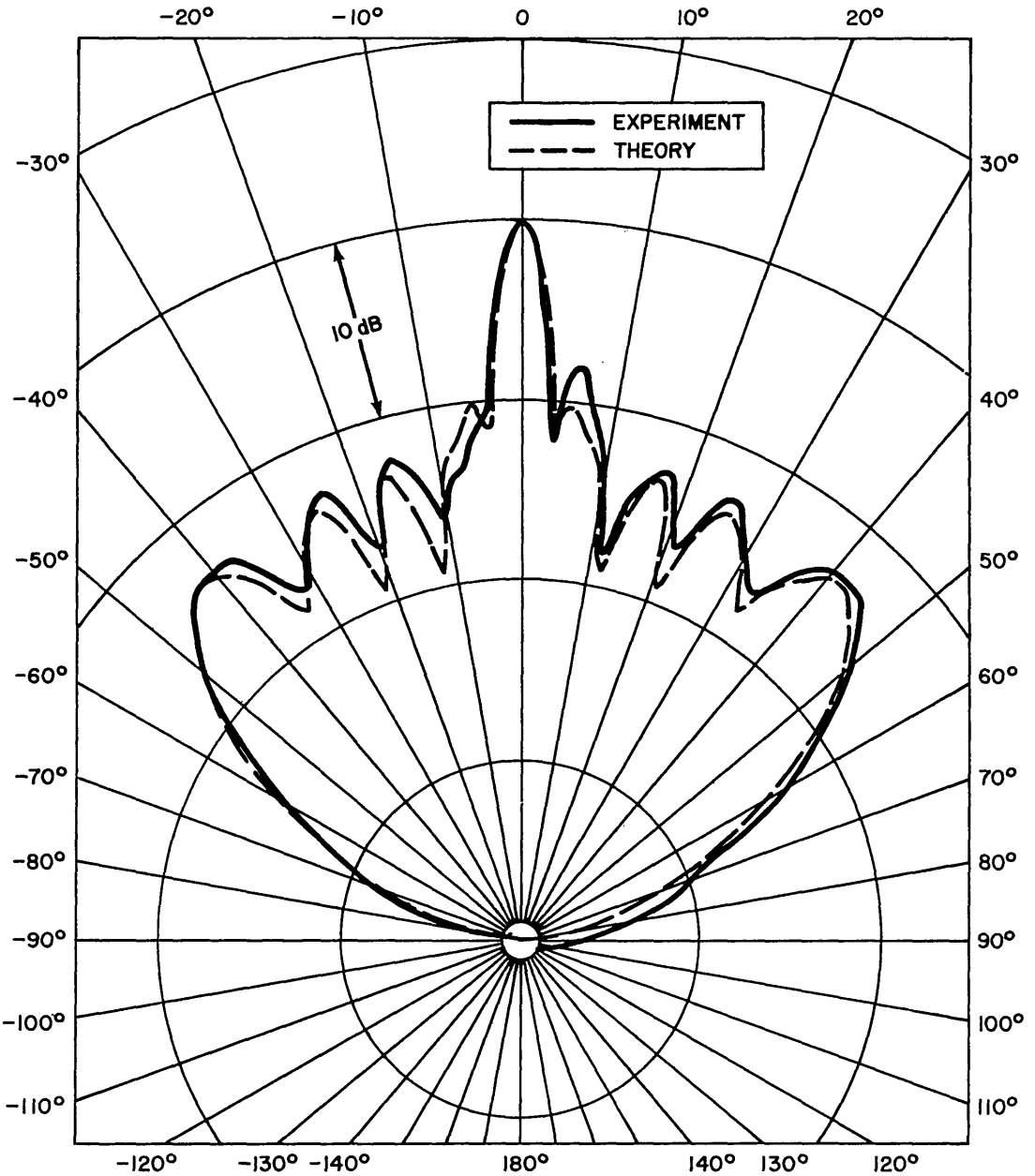

Fig. 5i—Radiation patterns in the median plane of the shallow (4.0-inch-focal-length) reflector for R = 20 feet and f = 30 kHz

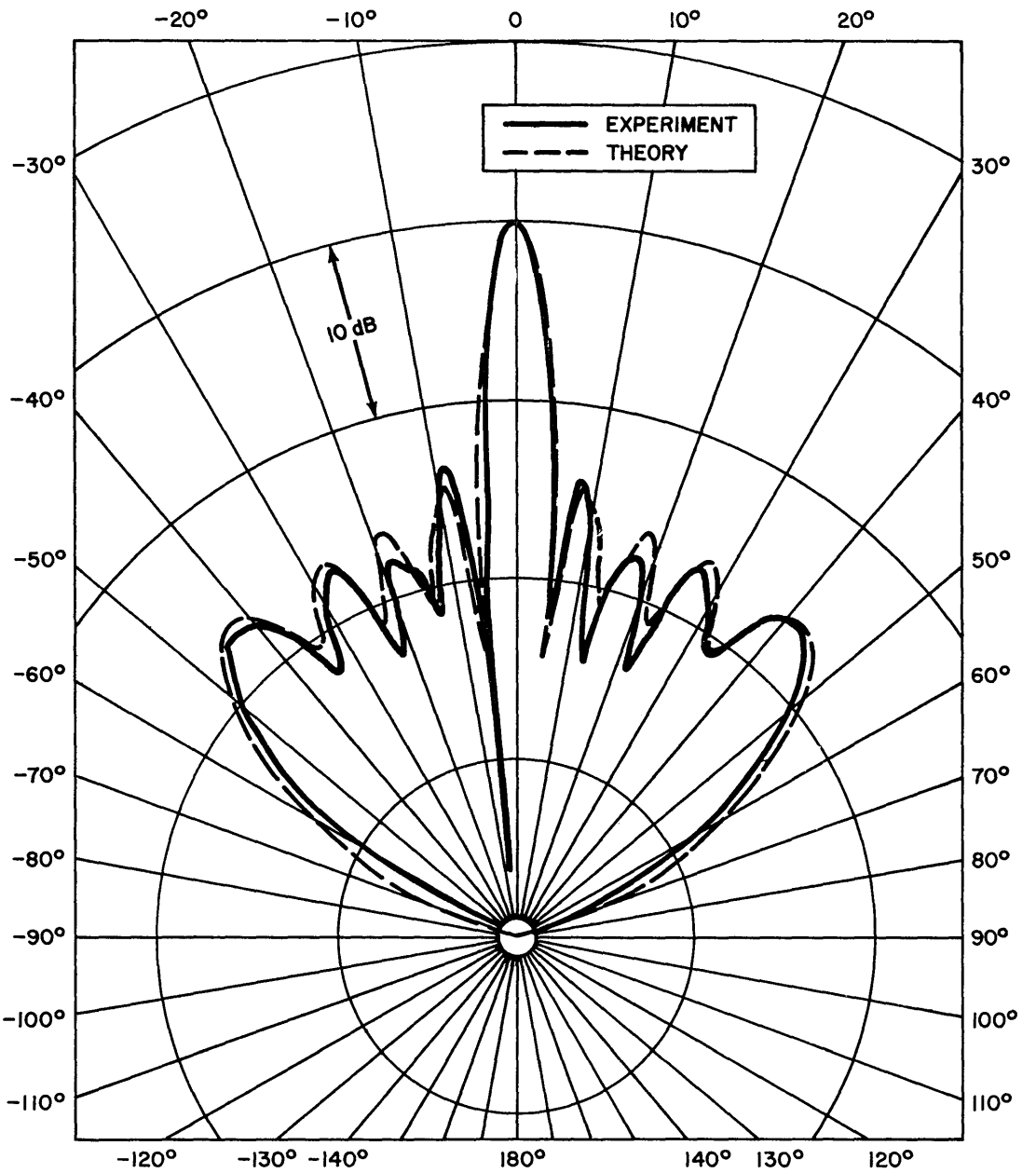

Fig. 5j—Radiation patterns in the median plane of the shallow (4.0-inch-focal-length) reflector for R = 20 feet and f = 33 kHz

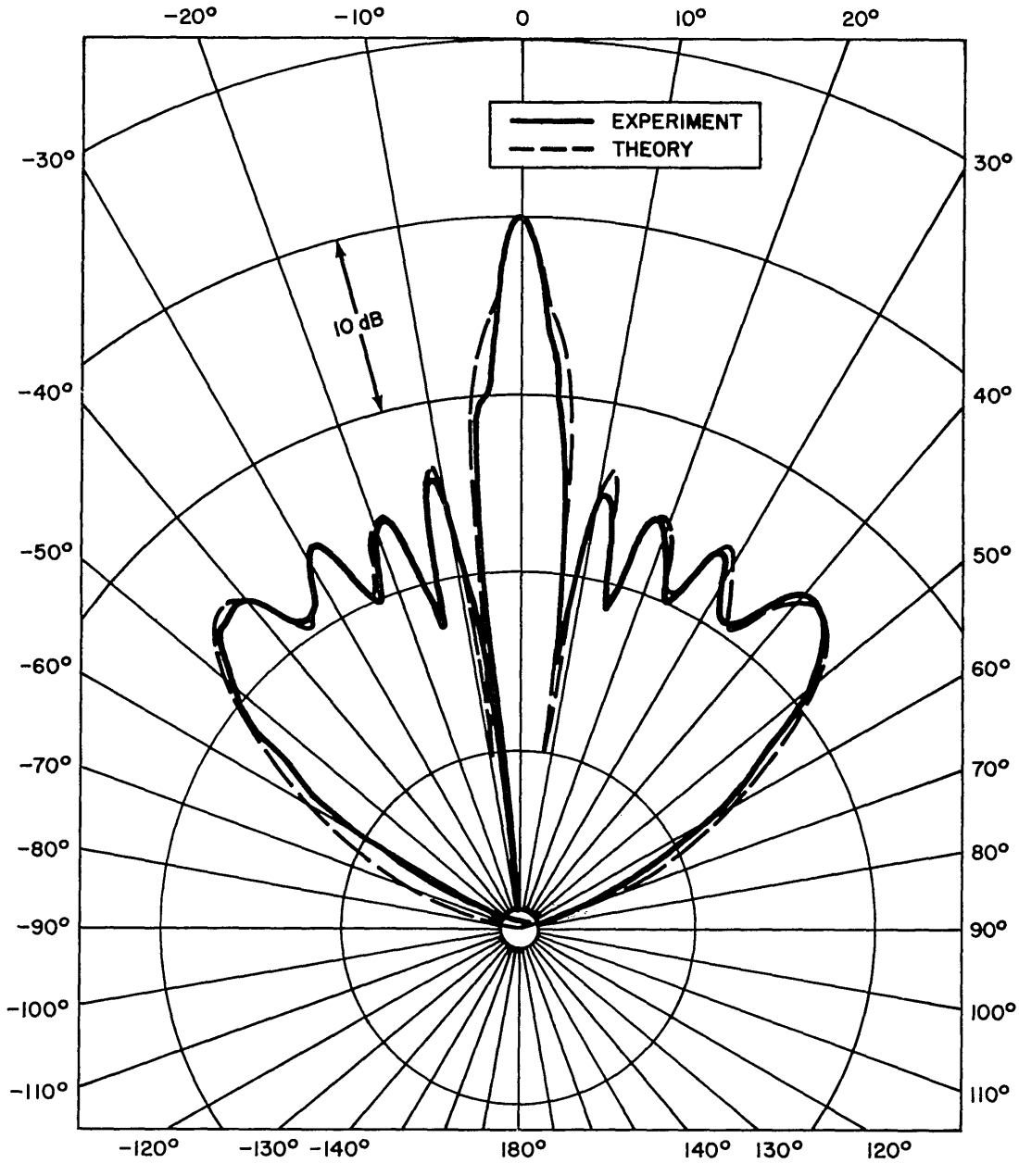

Fig. 5k—Radiation patterns in the median plane of the shallow (4.0-inch-focal-length) reflector for R = 20 feet and f = 35 kHz

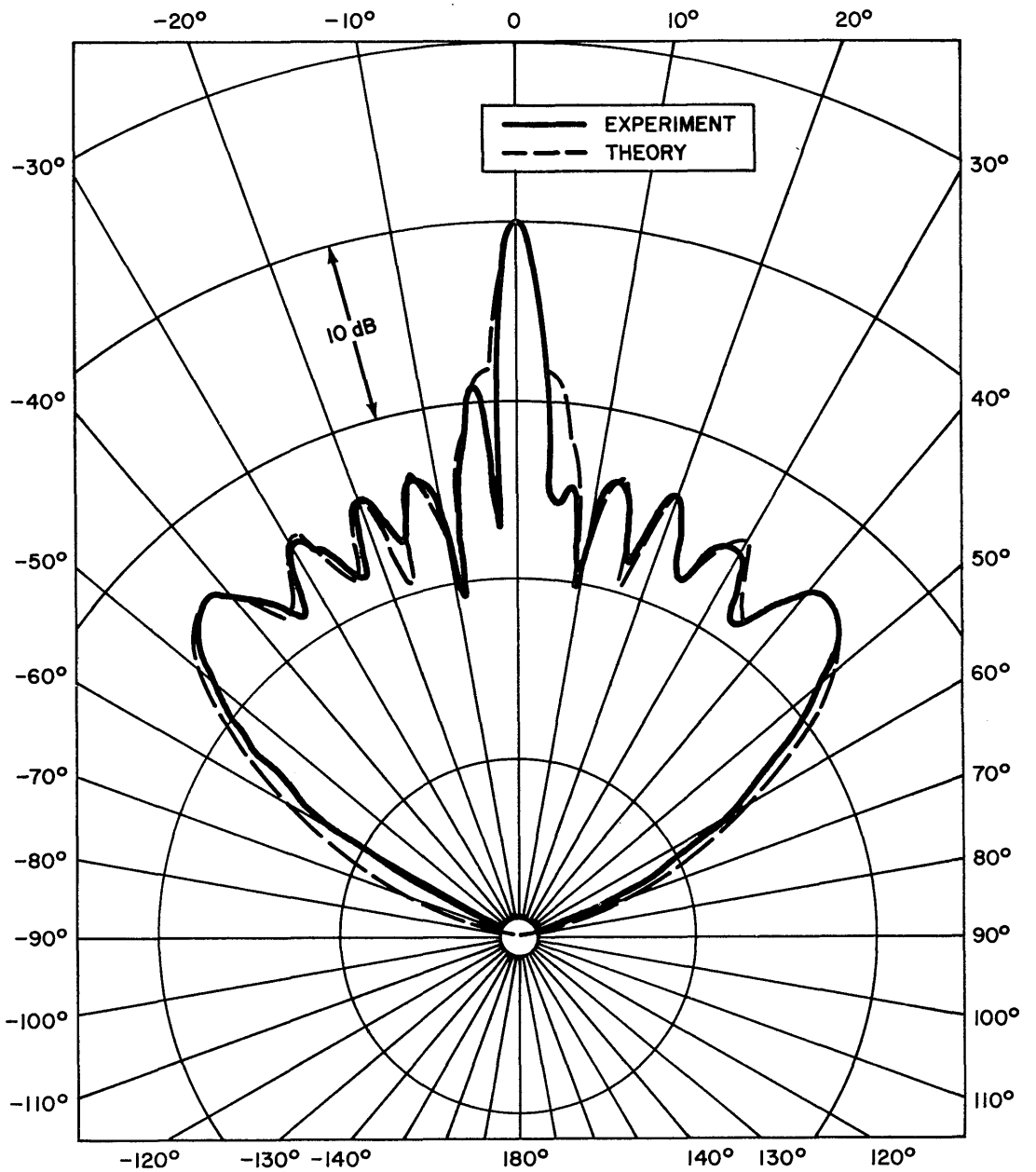

Fig. 51—Radiation patterns in the median plane of the shallow (4.0-inch-focal-length) reflector for R = 20 feet and f = 37 kHz

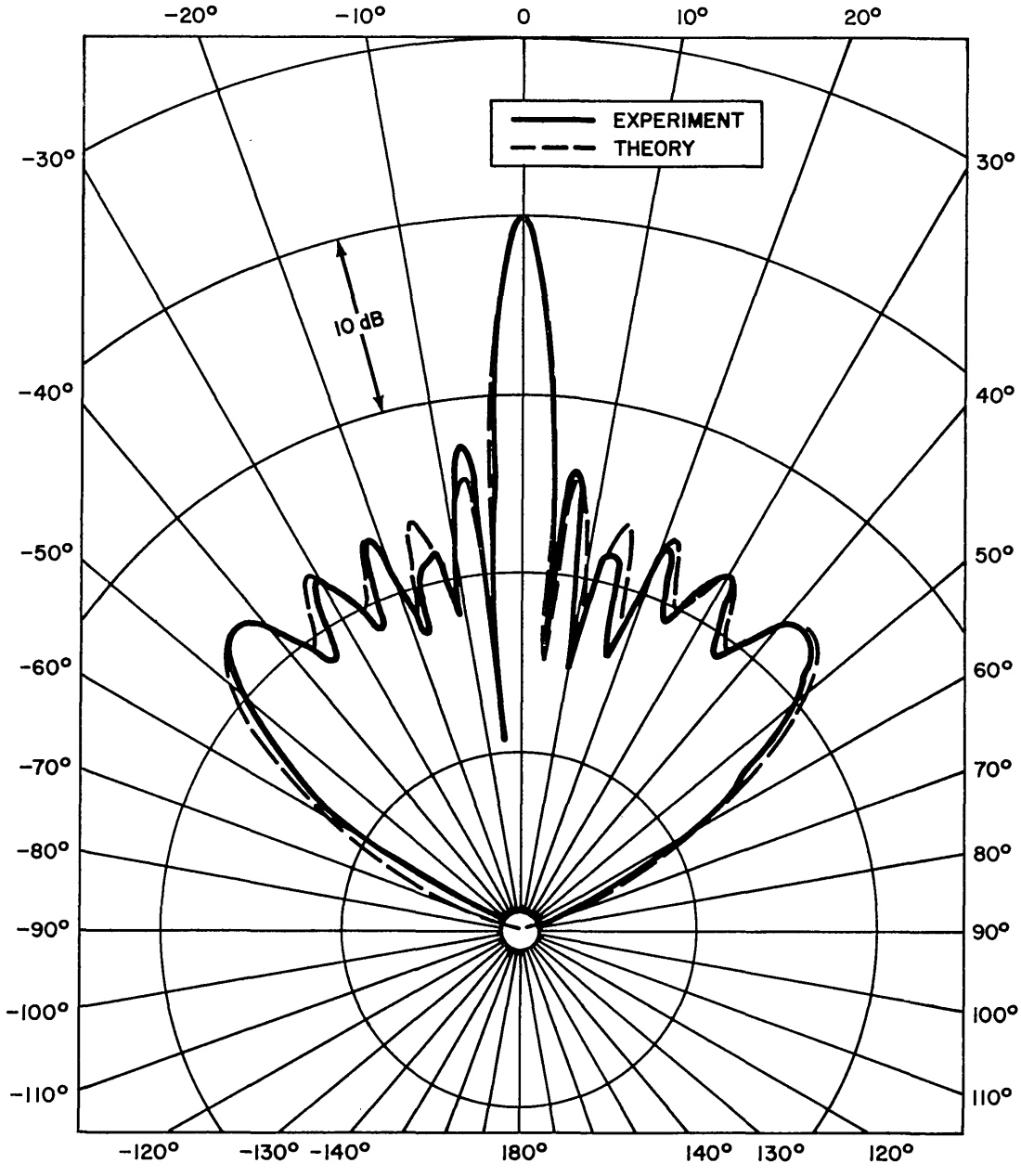

Fig. 5m—Radiation patterns in the median plane of the shallow (4.0-inch-focal-length) reflector for R = 20 feet and f = 40 kHz

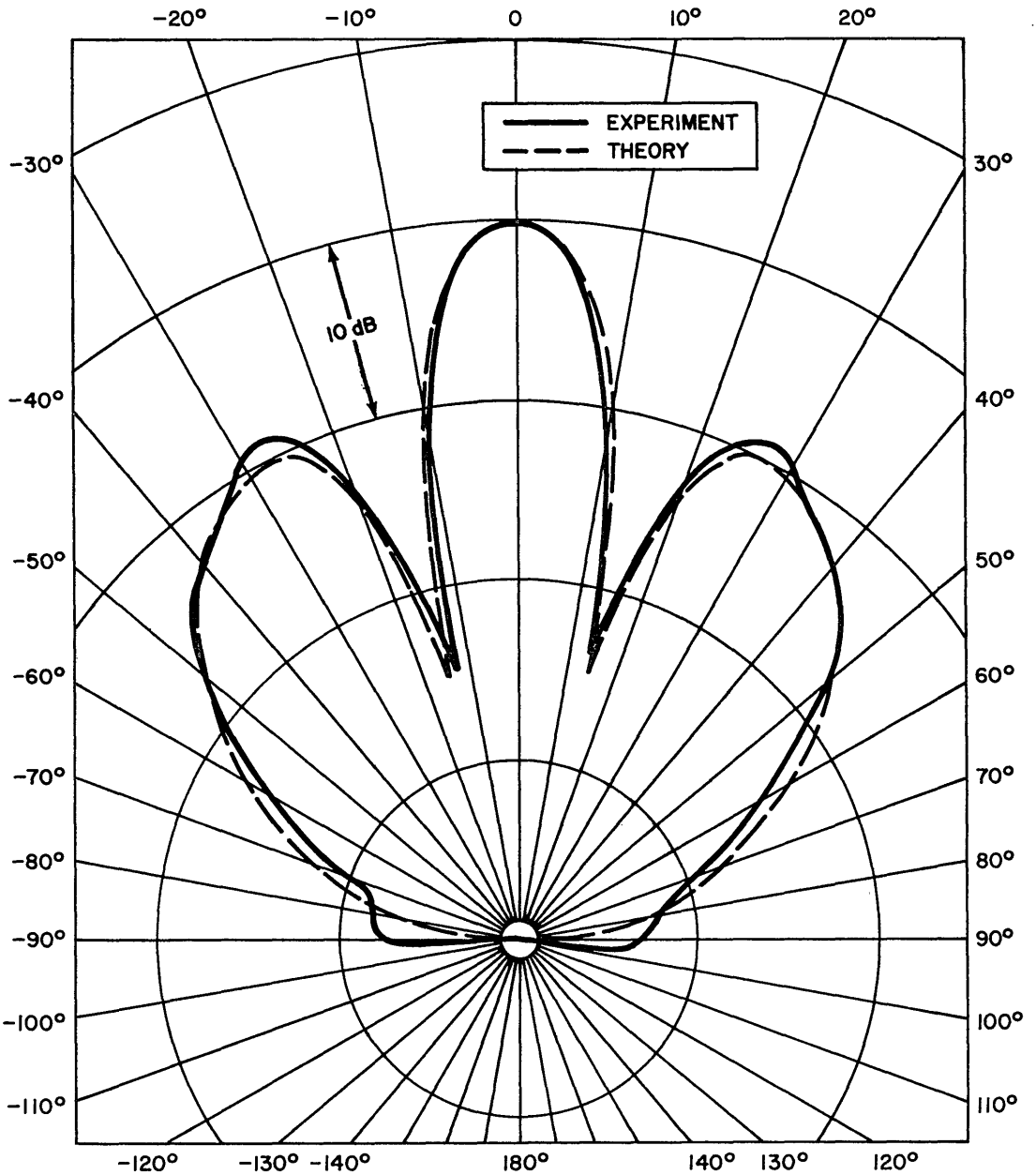

Fig. 5n—Radiation patterns in the median plane of the shallow (4.0-inch-focal-length) reflector for R = 10 feet 8 inches and f = 10 kHz

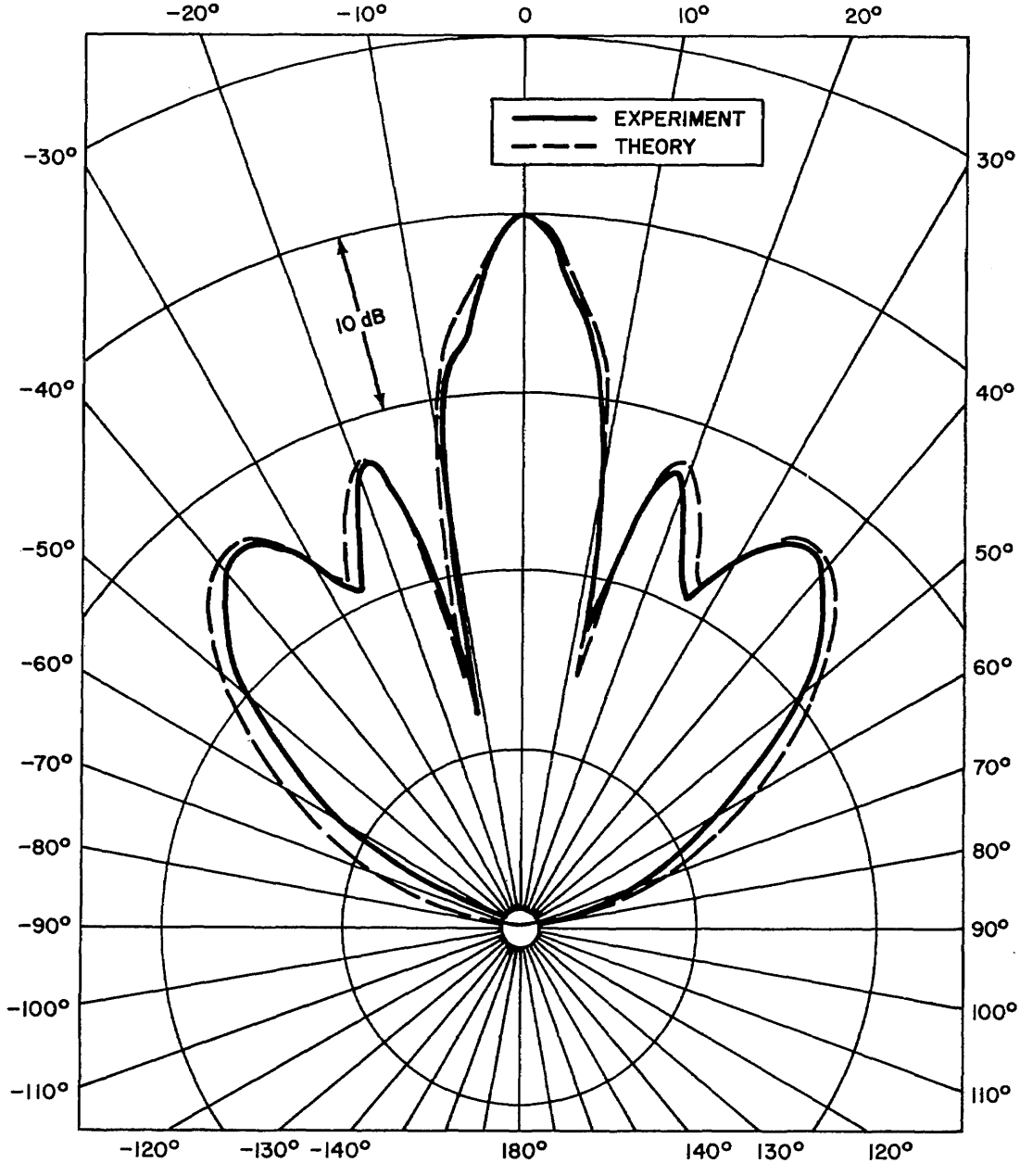

Fig. 5o—Radiation patterns in the median plane of the shallow (4.0-inch-focal-length) reflector for R = 10 feet 8 inches and f = 20 kHz

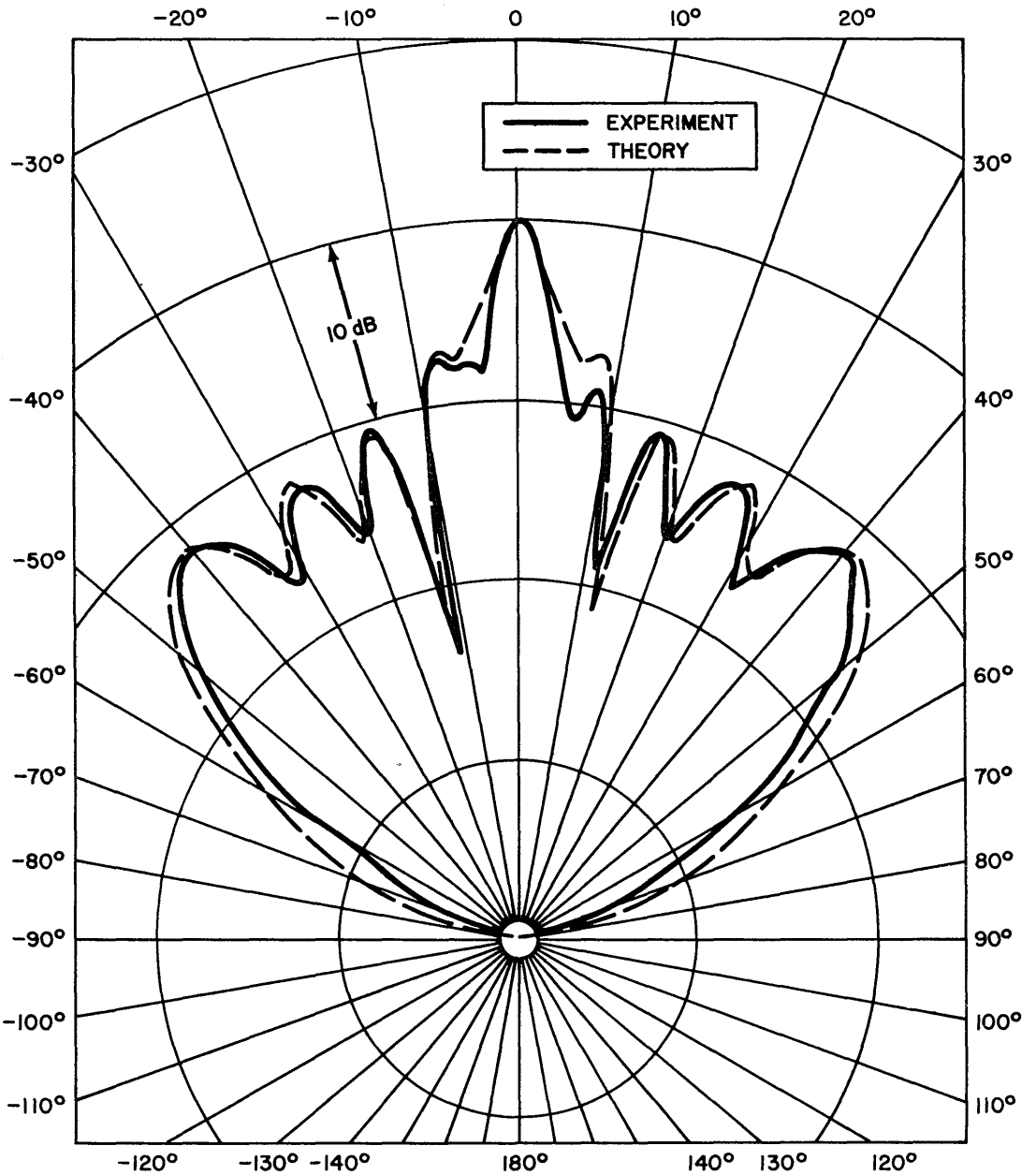

Fig. 5p—Radiation patterns in the median plane of the shallow (4.0-inch-focal-length) reflector for R = 10 feet 8 inches and f = 30 kHz

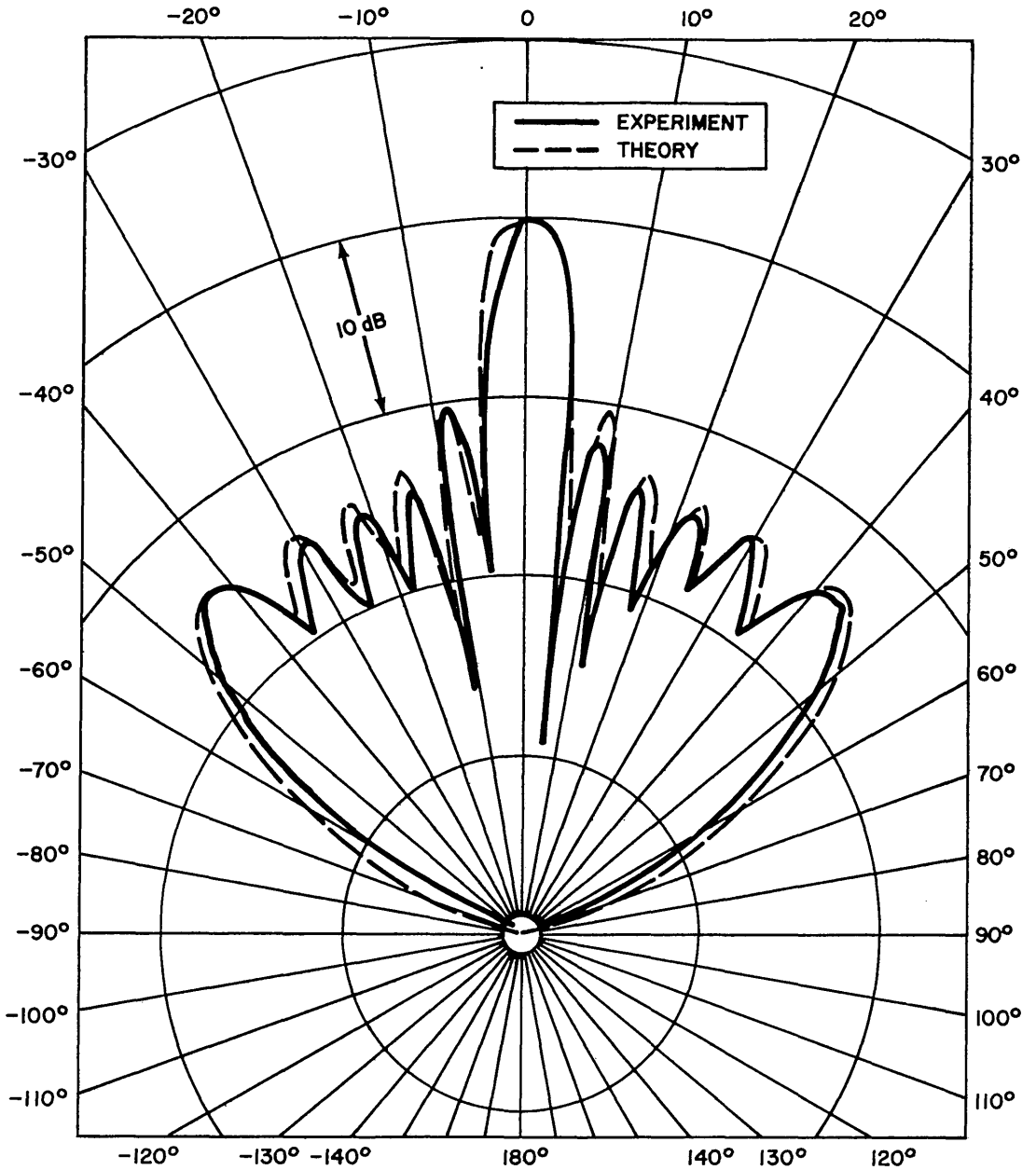

Fig. 5q—Radiation patterns in the median plane of the shallow (4.0-inch-focal-length) reflector for R = 10 feet 8 inches and f = 40 kHz

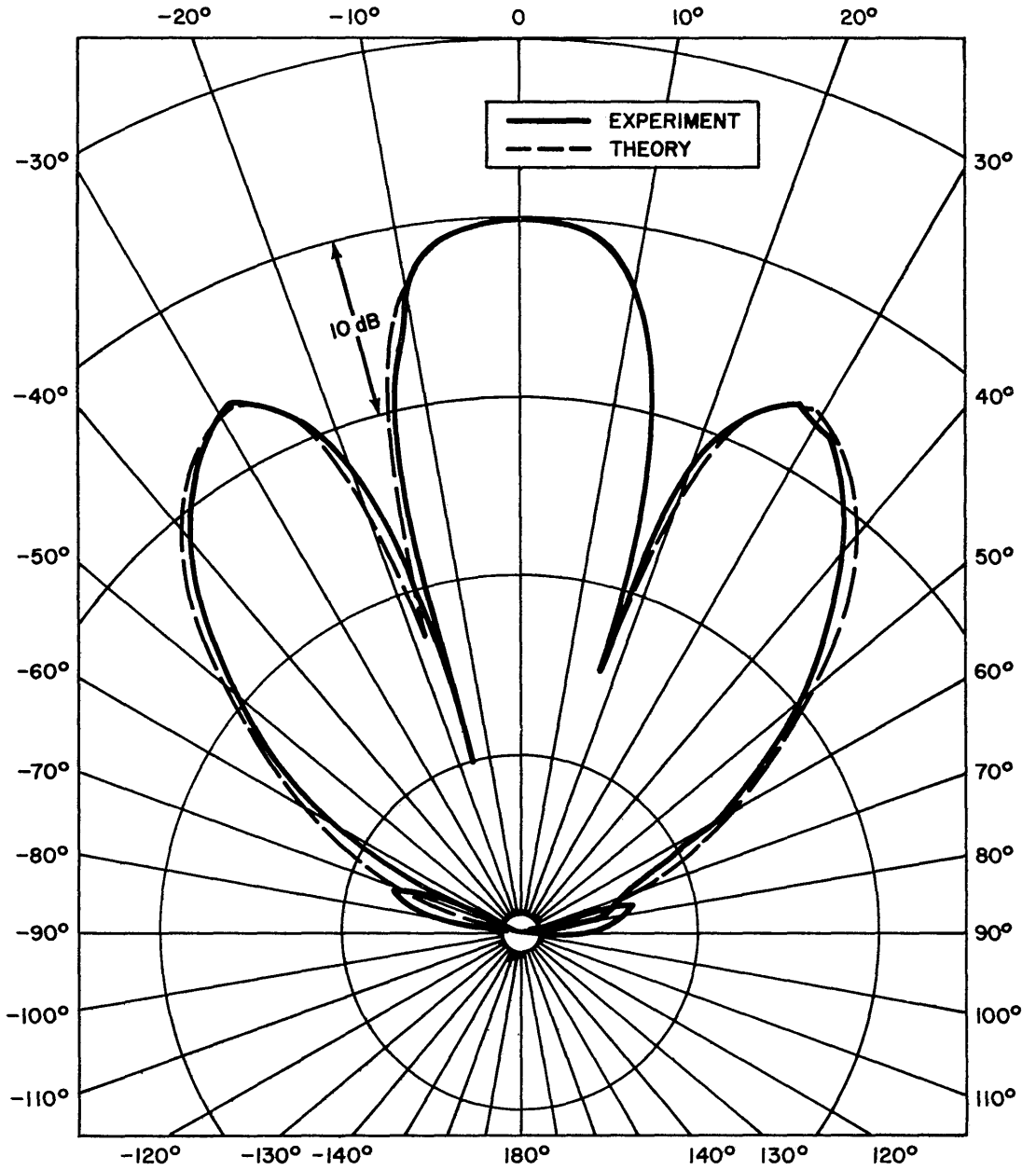

Fig. 5r—Radiation patterns in the median plane of the shallow (4.0-inch-focal-length) reflector for R = 40 inches and f = 10 kHz

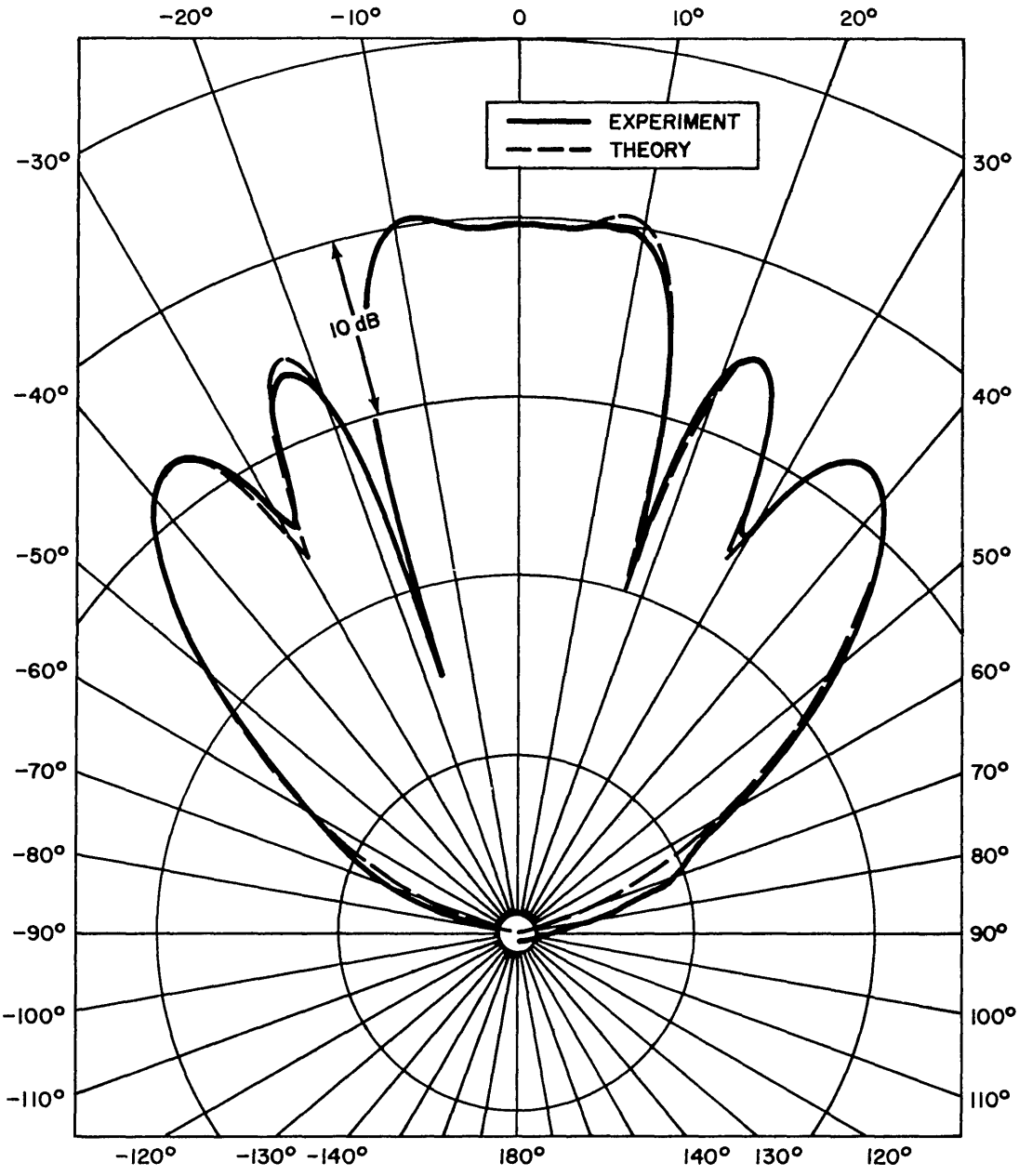

Fig. 5s—Radiation patterns in the median plane of the shallow (4.0-inch-focal-length) reflector for R = 40 inches and f = 20 kHz

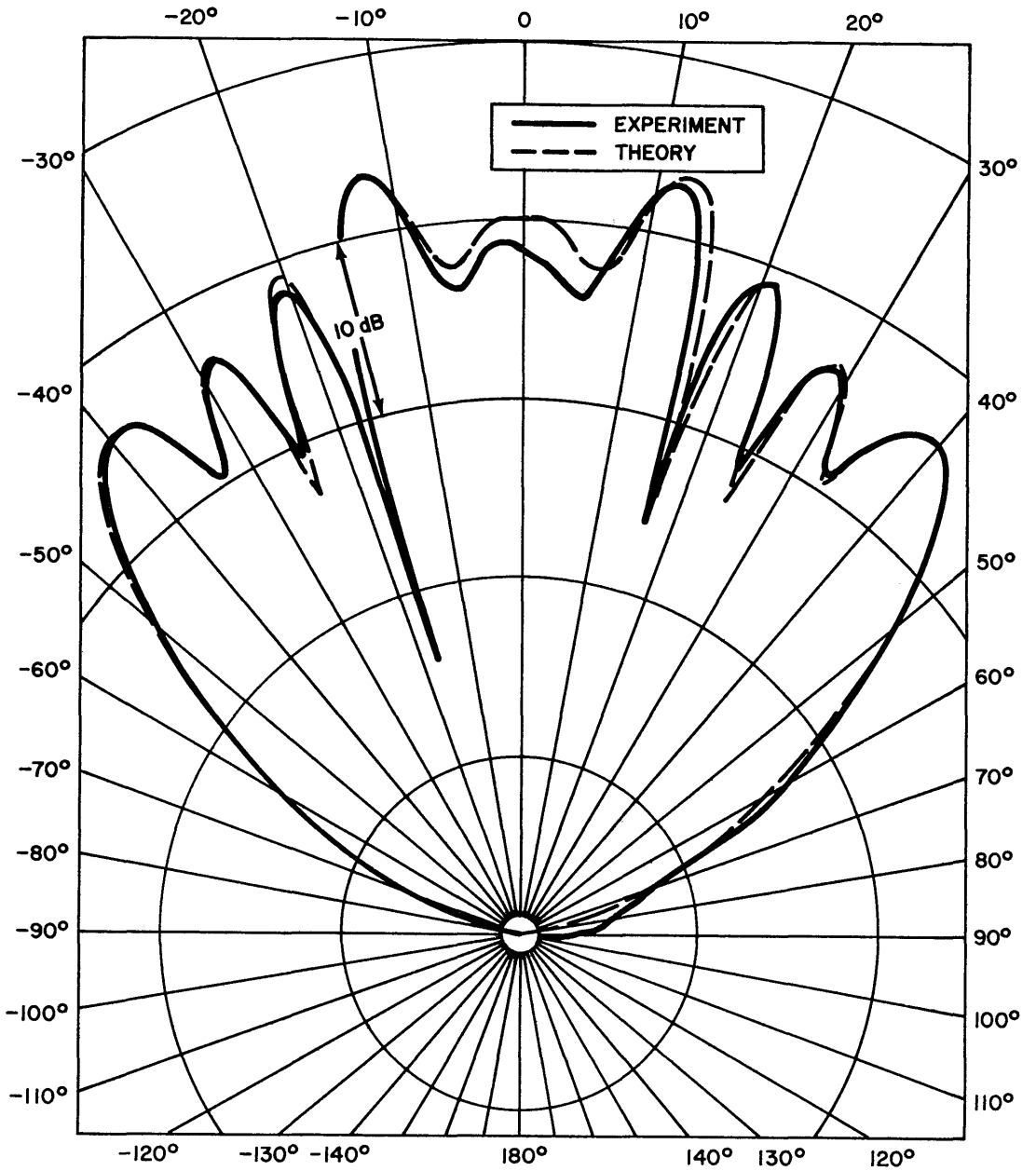

Fig. 5t—Radiation patterns in the median plane of the shallow (4.0-inch-focal-length) reflector for R = 40 inches and f = 30 kHz

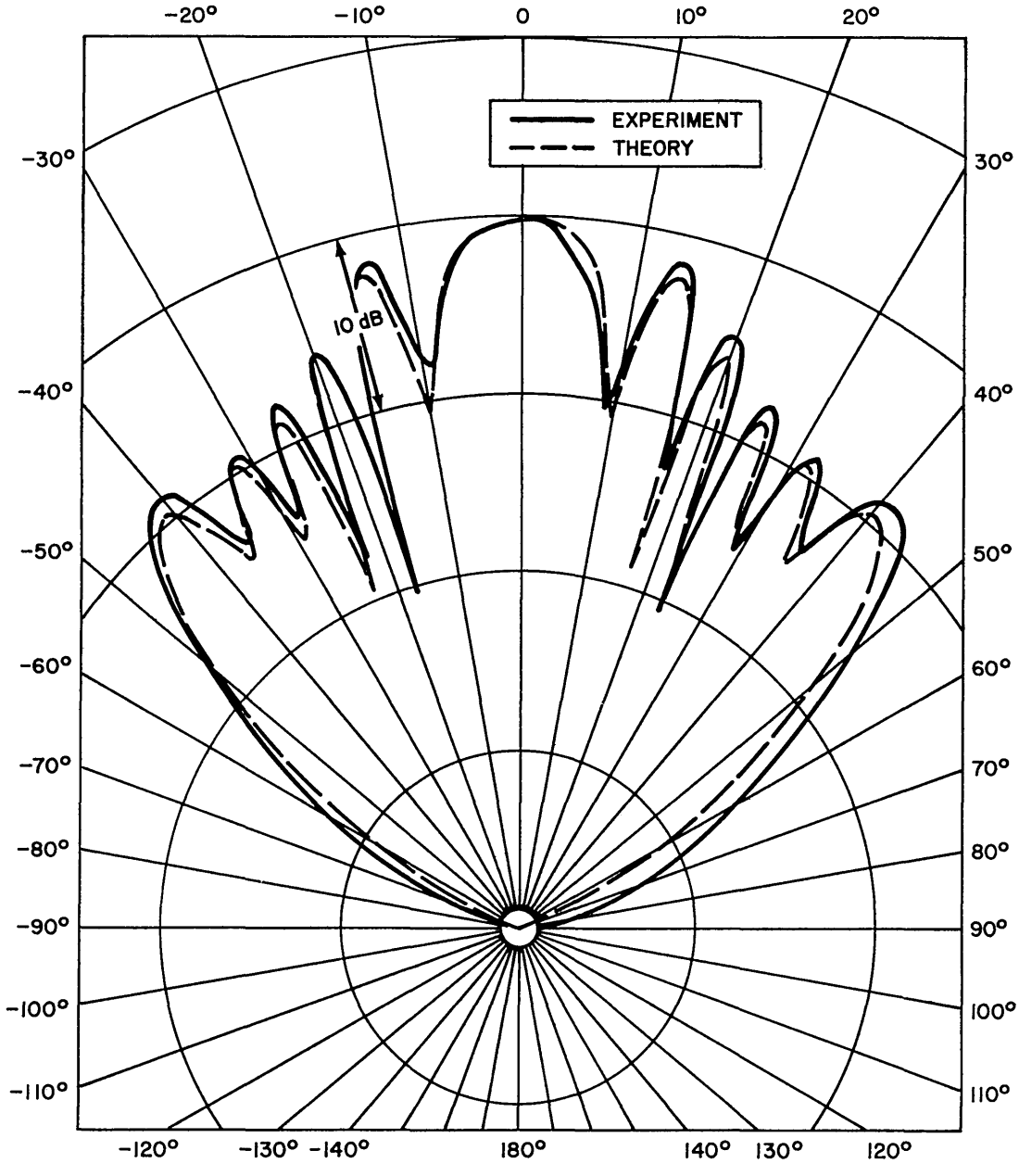

Fig. 5u—Radiation patterns in the median plane of the shallow (4.0-inch-focal-length) reflector for R = 40 inches and f = 40 kHz

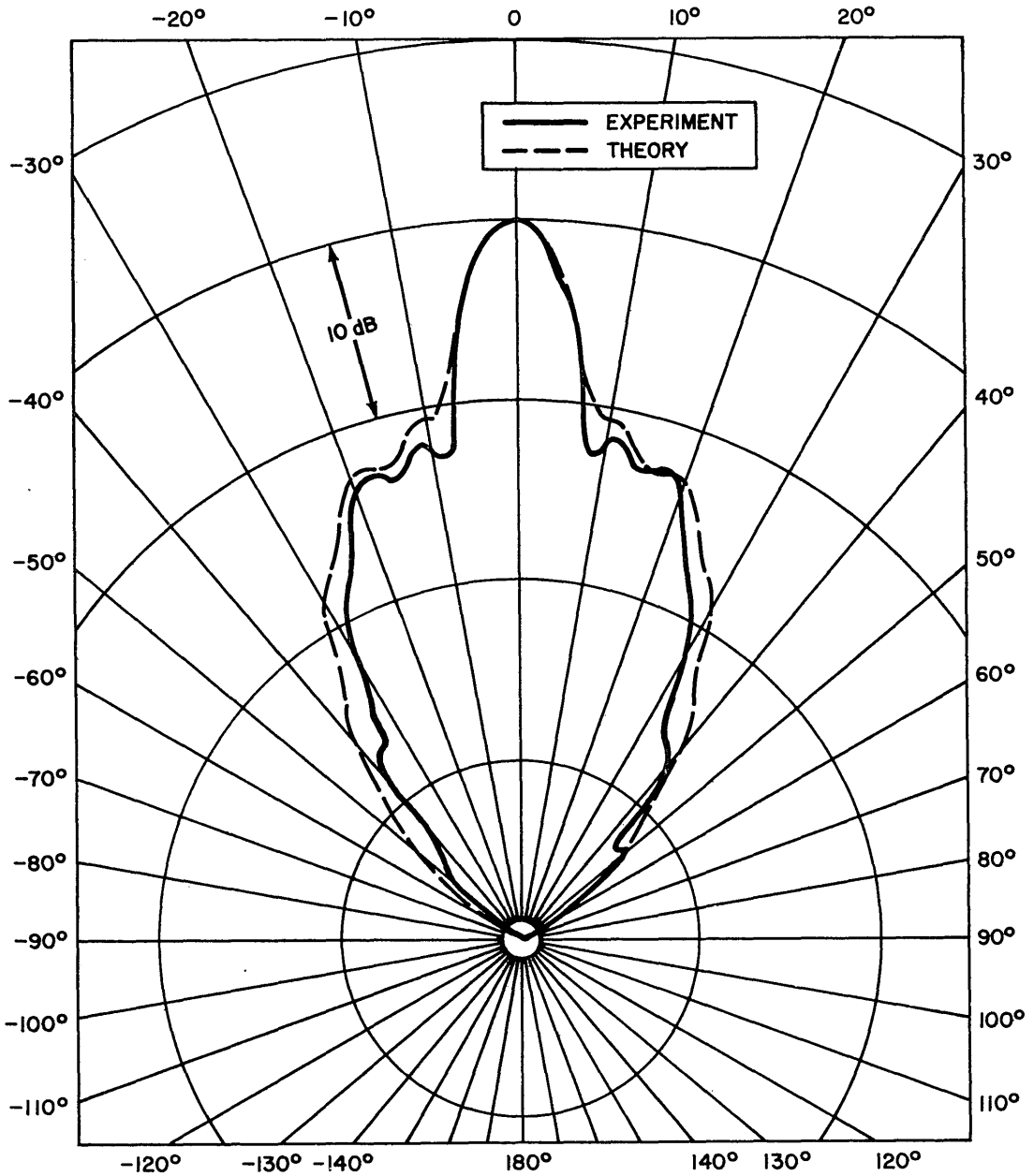

Fig. 6a—Radiation patterns in the median plane of the deep (2.0-inch-focal-length) reflector for R = 20 feet and f = 15 kHz

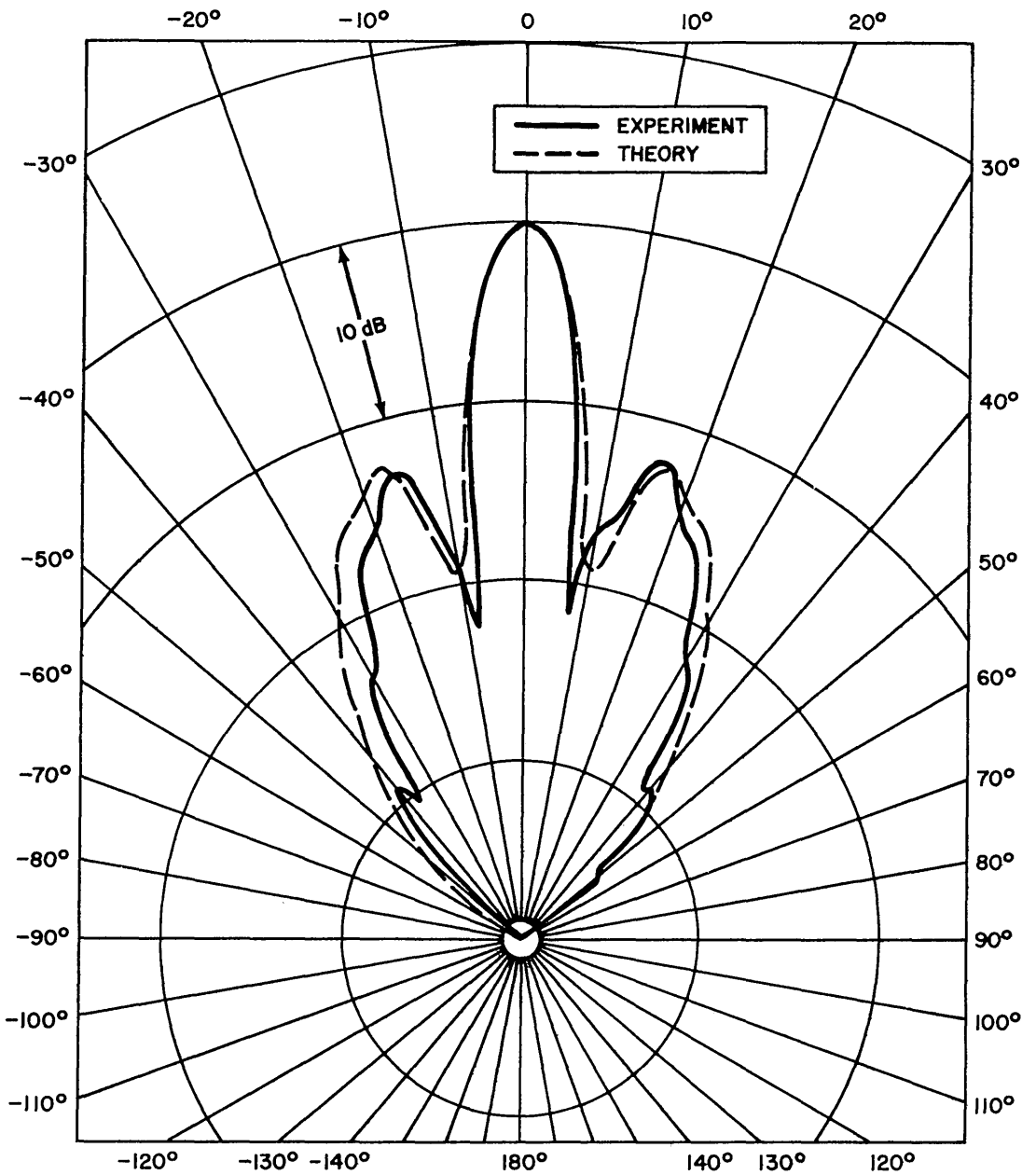

Fig. 6b—Radiation patterns in the median plane of the deep (2.0-inch-focal-length) reflector for R = 20 feet and f = 17 kHz

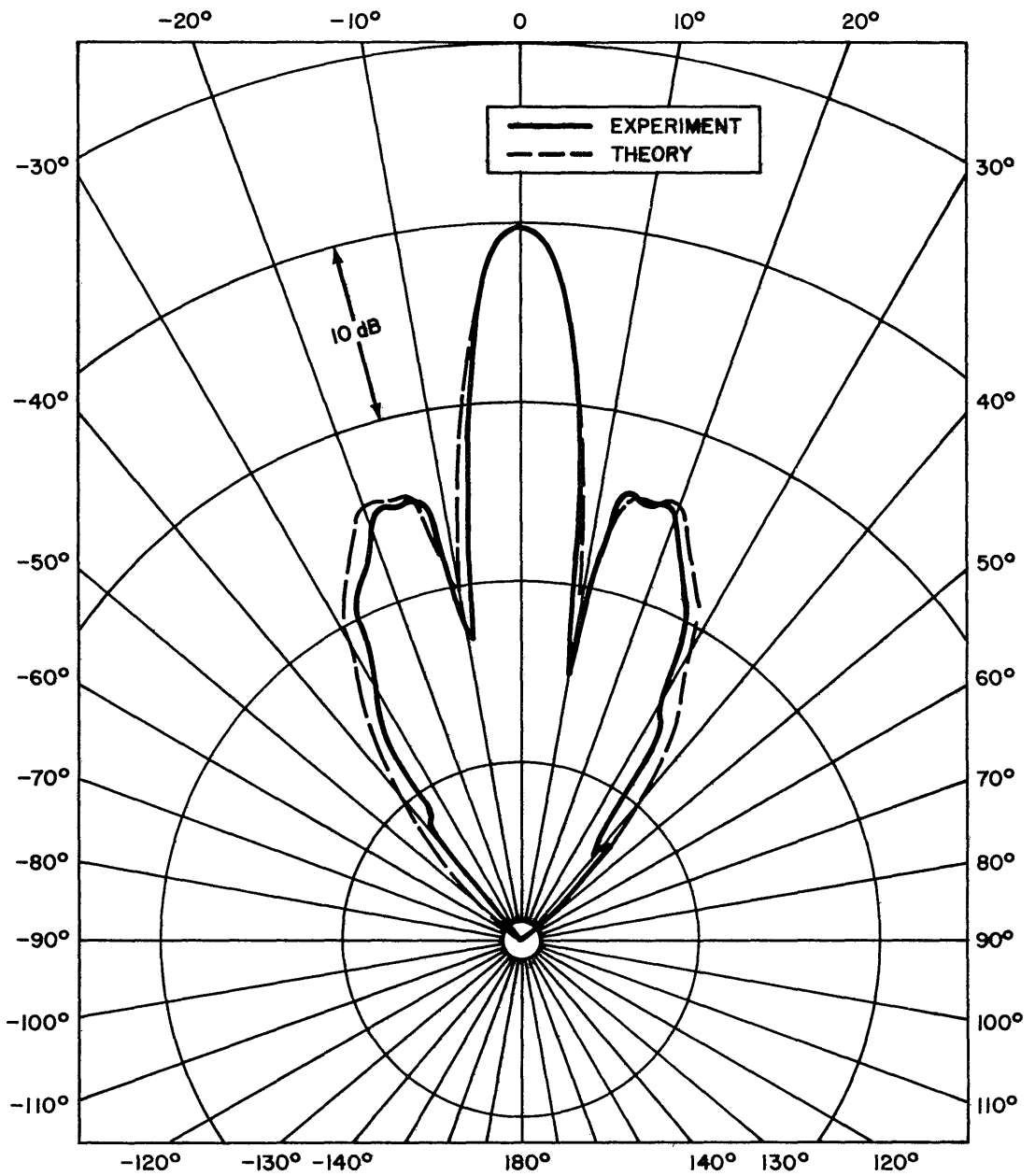

Fig. 6c—Radiation patterns in the median plane of the deep (2.0-inch-focal-length) reflector for R = 20 feet and f = 20 kHz

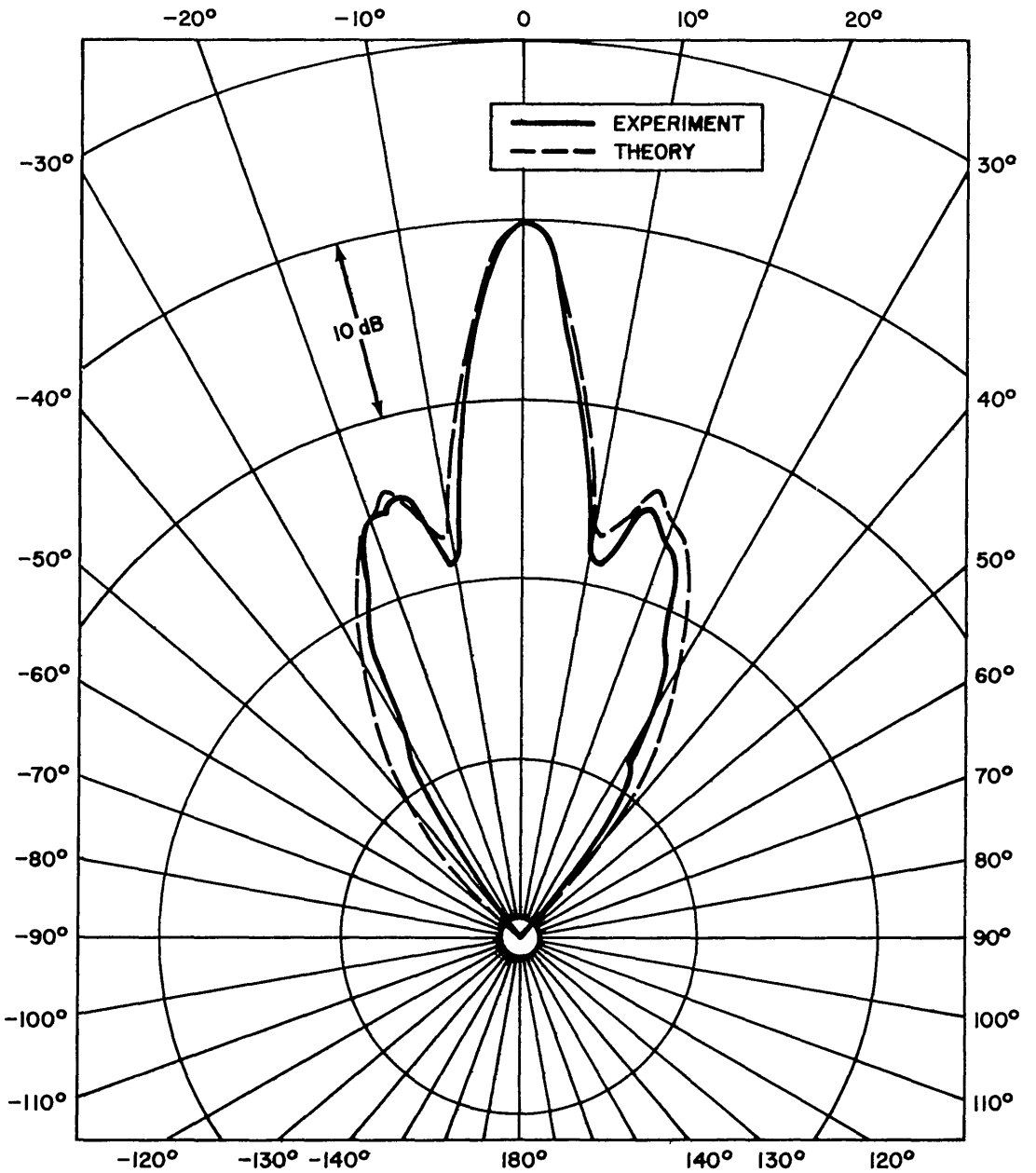

Fig. 6d—Radiation patterns in the median plane of the deep (2.0-inch-focal-length) reflector for R = 20 feet and f = 23 kHz

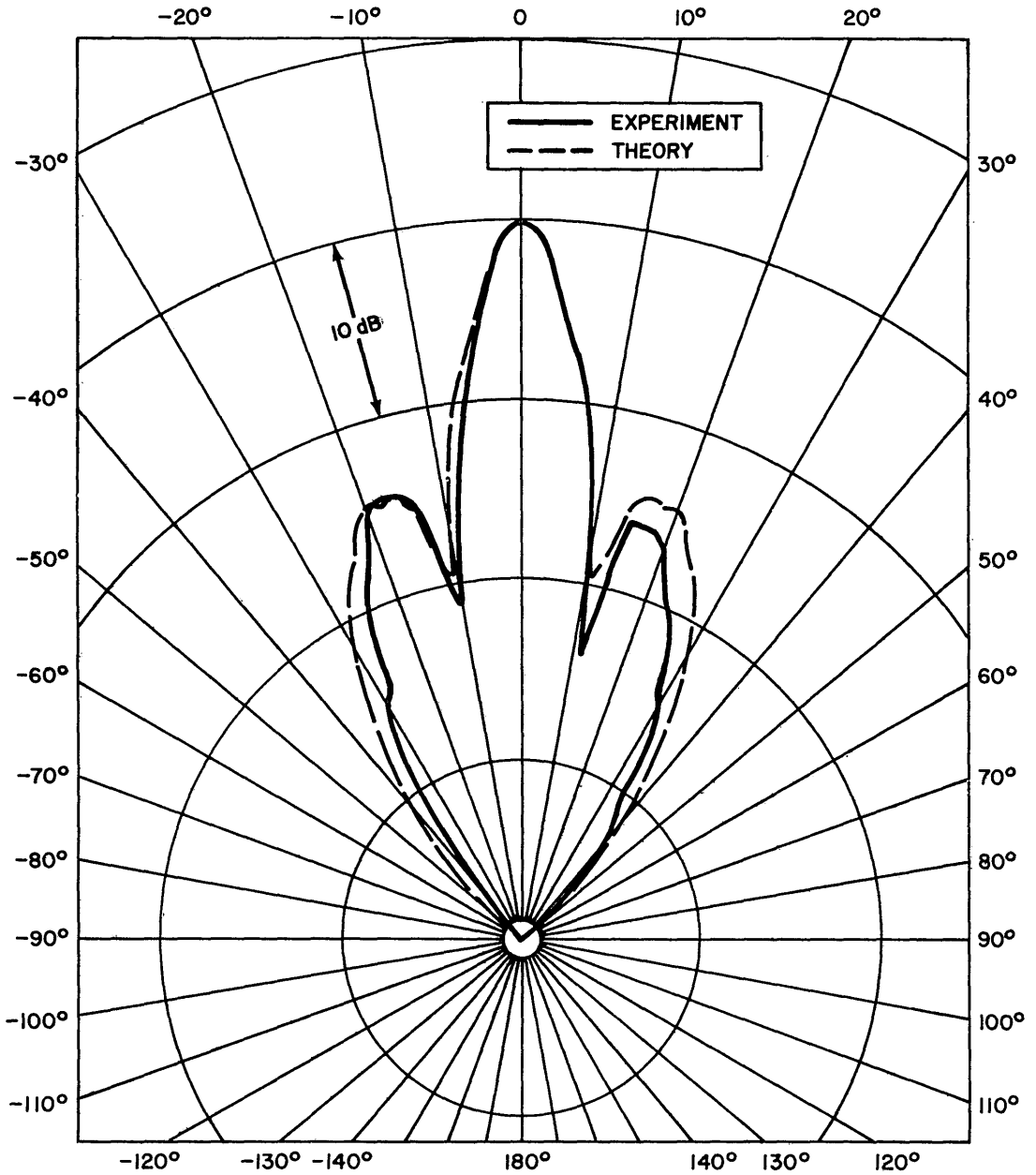

Fig. 6e—Radiation patterns in the median plane of the deep (2.0-inch-focal-length) reflector for R = 20 feet and f = 25 kHz

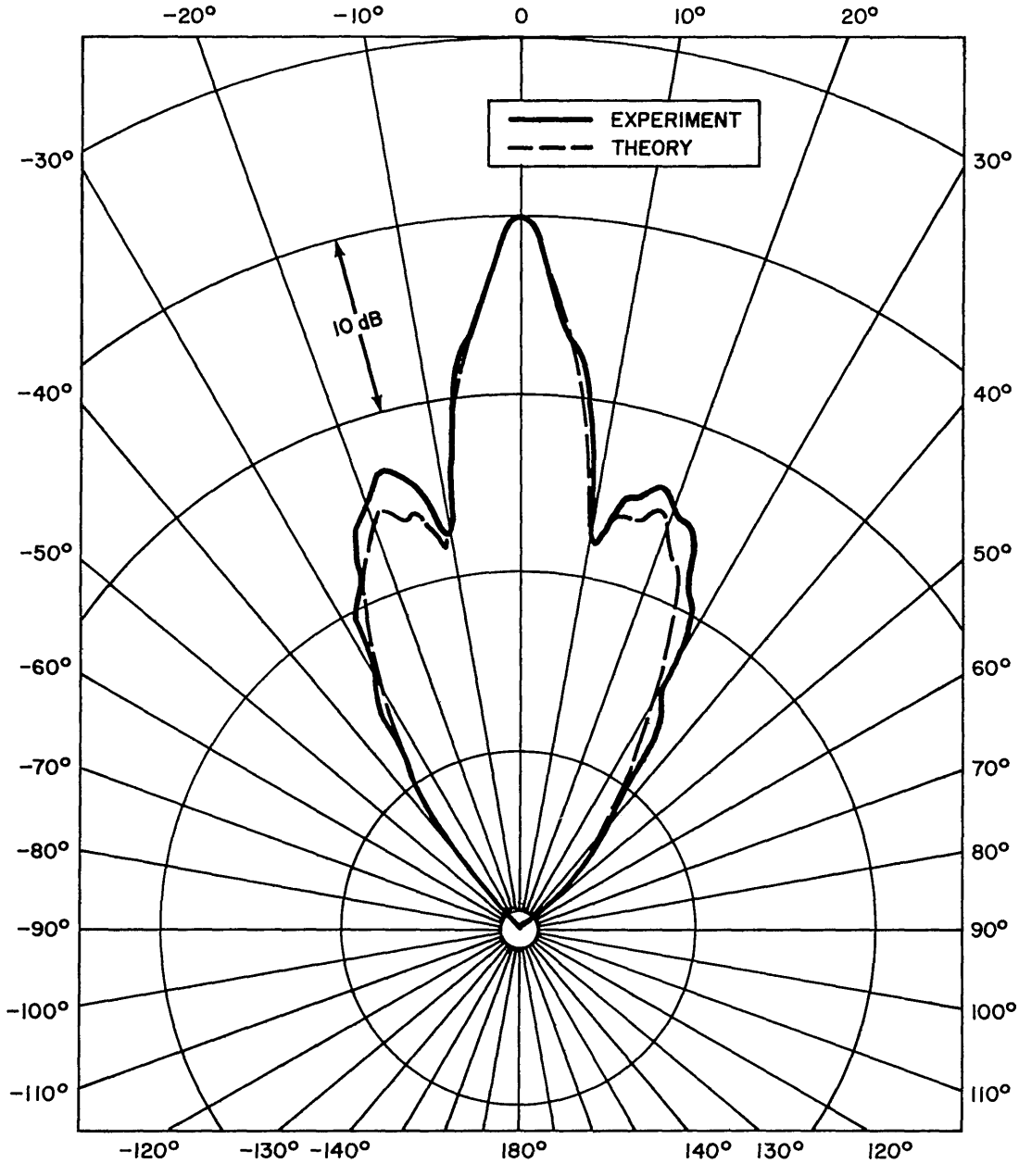

Fig. 6f—Radiation patterns in the median plane of the deep (2.0-inch-focal-length) reflector for R = 20 feet and f = 27 kHz

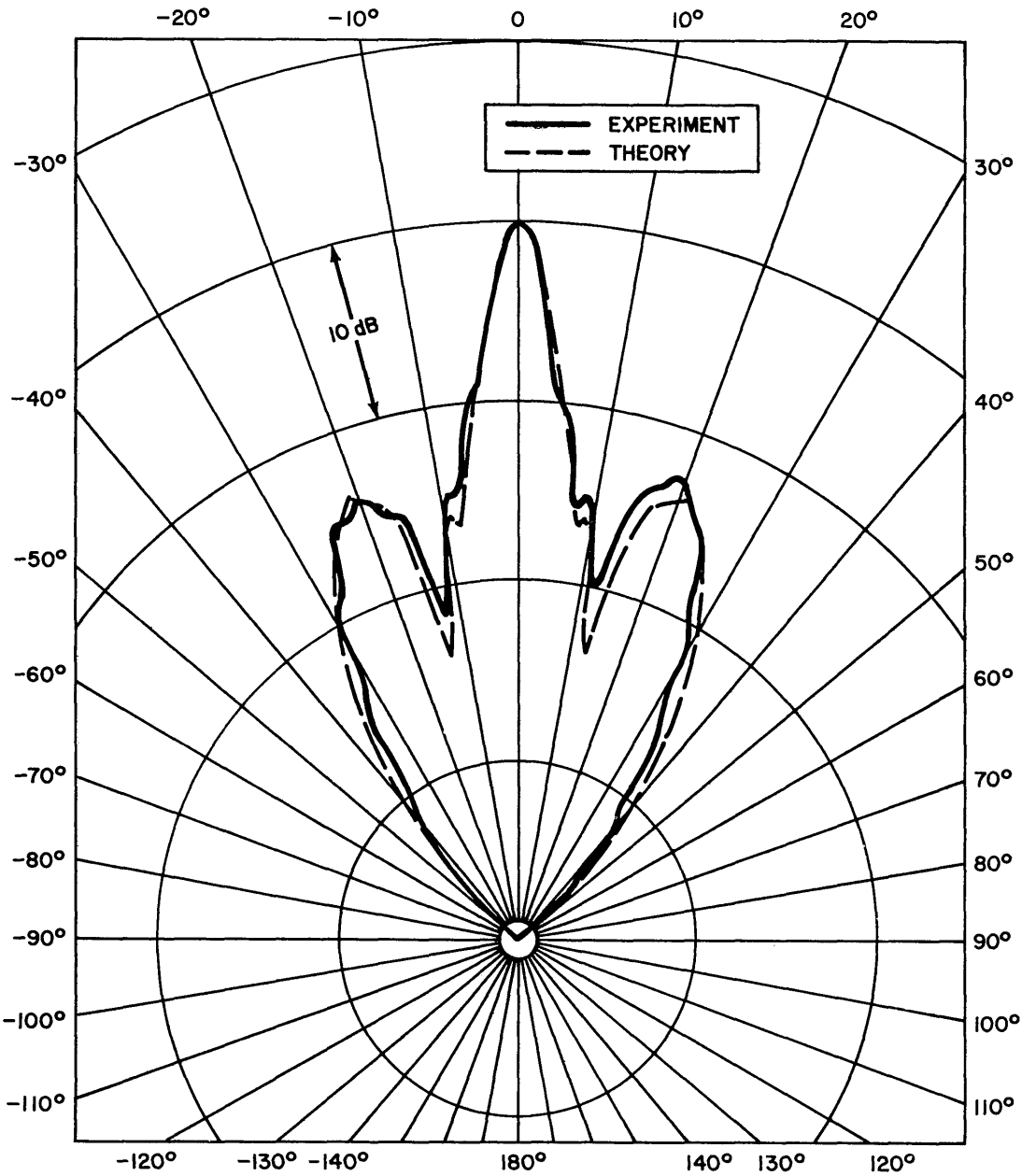

Fig. 6g—Radiation patterns in the median plane of the deep (2.0-inch-focal-length) reflector for R = 20 feet and f = 30 kHz

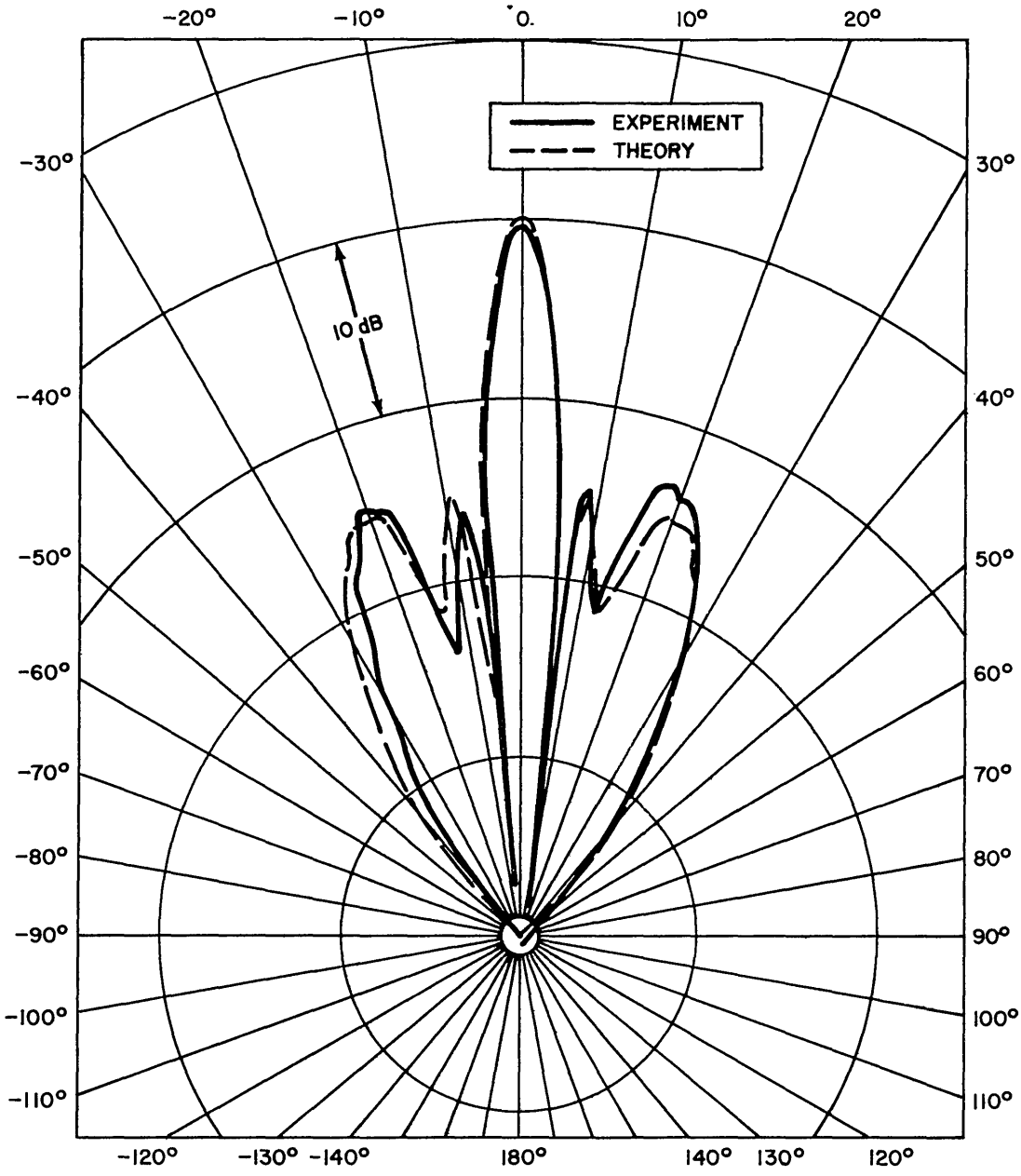

Fig. 6h—Radiation patterns in the median plane of the deep (2.0-inch-focal-length) reflector for R = 20 feet and f = 33 kHz

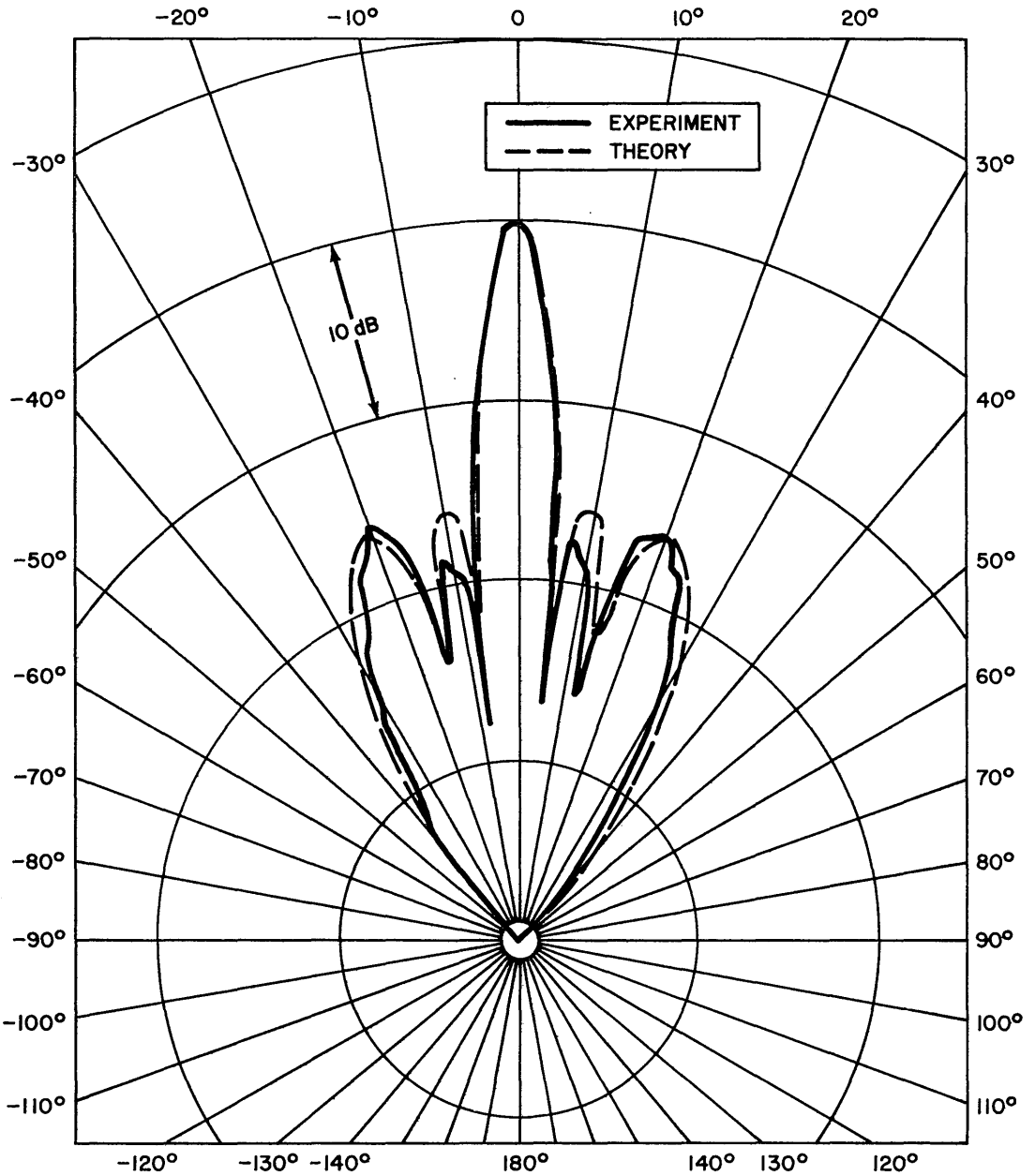

Fig. 6i—Radiaition patterns in the median plane of the deep (2.0-inch-focal-length) reflector for R = 20 feet and f = 35 kHz

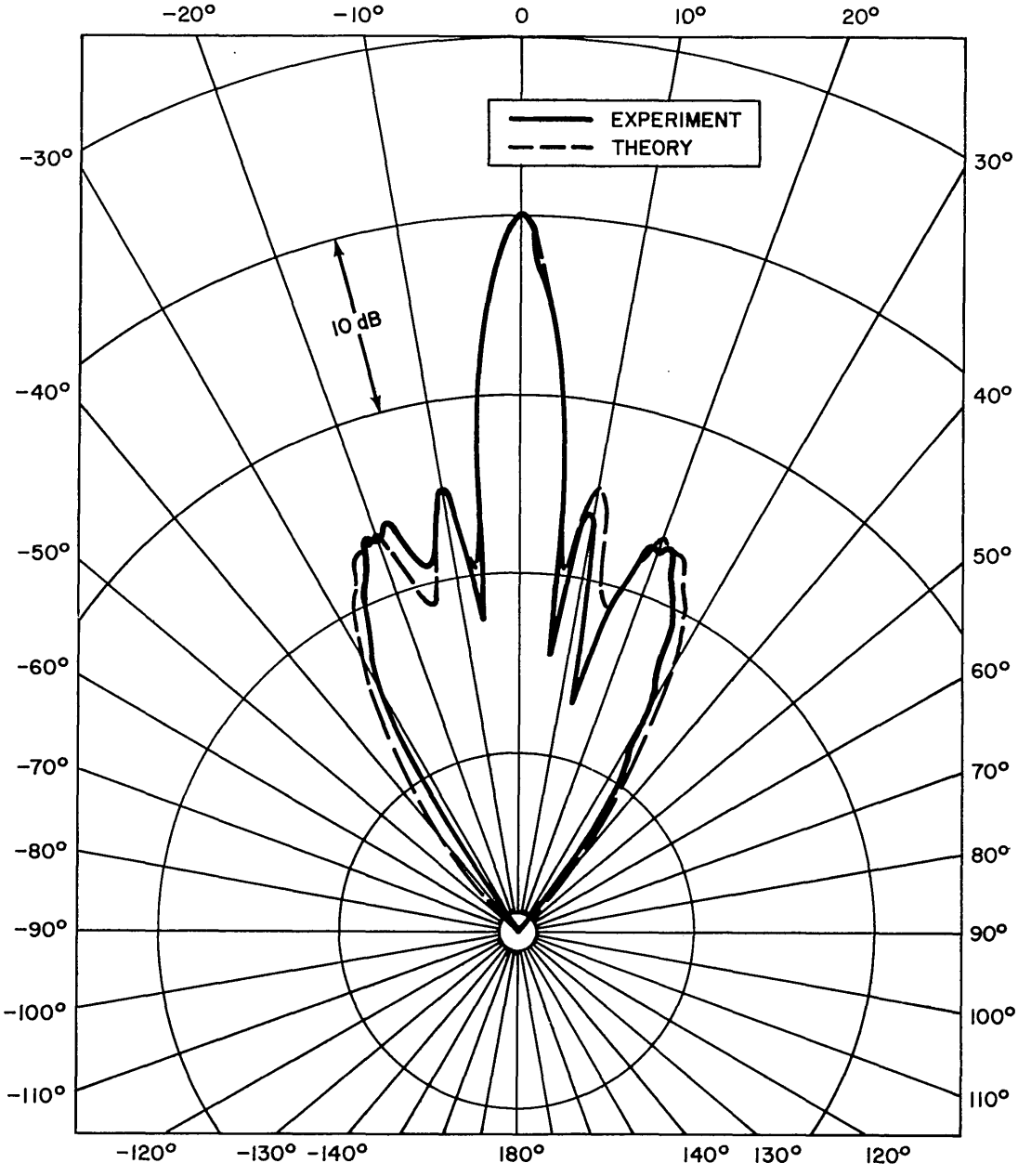

Fig. 6j—Radiation patterns in the median plane of the deep (2.0-inch-focal-length) reflector for R = 20 feet and f = 37 kHz

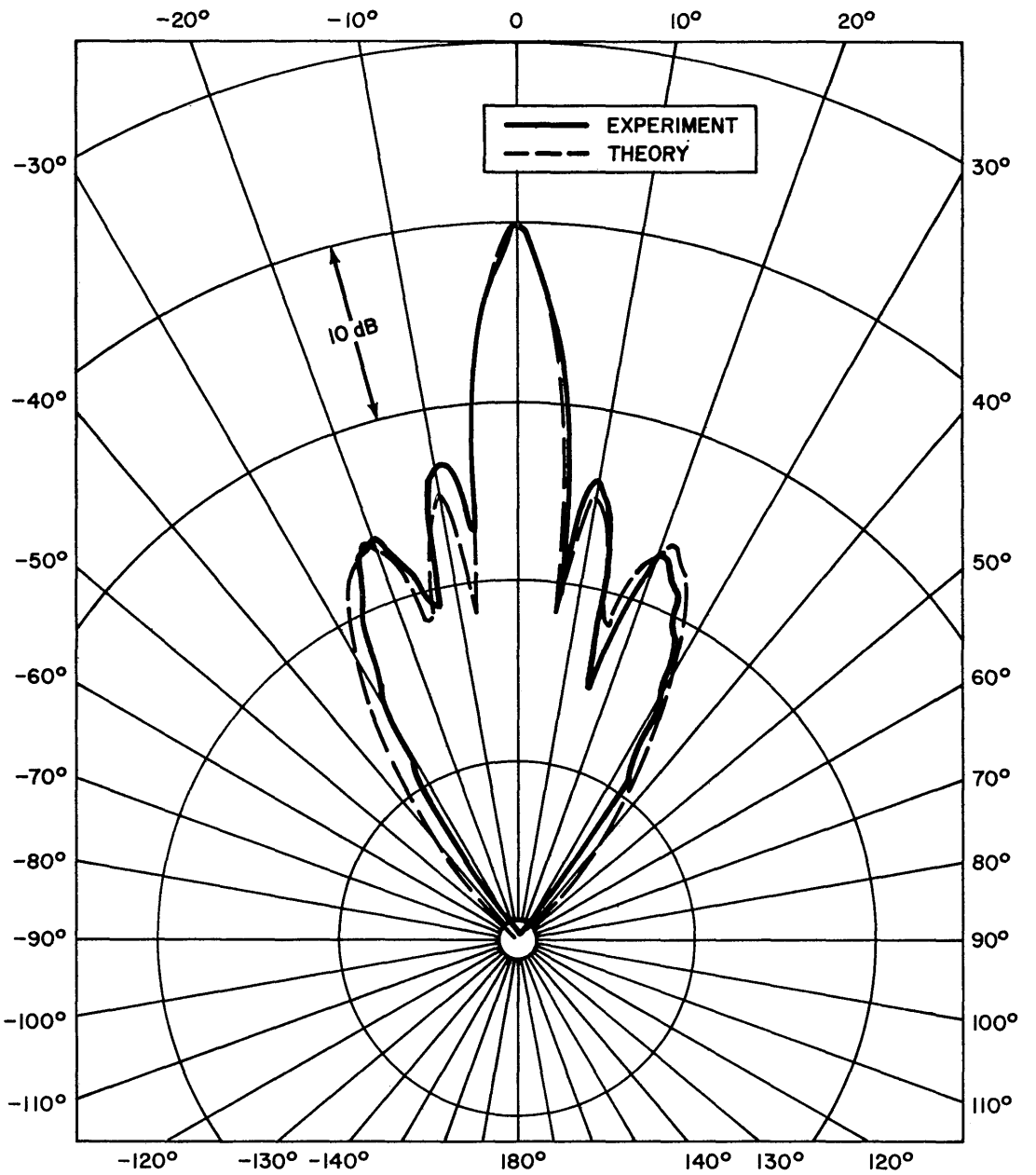

Fig. 6k—Radiation patterns in the median plane of the deep (2.0-inch-focal-length) reflector for R = 20 feet and f = 40 kHz

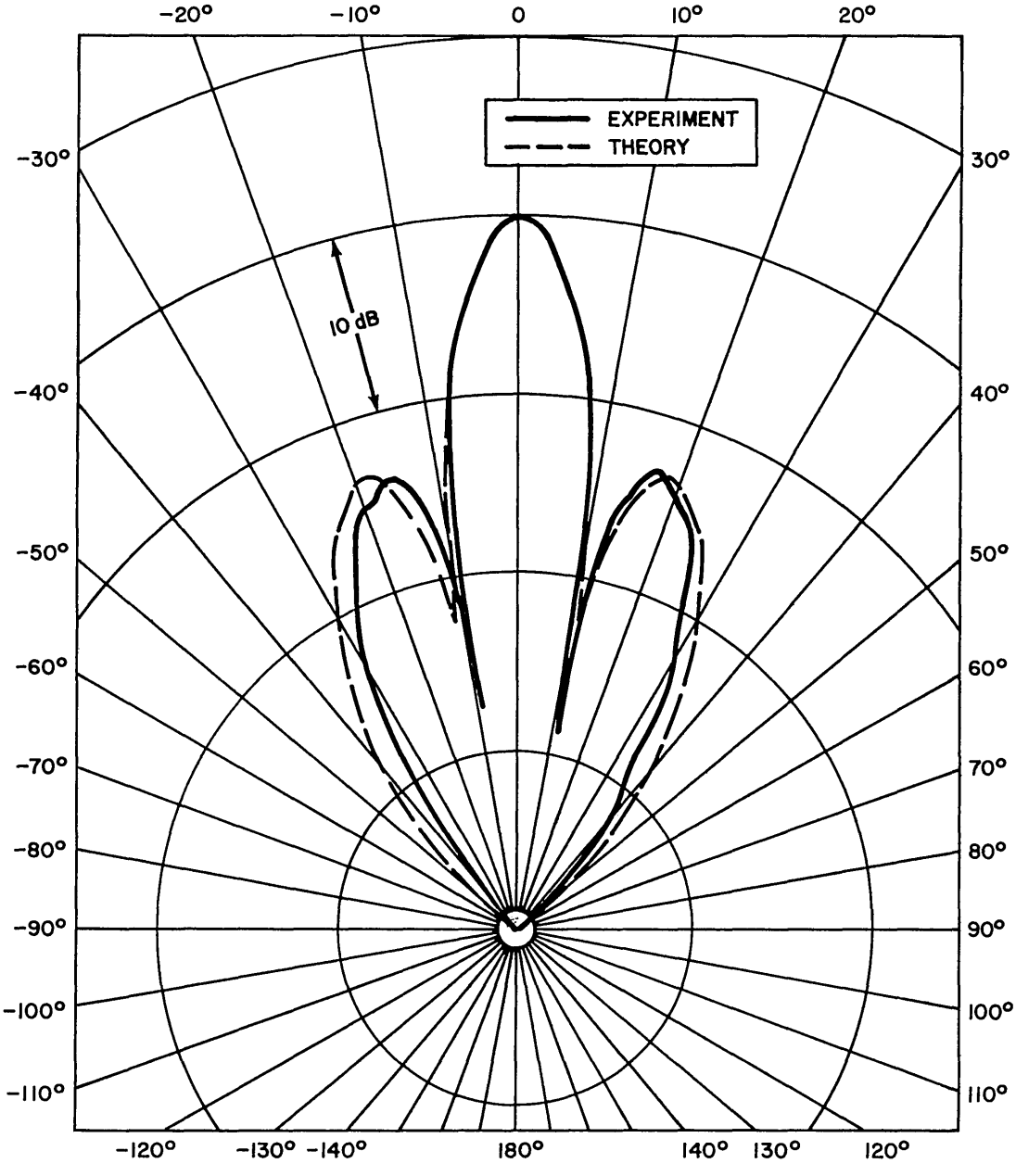

Fig. 6l—Radiation patterns in the median plane of the deep (2.0-inch-focal-length) reflector for R = 10 feet 8 inches and f = 20 kHz

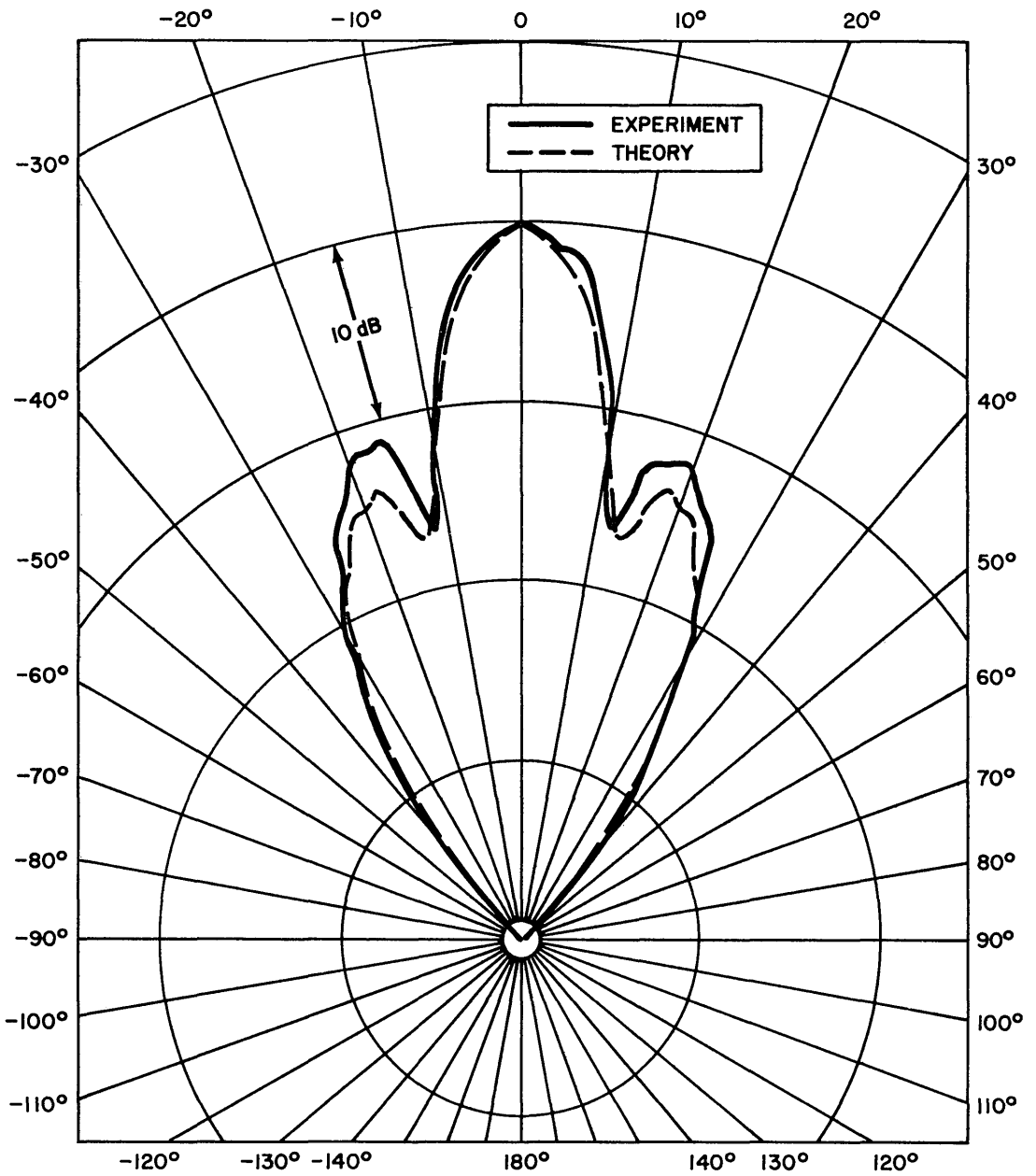

Fig. 6m—Radiation patterns in the median plane of the deep (2.0-inch-focal-length) reflector for R = 10 feet 8 inches and f = 27 kHz

water pressure in the environment of the experiment. The resulting underwater dimensions of the reflectors are analyzed and their conformity to those of a parabola is represented by the stated errors in the focal lengths. In Appendix D radiation patterns show the effects of displacing the line source in the X and Y directions (Fig. 2) from the focal line. The conclusions reached as a result of the tests described in Appendix D are: a misalignment of the line source within the estimated errors cannot account for asymmetries in the radiation patterns but can account for incorrect amplitude-level differences between the patterns' main beam and side lobes. No systematic disagreement is perceived between the experimental and theoretical patterns, and the disagreement does not in general exceed 2 dB. Consequently the physical properties of the reflectors and line source must have agreed reasonably well with the theoretical assumptions of omnidirectionality, parabolicness, and alignment.

The upper limit of the frequency range of the experiment was determined by the frequency-dependent response characteristics of the F36 and the tolerance to which the reflector was constructed. The lower limit was more a result of the increased leakage of the sound through the reflector at low frequencies. The finite size of the NRL Acoustic Research Tank limited the distance between the hydrophone and the reflector to 20 feet for this experiment. At separation distances greater than 20 feet the radiated sound reflected from the walls of the tank could not be excluded when the receive signal gate was opened just enough to see the pulsed radiation coming directly form the source. The far field of the reflector was approximated only beyond a minimum source distance such that [4]

$$r > \frac{\pi a^2}{\lambda},$$

where a is the largest radius or half length of the reflector, r is the source distance from the field point, and λ is the wavelength of sound, which is c/f, in which c is the velocity of sound (4950 ft/sec) and f is the frequency. For the reflectors $a = B \approx 14$ inches = 14/12 feet; therefore

$$r > \frac{\pi\left(\frac{14}{12}\right)^2}{\lambda} = \frac{\pi\left(\frac{14}{12}\right)^2 f}{c} = \frac{\pi\left(\frac{14}{12}\right)^2 f}{4950} = 0.86 \times 10^{-3} f.$$

At 5 kHz, $r > 4.3$ feet; at 23 kHz, $r > 20$ feet; and at 50 kHz, $r > 43$ feet. Therefore the 20-foot-separation-distance patterns were approximately far field only for frequencies less than 23 kHz.

The mathematical model of the reflector is valid in the near field as well as the far field of the reflector, and only the separation distance between the hydrophone and a reference point on the reflector need be specified for the calculations. The accuracy of the model in the near field was tested experimentally at separation distances between the hydrophone and the support shaft of 40 inches and 10 feet (Figs. 5n through 5u, 6l, and 6m).

THEORY

A two-dimensional mathematical model for a perfectly soft (zero-impedance) parabolic cylinder reflector driven by a line source coincident with its focal line has been developed

by one of the authors [1]. The model enables one to quickly ascertain the major features of the acoustic field (both near and far) when given only the acoustic size of the aperture ($2kB$) and focal length (kA, where k is the wavenumber). The mathematical model is based on the following two assumptions: a definite shadow zone exists behind the reflector, and the acoustic field in the region from the surface of the reflector to some locus bulging in front of the reflector (referred to as Region I in Ref. 1) depends primarily on the known boundary conditions on the front surface of the reflector. With this in mind, a reference circular cylinder of infinite length is constructed through the edges of the parabolic cylinder. The portion of the reference cylinder behind the reflector is assumed to be entirely within the shadow zone; the remainder of the reference cylinder is assumed to be entirely within Region I. The acoustic pressure in the shadow zone is assumed to be zero, so that if we are able to obtain an expression for the field in Region I, the problem would be reduced to solving a simple boundary-value problem in which the radiating surface is an infinite circular cylinder. Two methods can be used to obtain an approximate expression for the field in Region I. Method 1 uses an asymptotic expression for the field which is useful for $kA > 4$. Method 2 is essentially a method of images in which a number of image sources are employed to approximately satisfy the boundary condition on the reflecting surface. Method 2 is much slower than Method 1 but is useful for smaller values of kA. Once the field in Region I has been determined by either of these methods, the reduced problem is then easily solved by expanding the field in a series of cylindrical harmonics. The coefficients of the expansion are evaluated with the aid of the fast Fourier transform (FFT) algorithm. Further details concerning the mathematical model can be found in Ref. 1.

The mathematical model was implemented in a Fortran computer program for use on the NRL CDC 3800 computer. For each of the numerical examples presented in this report 120 terms in the cylindrical harmonic expansion were evaluated using a 512-point FFT. Whenever Method 2 was used to determine the field in Region I, 35 image sources were employed. The execution time when Method 1 was used was 5.4 seconds per example, as compared with 32.0 seconds when Method 2 was used. The use of the mathematical model as a tool to design a reflector whose radiation patterns will meet desired specifications is discussed in Appendix E.

If the fundamental assumptions were completely valid, the computed results would be independent of both the method used for obtaining the field in Region I and the choice of the reference cylinder. As one might expect, the results turn out to be only approximately independent of these parameters. The variation in the computed results which occurs when either the reference cylinder or method is changed provides a reasonable measure of the overall accuracy of the model. Figure 7a is a cross-sectional view of the shallow reflector showing four possible choices for the reference cylinder. Figure 7b shows the far-field patterns obtained by Method 1 at 10 kHz (right halves of patterns) and 25 kHz (left halves of patterns) when each of these cylinders is used as the reference cylinder. Figure 7c shows theoretical radiation patterns at 15 kHz (right halves) and 20 kHz (left halves) at a distance of 20 feet from the shallow reflector computed using reference cylinder 3. The solid line in the figure illustrates the results obtained using Method 1 to obtain the field in Region I; the dashed line illustrates the results obtained using Method 2. Method 1 was used for all of the 4.0-inch-focal-length-reflector patterns as well as for all of the 2.0-inch-focal-length-reflector patterns taken at frequencies above 30 kHz. Method 2 was used for the 2.0-inch-focal-length-reflector patterns taken at frequencies below 30 kHz. These figures indicate that the model is probably accurate to within 1 dB except at the minima, where it may be accurate only to within 2 dB. As would be expected, the model is more accurate for the main beam than for the side lobes.

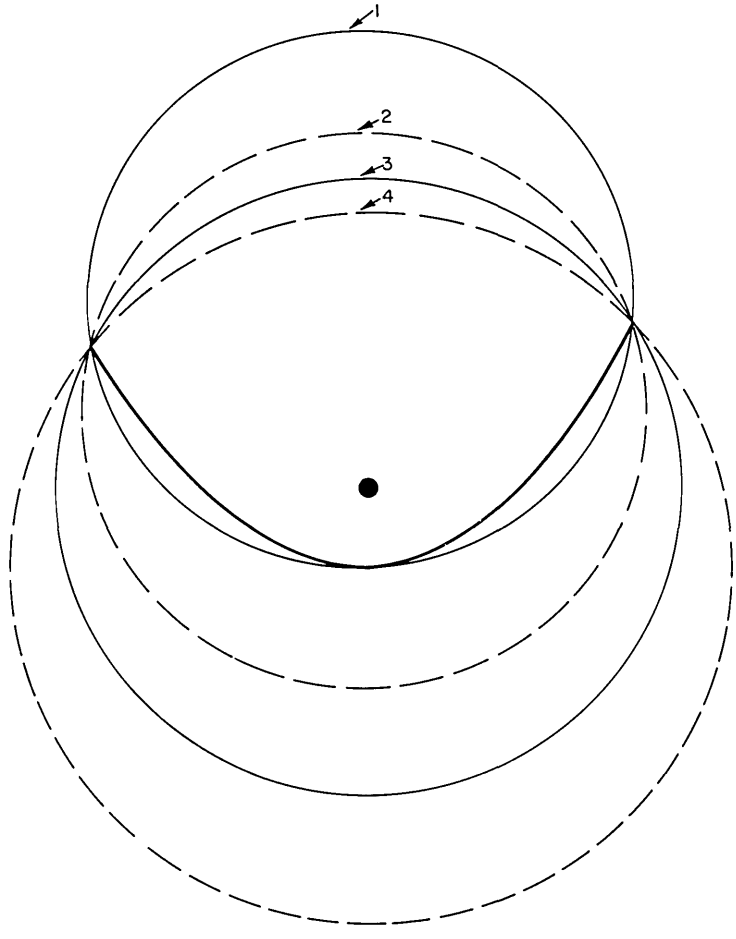

Fig. 7a—Four possible reference cylinders for the shallow reflector

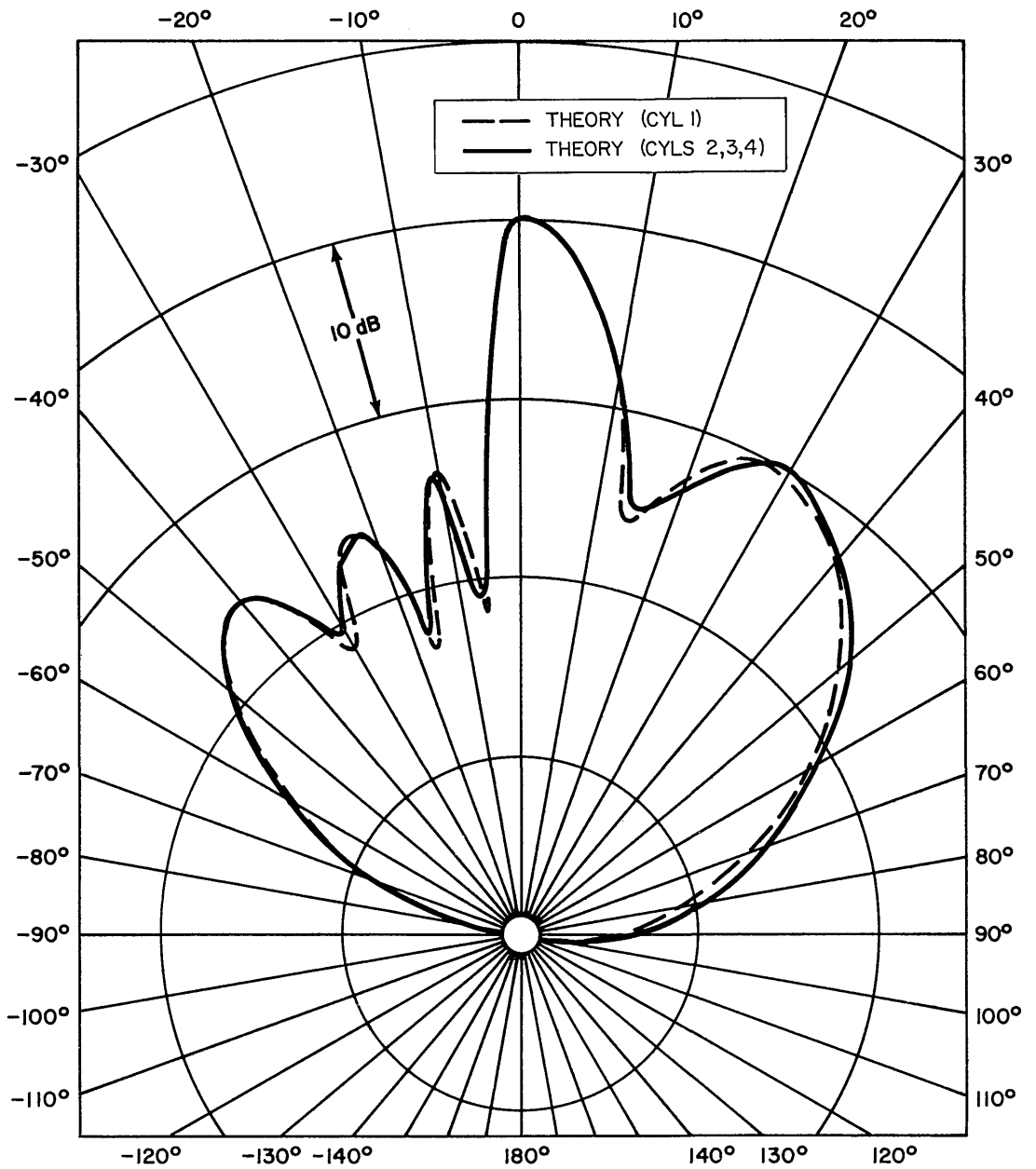

Fig. 7b—Far-field patterns computed at 10 kHz (right halves) and at 25 kHz (left halves) using Method 1 and the reference cylinders of Fig. 7a

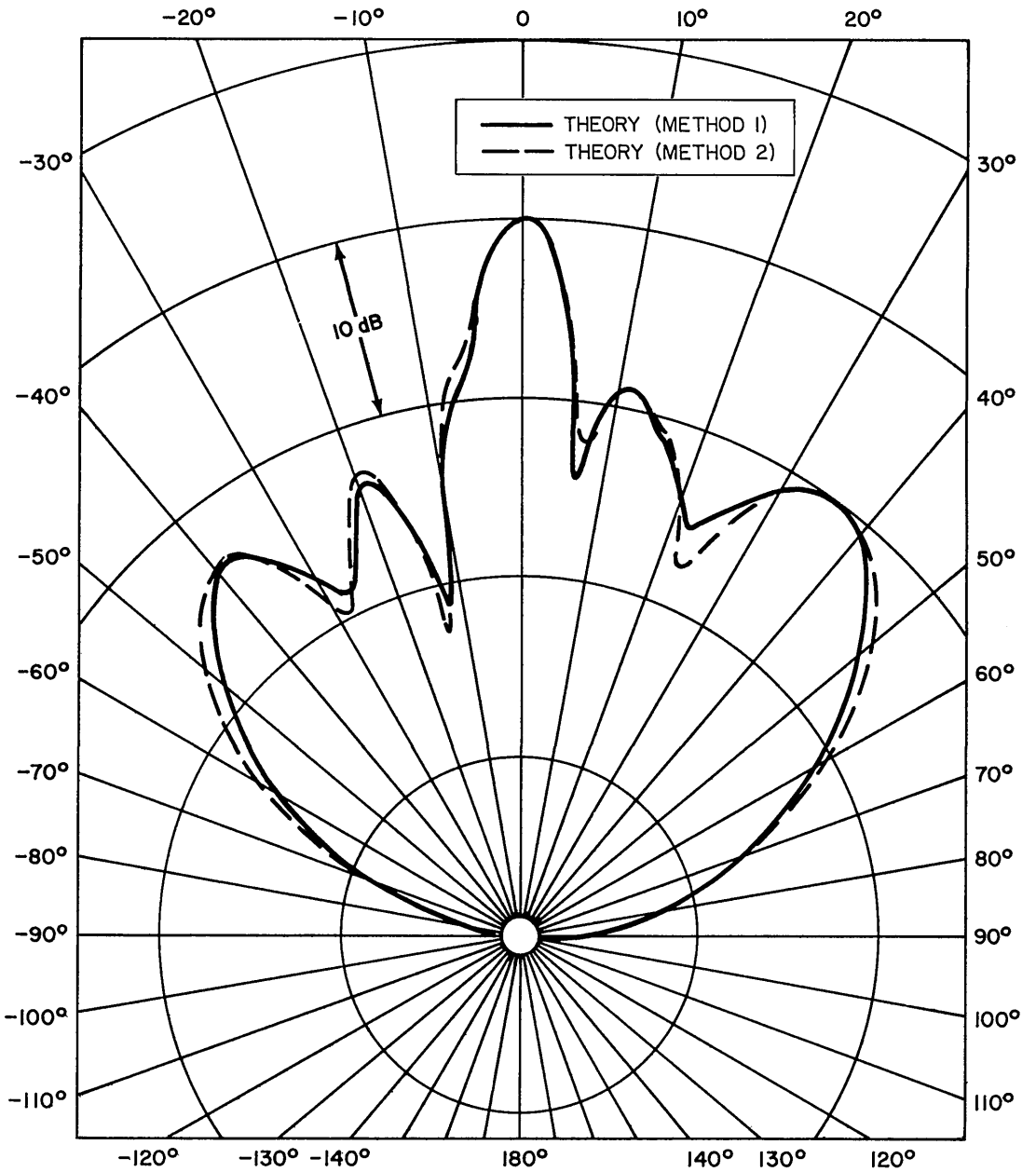

Fig. 7c—Radiation patterns at 20 feet from the shallow reflector computed at 15 kHz (right halves) and at 20 kHz (left halves) using reference cylinder 3

CONCLUSIONS

A mathematical model for the acoustic radiation from an ideal parabolic cylinder reflector driven by a line source coincident with its focal line has been verified experimentally to within the tolerances of the model and the experiment over a wide range of reflector parameters. The agreement between theory and experiment confirms the accuracy of the theory, the careful construction of the reflector, and the precision performance of the experiment. Thirty-four radiation patterns recorded over a wide range of reflector parameters are included in this report to show the agreement and to be used as reference material for any subsequent reflector work. A detailed error analysis indicates the validity of the stated assumptions, the possible problem areas in a reflector experiment, and a quantitative measure of the experimental uncertainties. The mathematical model is a tool to design a reflector which will meet desired radiation pattern specifications.

ACKNOWLEDGMENTS

The authors are grateful for the assistance of J. Chervenak at the inception of the experiment and J. Neeley, D. Gregan, D. Dorsey, and G. Wiedemann at its conclusion.

REFERENCES

1. P. Rogers, "A Two-Dimensional Mathematical Model for an Acoustically Soft Parabolic Cylinder Reflector," submitted for publication to the Journal of the Acoustic Society of America.
2. R. J. Bobber, *Underwater Electroacoustic Measurements*, Washington, D.C. Naval Research Laboratory, 1970, pp. 251-252.
3. J. Chervenak, "A New NRL Acoustic Research Tank Facility," NRL Report 6822, 1969.
4. "USA Standard Procedures for Calibration of Electroacoustic Transducers Particularly Those for Use in Water," United States of America Standards Institute, 1958, p. 11.

APPENDIX A
DIMENSIONS OF THE REFLECTORS

The underwater dimensions of the reflectors were found by measuring the reflectors in air and correcting the measurements for the underwater compression of the closed-cell rubber. The measurements, which were made at only the top surface of the reflector, were valid for the entire surface of the parabolic cylinder. A straight edge and carpenter's level were used to confirm that there were no visible indentations or high spots in the closed-cell rubber and that the reflector surface was a section of an unwarped right parabolic cylinder.

As shown in Fig. A1, a line $X'X''$ was drawn parallel to the directrix of the parabola. Pairs of lines perpendicular to $X'X''$ were drawn between $X'X''$ and the front of the reflector surface at either side of the vertex such that the lines were of equal length. The length of the line segments between $X'X''$ and the reflector surface was denoted Y_0 and the perpendicular distance between the line pairs was denoted $2X_0$. Five such pairs of lines were drawn and measured for each reflector, and the results are shown in Table A1. The estimated error for this procedure was the uncertainty of locating the points on the $X'X''$ line corresponding to a value of Y_0. The uncertainty in the precise location of each point on

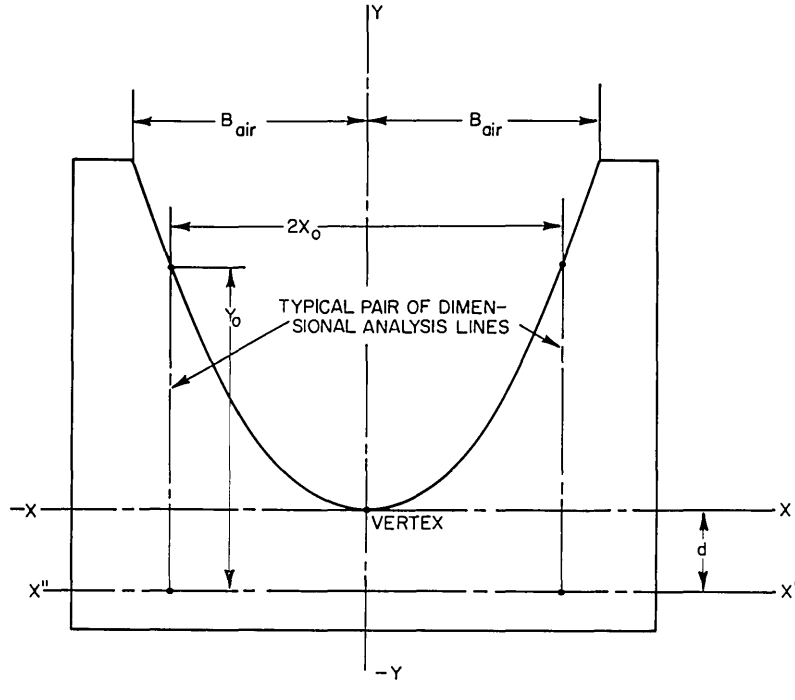

Fig. A1—Dimensions of the reflectors as measured in air

Table A1
Measurements on the Reflectors in Air
as Shown in Fig. A1

Y_0 (in.)	$2X_0$ (in.)
Shallow Reflector (4.0-inch focal length	
3	12-21/32
4-9/32	15-19/32
6-1/2	19-5/8
9	23-1/4
11	25-7/8
Deep Reflector (2.0-inch focal length)	
3-7/32	10-7/32
6-21/32	14-5/8
9-1/2	17-1/2
14-11/16	21-25/32
20-31/32	26

$X'X''$ was ±1/32 inch; therefore the root mean square error in $2X_0$ for a given Y_0 was $[(1/32)^2 + (1/32)^2]^{1/2} = \sqrt{2}/32$ inch, since each value of $2X_0$ depended on the location of two points. The error resulted from the difficulty in locating the distance Y_0 accurately because it terminated at the curved rubber surface of the reflector. The aperture width $2B$ was separately measured and found to be 28.2 ± 0.1 inches for the shallow reflector and 28.3 ± 0.1 inches for the deep reflector. The 0.1-inch error was due to the vagueness of the edges of the closed-cell rubber due to cutting and finishing.

The correction to the dimensions of the reflector due to the compression of the closed-cell rubber by the water pressure at the depth of the experiment was determined by the manufacturer's compression-deflection data. The neoprene closed-cell rubber compresses 25 percent for a pressure of 13 pounds per square inch, and the compression is assumed to be a linear function of pressure. At a depth of 10 feet, where the experiment was done, the water pressure was:

$$\text{pressure} = \frac{62.4}{(12)^3} \text{ pounds/(inch)}^3 \times 120 \text{ inches} = 4.33 \text{ pounds/(inch)}^2.$$

If compression is linear with pressure,

$$\text{percent compression} = \frac{4.33}{13} \times 25\% = 8.3\%.$$

For 0.5-inch-thick rubber, the compression is

$$0.083 \times 0.5 \text{ inch} = 0.042 \text{ inch.}$$

Bench experiments on a 2-inch-square, 0.5-inch-thick pad of the closed-cell rubber verified the manufacturer's data as well as the compression being a linear function of pressure.

The change in the dimension of the air-cell rubber due to water pressure was normal to the reflector surface. Therefore the resulting correction to Y_0 must be calculated from the geometry of the reflector (Fig. A2). Because the surface of the reflector is assumed to be nearly parabolic, the X and Y coordinates of a point on the surface are related by

$$\frac{X^2}{4A} = Y - d,$$

where A is the focal length of the parabola and d is the perpendicular distance between $X'X''$ and the X axis. Differentiating the preceding formula with respect to X,

$$\frac{dY}{dX} = \frac{X}{2A} .$$

From Fig. A2,

$$\frac{dY}{dX} = \tan \phi .$$

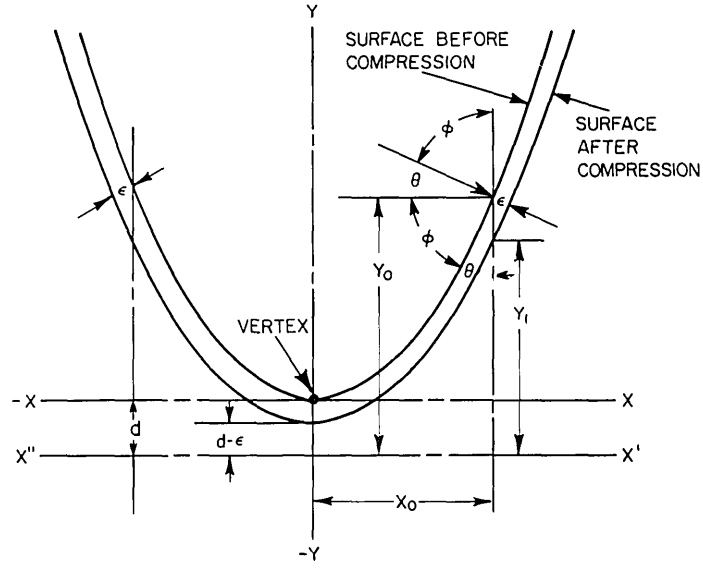

Fig. A2—Effect of water-pressure compression on the dimension Y_0 as measured in air

Therefore

$$\phi = \tan^{-1}\left(\frac{X}{2A}\right).$$

To a first approximation

$$(Y_0 - Y_1)\cos\phi \approx \epsilon,$$

where ϵ, the compression-deflection of the closed-cell rubber normal to the surface = 0.042 inch and $Y_0 - Y_1$ is the component of the compression-deflection of the closed cell rubber in the Y direction at the surface point (X, Y_0). Thus

$$Y_1 \approx Y_0 - \frac{\epsilon}{\cos\phi}$$

$$= Y_0 - \frac{\epsilon}{\cos\left[\tan^{-1}\left(\frac{X}{2A}\right)\right]}$$

$$= Y_0 - \frac{\epsilon\sqrt{4A^2 + X^2}}{2A}.$$

At $X = 0$, $Y_0 = d$, and the obvious result is obtained:

$$Y_1 = d - \epsilon.$$

For a given X value a point (X, Y_0) on the reflector surface in air is replaced by a point (X, Y_1) on the reflector surface in water. The computed values of Y_1 corresponding to the measured values of Y_0 given in Table A1 for both reflectors are tabulated in Table A2.

For the shallow reflector (A = 4.0 inches) the measured value of d = 7/16 ± 1/32 inch. For the deep reflector (A= 2.0 inches) the measured value of d = 0 ± 1/32 inch.

The analysis of the reflector dimensions is completed by using the method of least squares to find the focal length A of the best parabola through the data points corresponding to the corrected dimensions (X, Y_1). The parabola which best fits the five data points for each reflector is the one whose focal length $\bar{A}$ minimizes the summation

$$\sum_{i=1}^{5}\left[(Y_{1i} - d_u) - \frac{X_i^2}{4A}\right]^2,$$

where (X_i, Y_{1_i}) are the corrected underwater coordinates of a data point and d_u is the underwater distance from the $X'X''$ axis to the vertex. For the shallow reflector

$$d_u = d - \epsilon = 7/16 - 0.042 = 0.40 \text{ inch},$$

and for the deep reflector

Table A2
Measurements on the Reflectors in Air
and as Corrected for Underwater
Compression of the Rubber

Y_0 (in.)	Y_1 (in.)
Shallow Reflector (4.0-inch focal length)	
3	2.95
4-9/16	4.22
6-1/2	6.43
9	8.93
11	10.92
Deep Reflector (2.0-inch focal length)	
3-7/32	3.15
6-21/32	6.57
9-1/2	9.40
14-11/16	14.57
20-31/32	20.83

$$d_u = d - \epsilon = 0 - 0.042 = -0.04 \text{ inch.}$$

The focal length $\bar{A}$ is the value of A which satisfies the equation

$$\frac{d}{dA}\left[\sum_{i=1}^{5}\left(Y_{1_i} - d_u - \frac{X_i^2}{4A}\right)^2\right]\Bigg|_{A=\bar{A}} = 0$$

or

$$\sum_{i=1}^{5}\left(Y_{1_i} - d_u - \frac{X_i^2}{4\bar{A}}\right)X_i^2 = 0$$

or

$$\bar{A} = \frac{\sum_{i=1}^{5} X_i^4}{4\sum_{i=1}^{5}(Y_{1_i} - d_u)X_i^2}.$$

For the shallow reflector

$$\overline{A} = 3.98 \text{ inches},$$

and for the deep reflector

$$\overline{A} = 2.03 \text{ inches}.$$

The quality of the parabolas used in this experiment is seen by a comparison of the values of A_i, the focal lengths of parabolas defined by the individual data points (X_i, Y_{1_i}), with A. Consistently small values of $A_i - \overline{A}$ for each A_i indicate the reflector surface is approximately uniform and parabolic.

The individual A_i values corresponding to the data points (X_i, Y_{1_i}) are given by

$$A_i = \frac{X_i^2}{4(Y_{1_i} - d_u)} .$$

But $X_i = \tilde{X}_i \pm \Delta$ and $d_u = \tilde{d}_u \pm \delta$, where Δ and δ are the independent measurement errors in X_i and d_u ($\Delta = \pm\sqrt{2}/64$ inch and $\delta = \pm$ 1/32 inch) and where $\tilde{X}_i$ and $\tilde{d}_u$ represent the measured values without error. Therefore

$$A_i = \frac{(\tilde{X}_i \pm \Delta)^2}{4[Y_{1_i} - (d_u \pm \delta)]}$$

or, using the binomial expansion,

$$A_i \approx \frac{\tilde{X}_i^2}{4(Y_{1_i} - \tilde{d}_u)} \pm a_i,$$

where

$$a_i \approx \pm \frac{2\tilde{X}_i\Delta}{4(Y_{1_i} - \tilde{d}_u)} \pm \frac{\delta\tilde{X}_i^2}{4(Y - \tilde{d}_u)^2} .$$

The root-mean-square value of a_i based on the worst-case values of Δ and δ is

$$a_{rms_i} = \left\{ \left[\frac{\tilde{X}_i\Delta}{2(Y_{1_i} - \tilde{d}_u)} \right]^2 + \left[\frac{\delta\tilde{X}_i^2}{4(Y_{1_i} - \tilde{d}_u)^2} \right]^2 \right\}^{1/2}$$

Table A3 lists each value of Y_1, the corresponding calculated value of A, and the derived error $\pm a_{rms}$ in A. The calculated values of A for the shallow reflector vary by less than

$$\frac{3.99 - 3.93}{3.98} \times 100\% = 1.5\%$$

and for the deep reflector by less than

$$\frac{2.05 - 2.02}{2.03} \times 100\% = 1.5\%,$$

which indicates that both reflector surfaces were nearly parabolic underwater.

Table A3
Calculated Values of the Focal Length A and the Error in A for Each Value Y_1

Y_1 (in.)	A (in.)	a_{rms} (in.)
Shallow Reflector		
2.95	3.93	±0.055
4.22	3.98	±0.039
6.43	3.99	±0.027
8.93	3.96	±0.021
10.92	3.98	±0.018
Deep Reflector		
3.15	2.05	±0.027
6.57	2.02	±0.015
9.40	2.03	±0.012
14.57	2.03	±0.009
20.83	2.02	±0.007

As a measure of the consistent quality of the parabolic reflectors, $\sigma_{\overline{A}}$, the mean-square deviation of the least-squares fit, is calculated from the individual A_i values and $\overline{A}$. The calculation however must be weighted to reflect the reliability of the A_i values implied in the errors a_{rms_i}, which are derived from the measurement errors. The weighting scheme chosen is to let the weighting factor be

$$W_i = \frac{2}{1 + \left| \frac{a_{rms_i}}{\overline{a}} \right|},$$

where a_{rms_i} is the individual derived error in A_i and $\overline{a}$ is the average of the a_{rms_i} values. If every determination of $a_{rms_i} = \overline{a}$ (all errors are equal), then $W_i = 1$ for each A_i. If there were no measurement error for a data point (X_i, Y_{1_i}), then $a_{rms_i} = 0$ and $W_i = 2$ for that point. (If the measurement error for a data point is infinite (the location of the point is completely uncertain), then $a_{rms_i} = \infty$ and $W_i = 0$.)

The weighted mean-square deviation of the focal length corresponding to the least-squres fit is

$$\sigma_{\overline{A}} = \sqrt{\frac{\sum_{i=1}^{5} W_i(A_i - \overline{A})^2}{(5-1)\sum_{i=1}^{5} W_i}}.$$

For the shallow reflector $\sigma_{\overline{A}} = 0.011$ inch; therefore

$$\overline{A} = 3.98 \pm 0.011 \text{ inches.}$$

For the deep reflector $\sigma_{\overline{A}} = 0.005$ inch; therefore

$$\overline{A} = 2.03 \pm 0.005 \text{ inches.}$$

The aperture size $2B_{\text{air}}$ of the reflectors was also corrected for underwater compression. From Figs. A1 and A2 the corrected aperture size is

$$\begin{aligned} 2B &= 2B_{\text{air}} + 2\epsilon \sin\phi \\ &= 2B_{\text{air}} + 2\epsilon \sin\left[\tan^{-1}\left(\frac{X}{2A}\right)\right] \\ &= 2B_{\text{air}} + \frac{2\epsilon X}{\sqrt{4A^2 + X^2}}. \end{aligned}$$

At the aperture $X = B_{\text{air}}$; hence

$$\begin{aligned} 2B &= 2B_{\text{air}} + \frac{2\epsilon B_{\text{air}}}{\sqrt{4A^2 + B_{\text{air}}^2}} \\ &= 2B_{\text{air}}\left(1 + \frac{\epsilon}{\sqrt{4A^2 + B_{\text{air}}^2}}\right). \end{aligned}$$

For the shallow reflector

$$\begin{aligned} 2B &\approx 2B_{\text{air}}\left(1 + \frac{0.042}{\sqrt{4 \times 16 + 14^2}}\right) = 2B_{\text{air}}(1 + 0.0026) \\ &= (28.2 \pm 0.1)(1 + 0.0026) = 28.2\ (1 + 0.0026) \pm 0.1 \\ &= 28.3 \pm 0.1 \text{ inches.} \end{aligned}$$

For the deep reflector

$$2B \approx 2B_{\text{air}}\left(1 + \frac{0.042}{\sqrt{4 \times 4 + 14^2}}\right) = 2B_{\text{air}}(1 + 0.0029)$$

$$= (28.3 \pm 0.01)(1 + 0.0029) = 28.3\ (1 + 0.0029) \pm 0.1$$

$$= 28.4 \pm 0.1 \text{ inches.}$$

APPENDIX B
OMNIDIRECTIONALITY OF THE LINE SOURCE

An important assumption of the reflector theory was that the line-source near-field radiation was omnidirectional. Because the axis of symmetry of the transducer was coincident with the focal line of the reflector, the reflecting surface was in the near field of the transducer. Therefore the omnidirectionality of the near-field radiation of the F36 transducer required verification. The F36 was removed from the reflector and suspended in the water vertically from the Scientific Atlanta rotating head, and the LC-10 hydrophone was brought to within 1 inch of the F36 outside surface and in its median plane. At this separation the acoustic center of the LC-10 was approximately 2-1/4 inches from the axis of the line source.

It was necessary to design a special support system for the F36 near-field omnidirectionality measurements. Transducers are usually supported in the NRL Research Tank by pinned sections of stainless steel rods fitted with adjustable collars. The Scientific Atlanta rotator slips over the upright section of rod and rotates the transducer-and-support-rod assembly. For applications in which the transducer is light, as is the F36, the transducer-and-support-rod assembly wobbles as much as 1 inch while rotating through 360 degrees. For near-field measurements with the hydrophone as close as 1 inch from the transducer, the 1-inch wobble was not tolerable, and modifications were needed in the support system. The F36 was tied to a flexible brass strip 1/8 inch thick, 3/4 inch wide, and 14 feet long, and the strip was clamped in the rotator. A 25-pound lead brick was hung from the F36. The brass support strip and the F36 functioned as a plumb line and the lead brick as a plumb bob, and the wobble was reduced to less than ±1/12 inch, the minimum observable amount.

The radiating transducer was rotated while the hydrophone position remained stationary and the horizontal beam patterns were recorded. Patterns were taken every 5 kHz at the frequencies from 10 to 40 kHz and at displacements between hydrophone tip and transducer boot of from 1 to 3 inches. At approximately a 1-inch separation between the tip of the hydrophone and the F36 boot, the recorded pressure patterns with no correction made for the ±1/12-inch wobble were omnidirectional to within 0.5 dB from 10 kHz to 35 kHz and omnidirectional to within 2 dB from 37 kHz to 40 kHz. At 40 kHz however the received signal at the hydrophone changed by 2 dB for a 1/6-inch change in separation distance between the hydrophone and the transducer when their separation distance was 1 inch. Therefore, a ±1/12-inch wobble could account for the 2-dB departure from omnidirectionality for the 40-kHz pattern. At lower frequencies the gradient of the pressure with respect to separation distance was considerably less. Consequently the horizontal patterns in the near field as well as in the far field of the transducer were omnidirectional to within the accuracy of the instrumentation.

APPENDIX C
EFFICIENCY OF THE REFLECTOR

The efficiency of the reflector is defined as the ratio of the acoustic power radiated into the far field of the reflector to the real acoustic power emitted from the line source. An experimental determination of the efficiency depends on the assumptions that the vertical directivity of the radiation pattern of the line source in the reflector is equal to that of the line source alone and that the radiation loading of the line source in the reflector is approximately equal to that of the line source alone.

A far-field transmitting voltage response was taken of the line source in and out of the reflector. Also the voltage and current into the line source in and out of the reflector and the phase angle between the voltage and the current were recorded. From these data, and with the two preceding assumptions, the efficiency of the reflector can be calculated at any frequency. As an illustration of the calculation, consider the data at 20 kHz from the shallow reflector (Table C1).

Table C1
Electrical Input and Pressure Output of the Line Source at 20 kHz

Configuration	RMS Voltage In (V)	RMS Current In (A)	Phase Between Current and Voltage (deg)	Maximum Sound Pressure in the Median Plane of the Transducer at 3.5 meters (dynes/cm^2)
Line source alone (out of the reflector)	25.8	0.192	-84	377
Line source in the shallow reflector	25.8	0.194	-84	2038

The expression for the average acoustic power P_a radiated into the far field is given by

$$P_a = \int_S \frac{|p|^2}{\rho c}\, dS,$$

where S is any closed far-field surface surrounding the source, $|p|$ is the absolute value of the rms pressure evaluated on the increment of surface area dS, and ρc is the characteristic

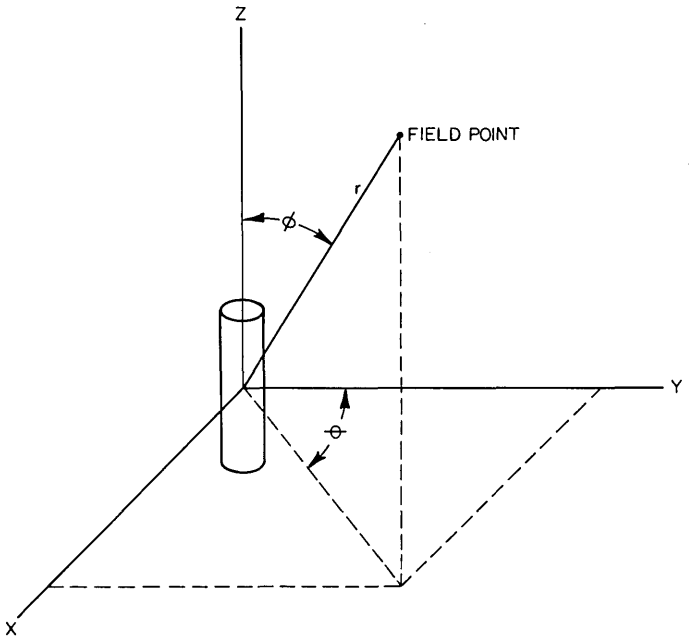

Fig. C1—Spherical coordinates of a field point

impedance of the medium. Figure C1 shows the spherical coordinates r, ϕ, and θ of a point in the field of the transducer; in these coordinates

$$dS = r^2 \sin\phi \, d\phi d\theta ,$$

where r is the distance between the hydrophone and the transducer. Hence

$$P_a = \int_0^{2\pi} \int_0^{\pi} \frac{|p|^2}{\rho c} r^2 \sin\phi \, d\phi d\theta .$$

At a fixed value of $r = R$

$$p(\theta, \phi) = \Theta(\theta)\Phi(\phi)$$

or

$$|p|^2 = |\Theta(\theta)|^2 |\Phi(\phi)|^2,$$

so that

$$P_a = \int_0^{2\pi} \int_0^{\pi} \frac{|\Theta(\theta)|^2 |\Phi(\phi)|^2}{\rho c} R^2 \sin\phi \, d\phi d\theta .$$

If

$$K = \int_0^{\pi} \frac{|\Phi(\phi)|^2}{\rho c} R^2 \sin\phi \, d\phi,$$

then

$$P_a = K \int_0^{2\pi} |\Theta(\theta)|^2 \, d\theta,$$

where $|\Phi(\pi/2)||\Theta(\theta)|$ is the absolute value of the rms pressure in the $\phi = \pi/2$ plane, which is the median plane of the transducer. If the subscript 1 denotes the parameters and variables corresponding to the line source alone (out of the reflector), and if the subscript 2 denotes the parameters and variables corresponding to the line source in the reflector, then $R_1 = R_2 = 3.5$ meters = 11 feet 6 inches (roughly corresponding to Fig. 5o), $K_1 = K_2$ by the assumption that the vertical directivity of the radiation pattern of the line source in the array is that of the line source alone, P_{a_1} is the acoustic power radiated into the far field of the line source alone, and P_{a_2} is the acoustic power radiated into the far field of the reflector, $|\Phi_1(\phi = \pi/2)||\Theta_1(\theta)|$ is the absolute value of the rms pressure in the $\phi = \pi/2$ plane of the line source alone and is 377 dynes/cm^2 for all θ (since the line-source radiation was omnidirectional in the median plane), and $|\Phi_2(\phi = \pi/2)||\Theta_2(\theta)|$ is the absolute value of the rms pressure in the $\phi = \pi/2$ plane of the reflector, with $|\Phi_2(\phi = \pi/2)||\Theta(0)|$ being 2038 dynes/cm^2 and the θ dependence of the pressure being given approximately in Fig. 5o. Thus

$$\frac{P_{a_2}}{P_{a_1}} = \frac{K_2 \int_0^{2\pi} |\Theta_2(\theta)|^2 \, d\theta}{K_1 \int_0^{2\pi} |\Theta_1(\theta)|^2 \, d\theta},$$

in which

$$\int_0^{2\pi} |\Theta_1(\theta)|^2 \, d\theta = \int_0^{2\pi} (377)^2 \, d\theta = 2\pi(377)^2$$

and, by a numerical integration of the pattern in Fig. 5o,

$$\int_0^{2\pi} |\Theta_2(\theta)|^2 \, d\theta = 0.0328 \times (2038)^2,$$

so that

$$\frac{P_{a_2}}{P_{a_1}} = \frac{.0328 \times (2038)^2}{(377)^2} = 0.959.$$

The efficiency of the reflector at 20 kHz was 95.9%. A detailed error analysis was not performed for this calculation, but the estimated error could make the calculated efficiency as high as 100% or as low as 90%. An additional indication that the efficiency of the reflector was nearly 100% was obtained by the good agreement of theory and experiment illustrated in Fig. 5o. The consequence of less than 100% efficiency is a lowering of the main-beam amplitude level in the reflector patterns with respect to the amplitude level of the minor lobes. The assumption of 100% reflector efficiency was used in the mathematical model to calculate the relative amplitudes of the pressure radiated directly from the line source in the reflector and the pressure radiated after bouncing off of the reflecting surface. Agreement of theory and experiment as well as the efficiency calculation support the assumption of total reflection of the sound at the reflector surface.

APPENDIX D
EFFECT OF A LINE-SOURCE MISALIGNMENT ON THE RADIATION PATTERN

Another important assumption of the reflector theory was that the line-source axis coincided with the focal line of the parabolic reflector. There were, however, possible sources of error in the alignment of the F36 in the reflector. The procedure involving the sliding of a metal spacer between the vertex line of the reflector and the back surface of the transducer boot was estimated to have a possible error of ±1/32 inch because of the compressibility of the rubber reflector material and the F36 boot. An associated source of error was an estimated ±1/32-inch deviation of the vertex line from the average parabolic surface. The reflector surface on the average was a parabola with the appropriate focal length but, as shown in Appendix A, individual points on the surface deviated from the mean parabola. If the vertex line was not exactly on the mean parabola, the alignment of the line source would have been detrimentally affected because of the metal spacer procedure. Because the F36 transducer was encased in an oil-filled compliant rubber boot, all alignment procedures were performed with respect to the outside surface of the boot. Errors associated with the softness of the boot were estimated to be ±1/32 inch in measuring the diameter of the boot and ±1/32 inch in the axis of the active ceramic elements of the F36 being coincident with the axis of symmetry of the rubber boot; either of these two errors could have been an independent cause of misalingment.

Four possible independent sources of misalignment error have been described, and each error was estimated to be ±1/32 inch. The uncertainty in alignment in the Y coordinate axis direction (Fig. 2) is $\pm\sqrt{4(1/32)^2}$ or ±1/16 inch. This uncertainty includes both the position of the axis of the line source as well as the line source being tilted from end to end in the Y plane.

The alignment of the F36 in the vertex plane ($X = 0$) depended on the optical procedure, which was estimated accurate to ±1/32 inch, and on the error in the acoustic axis of the F36 being coincident with the axis of the rubber boot, which was also estimated to be ±1/32 inch. The rms resultant of the two independent errors in alignment in the X-coordinate-axis direction is $\pm\sqrt{2(1/32)^2}$ or $\pm\sqrt{2}/32$ inch.

The focal line was at $X = 0$ and $Y = A$. Therefore, the acoustic axis of the F36 transducer was at $X = 0 \pm\sqrt{2}/32$ inch and $Y = A \pm 1/16$ inches.

An attempt was made to experimentally determine the effect on the radiation pattern of a misalignment of the line source. The line source was intentionally misaligned in the Y-coordinate-axis direction and in the X-coordinate-axis direction, and radiated horizontal far-field patterns were compared to the corresponding patterns of Figs. 5 and 6. First the line source was displaced along the Y coordinate axis from its presumed location coincident with the focal line to a new position 5/64 inch closer to the vertex line. This misalignment

was greater than the estimated uncertainty of 1/16 inch. The resulting patterns from the displaced line source are shown in Figs. D1 through D4. In this appendix the solid curves represent the original patterns as shown in the Experimental Data section of this report and the dashed curves represent the patterns when the line source was intentionally misaligned. Representative patterns were taken at 10 kHz, 20 kHz, 30 kHz, and 40 kHz.

In Fig. D1 except for a slight deepening of the nulls the pattern remained virtually unchanged. In Figs. D2 through D4 it appears as though the misaligned patterns are larger in amplitude than the original patterns except for the main beam. However the appearance is deceptive, because all of these patterns were drawn with the peak radiation on the main beam normalized to the same level on the dB scale. Therefore, the discrepancies in these patterns are explained by a lowering of the main beam by approximately 1 dB with respect to the side-lobe levels when the line source was misaligned. In effect, displacement of the line source in the Y-coordinate-axis direction unfocuses the patterns. When the line source was displaced yet another 3/64 inch in the Y-coordinate-axis direction, so that the total displacement was 1/8 inch, the main beam was lowered even more with respect to the side-lobe levels (Fig. D5). Misalignment of the line source in the Y coordinate direction left the symmetry of the patterns intact.

The line source was displaced 1/8 inch in the X-coordinate-axis direction from its initial position coincident with the focal line, and radiated patterns were recorded at the frequencies of interest. The displaced coordinate of the line source was $Y = A \pm 1/16$ inches, $X = 1/8 \pm \sqrt{2}/32$ inches, and $A = 4.0$ inches. The resulting patterns from the displaced line source agreed to within experimental uncertainty with the original patterns shown in the Experimental Data section of this report. There were no obvious right-left asymmetries in the patterns as a result of this 1/8-inch transverse displacement of the line source.

For a 1-1/8-inch transverse displacement of the line source ($Y = A - 5/64 \pm 1/16$ inches, $X = 1\text{-}1/8 \pm \sqrt{2}/32$ inches) the asymmetry in the patterns is pronounced (Fig. D6). In conclusion, experiments show that a misalignment of the line source from the hypothetical focal line of the reflector within the alignment uncertainty ($Y = A \pm 1/16$ inches, $X = 0 \pm \sqrt{2}/32$ inch) resulted in no measurable asymmetry and less than a 1-dB decrease of the main beam amplitude with respect to the amplitude of the side lobes.

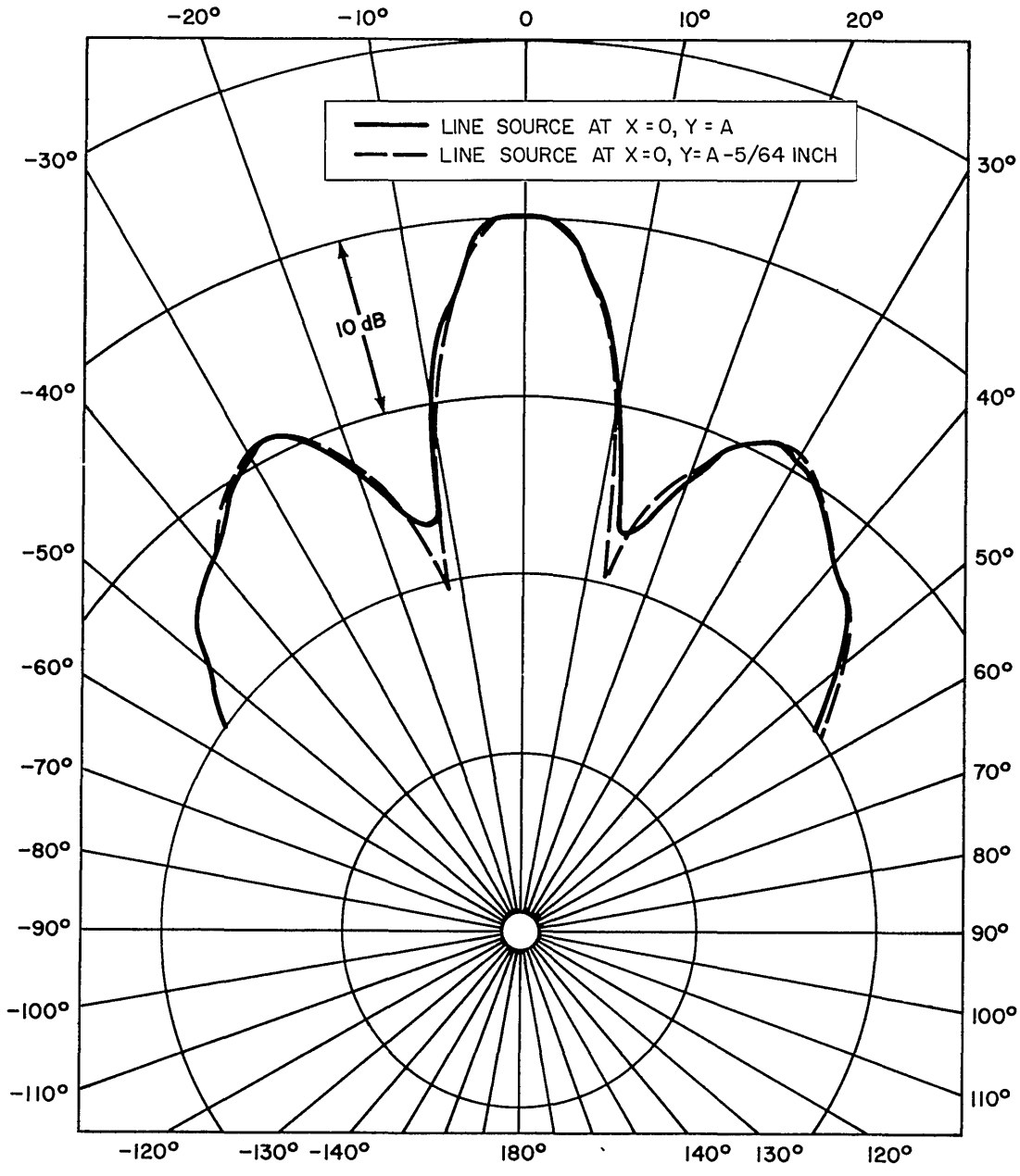

Fig. D1—Effect of intentional misalignment on the radiation pattern in the median plane of the shallow (4.0-inch-focal-length) reflector for R = 20 feet and f = 10 kHz

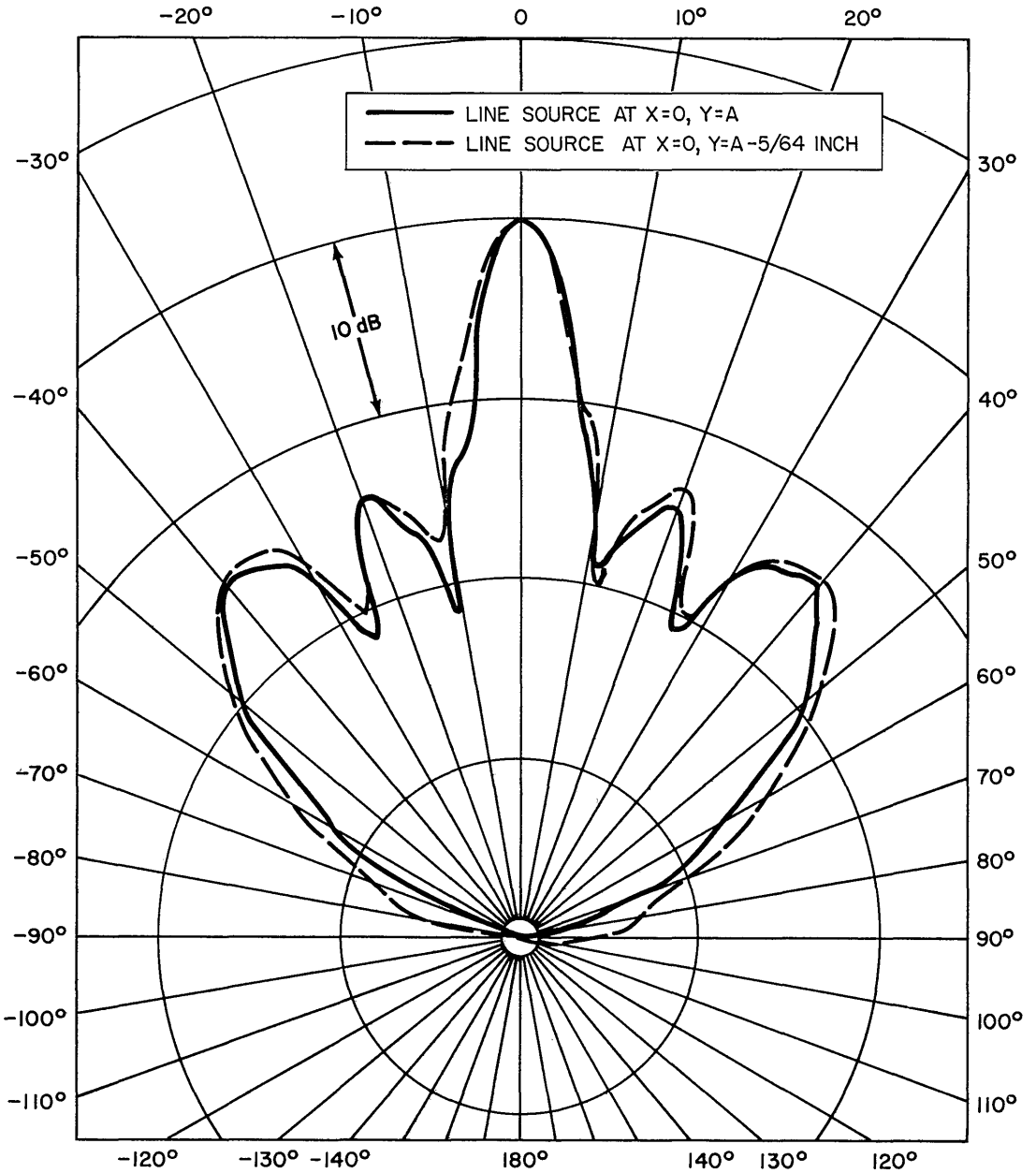

Fig. D2—Effect of intentional misalignment on the radiation patterns in the median plane of the shallow (4.0-inch-focal-length) reflector for R = 20 feet and f = 20 kHz

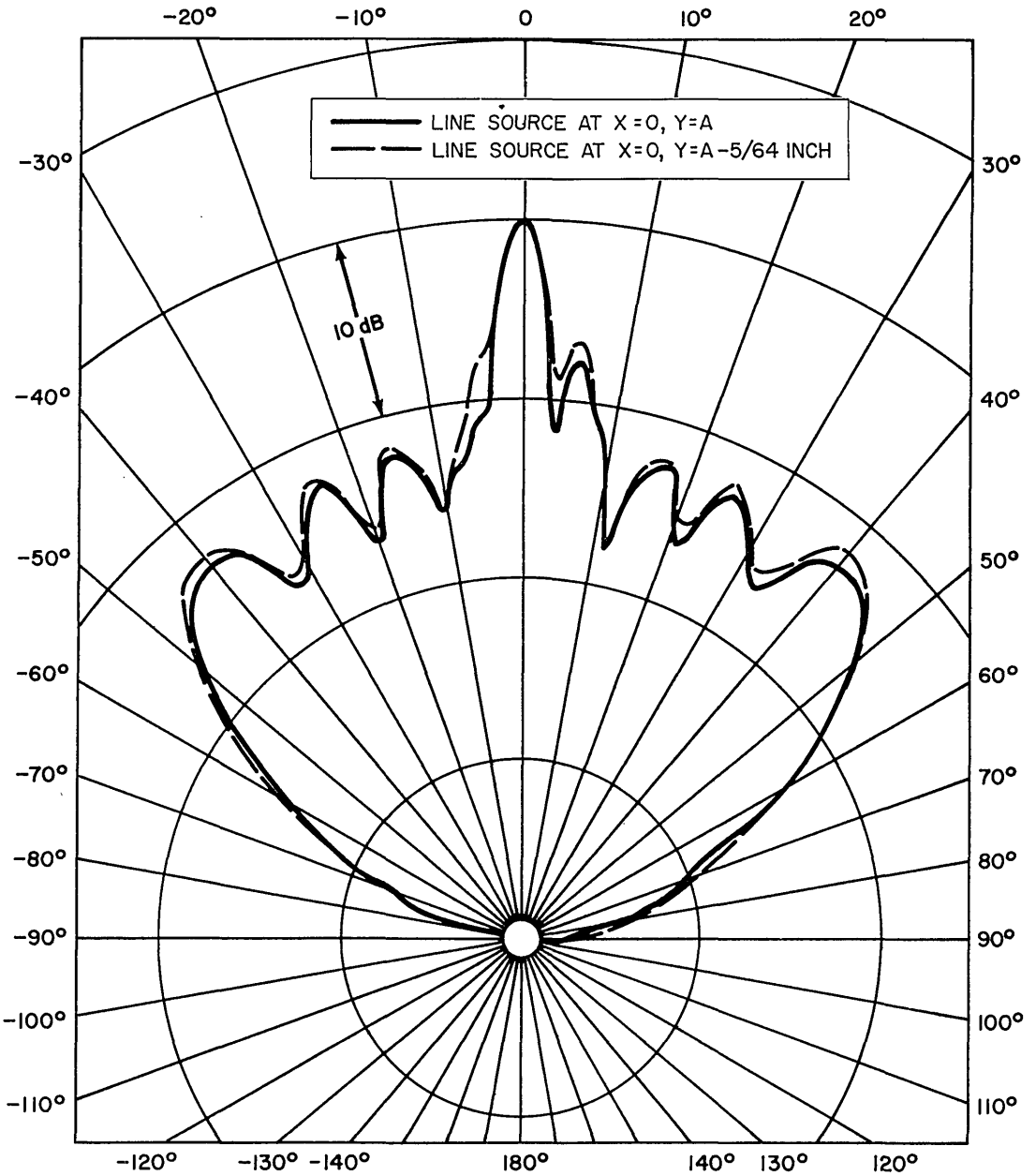

Fig. D3—Effect of intentional misalignment on the radiation pattern in the median plane of the shallow (4.0-inch-focal-length) reflector for R = 20 feet and f = 30 kHz

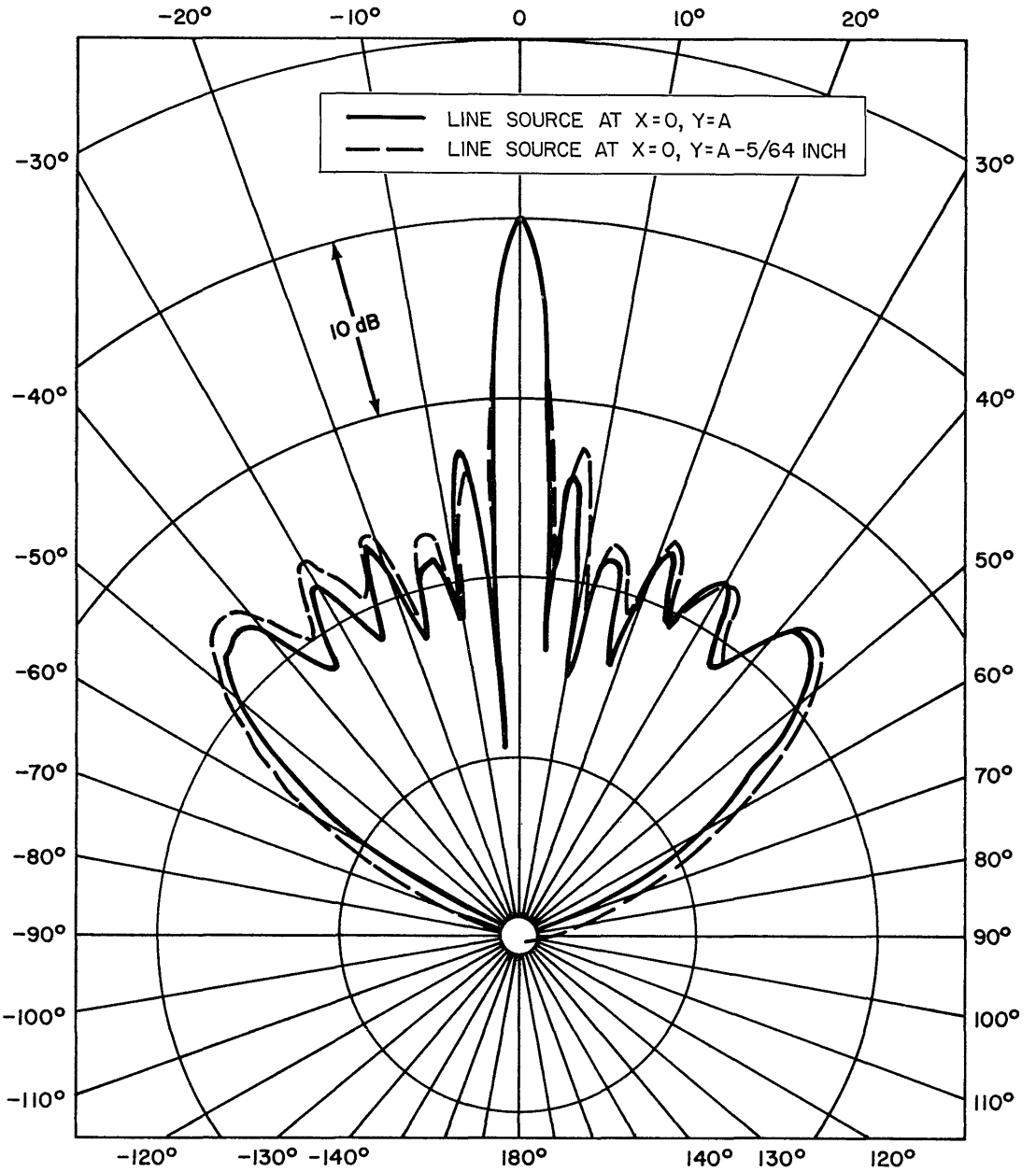

Fig. D4—Effect of intentional misalingment on the radiation pattern in the median plane of the shallow (4.0-inch-focal-length) reflector for R = 20 feet and f = 40 kHz

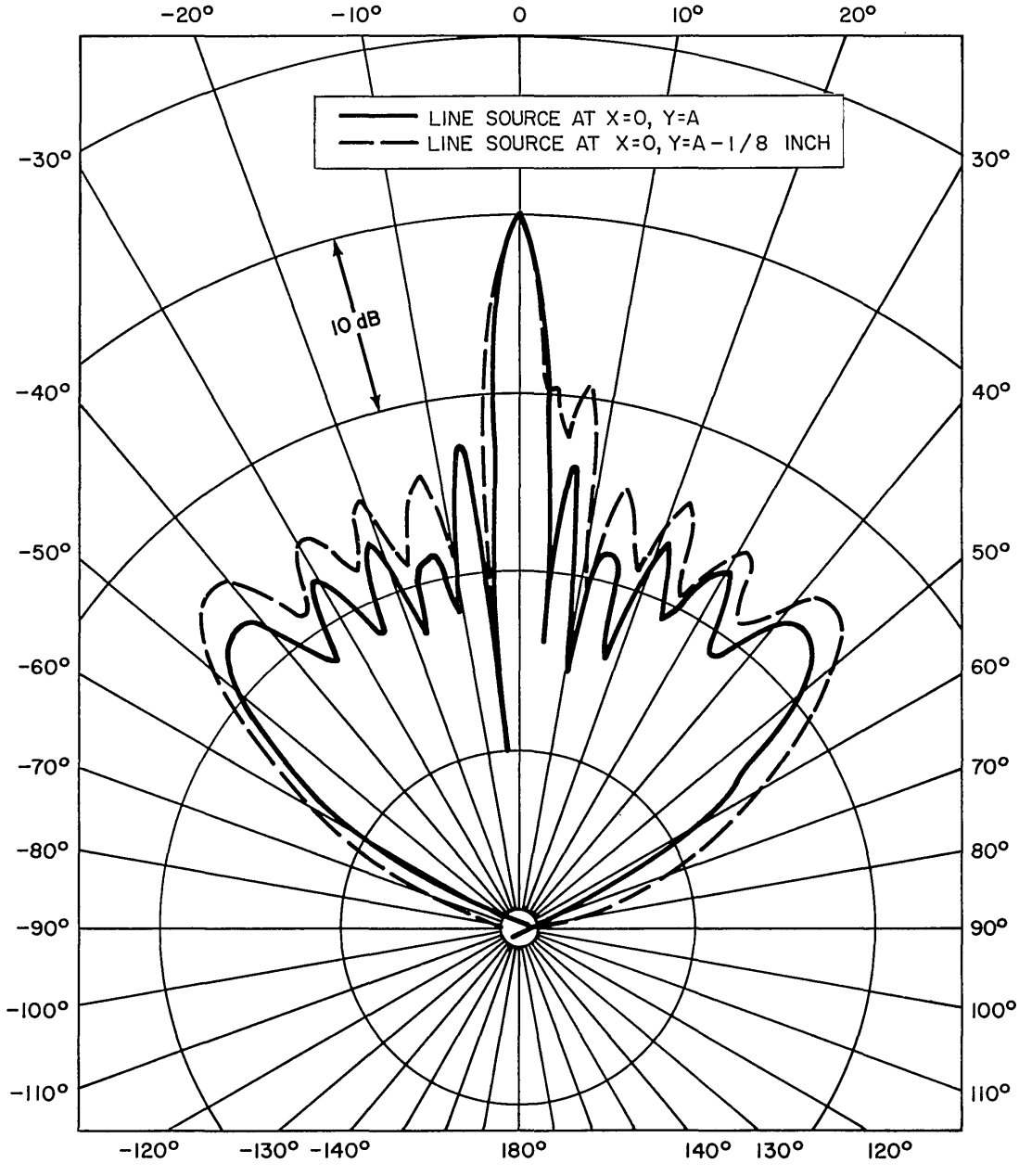

Fig. D5—Effect of intentional misalignment on the radiation pattern in the median plane of the shallow (4.0-inch-focal-length) reflector for R = 20 feet and f = 40 kHz

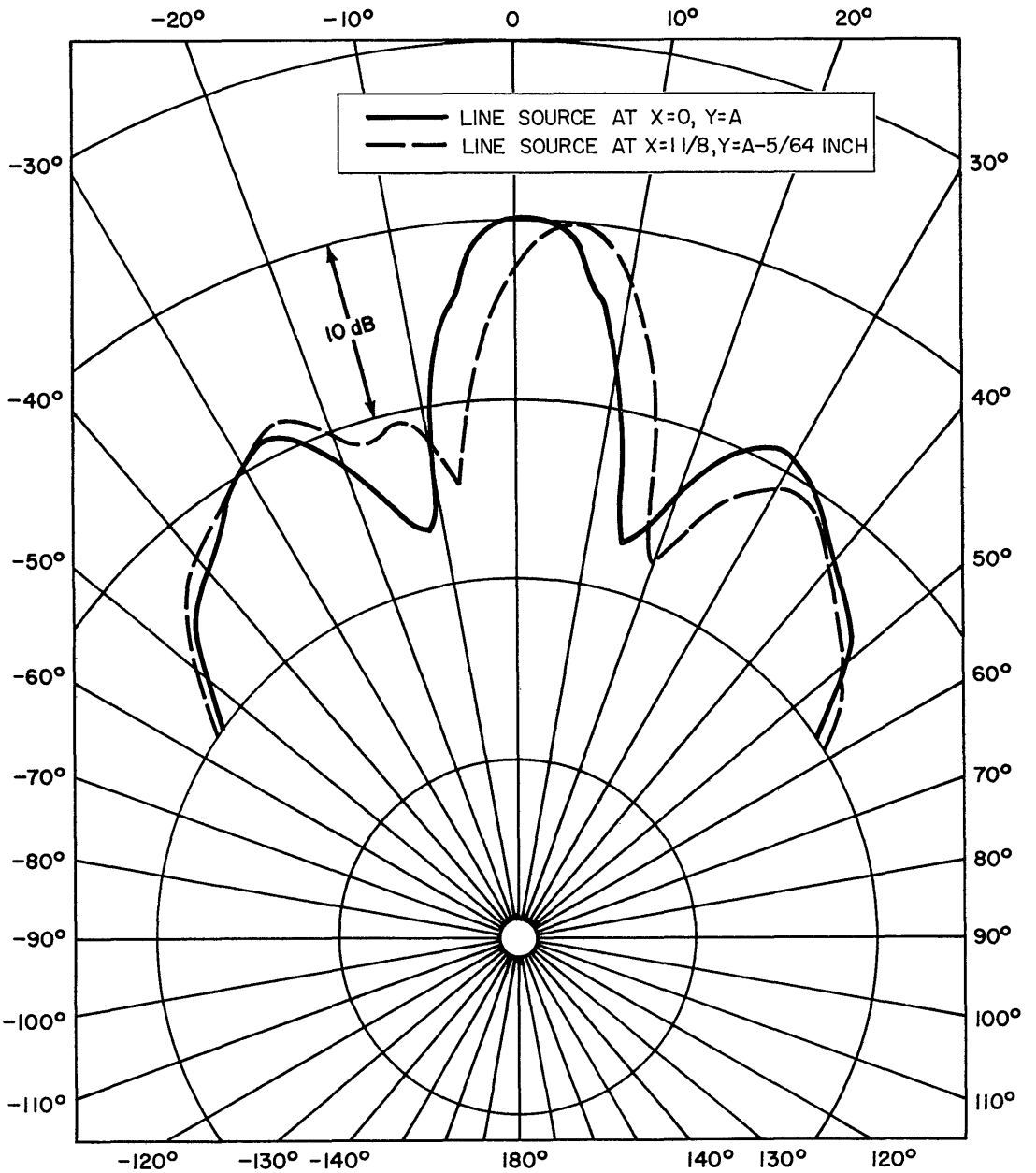

Fig. D6—Effect of intentional misalignment on the radiation pattern in the median plane of the shallow (4.0-inch-focal-length) reflector for R = 20 feet and f = 10 kHz

APPENDIX E
MATHEMATICAL MODEL OF THE REFLECTOR AS A DESIGN TOOL

The purpose of this experiment was to verify a mathematical model of an ideal parabolic-cylinder reflector. The accuracy of the reflector model has been confirmed by the excellent agreement between theory and experiment over a wide range of reflector parameters. In this experiment B/A, the half-aperture width divided by the focal length, was 14.2/4.0 = 3.5 for the shallow reflector and 14.2/2.0 = 7.1 for the deep reflector. For both reflectors the patterns shown in Figs. 5 and 6 represent values of B/λ, the half-aperture width divided by the wavelength of sound, over the range 2.4 to 9.6.

Additional calculations were made for the ranges $3 \leqslant B/A \leqslant 10$ and $2 \leqslant B/\lambda \leqslant 15$, and the resulting curves (Fig. E1) and data (Table E1) can be used to design a reflector to meet specifications of beamwidth and of first-discrete-minor-lobe amplitude-level

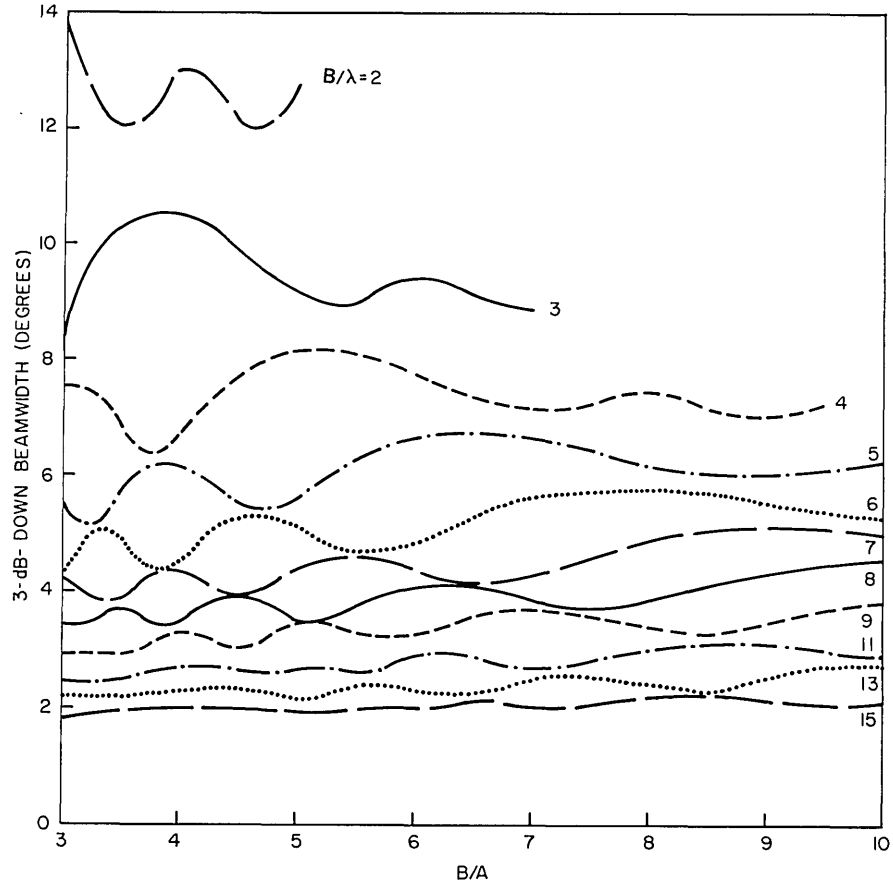

Fig. E1—Beamwidth of an ideal parabolic-cylinder reflector with an aperture width $2B$ and a focal length A

Table E1
Calculated Suppression and Location of the First Minor Lobes for an Ideal Parabolic-Cylinder Reflector With an Aperture Width $2B$ and a Focal Length A

B/A	Minor-Lobe Suppression for B/λ = 2, 3, 4, 5, 6, 7, 8, 9, 11, and 13 (dB)										Minor-Lobe Angle for B/λ = 2, 3, 4, 5, 6, 7, 8, 9, 11, and 13 (deg)									
	2	3	4	5	6	7	8	9	11	13	2	3	4	5	6	7	8	9	11	13
3	8.8	8.7	13.4	13.1	11.1	14.4	14.5	12.4	14.8	16.4	35	14	18	9	7	10	6	5	4	6
3.25	7.8	11.4	12.4	10.1	14.5	14.8	14.3	—	—	—	25	35	18	9	12	18	5	—	—	—
3.5	6.6	12.6	11.9	13.6	13.7	12.5	14.5	12.3	14.7	16.8	24	34	12	20	12	6	9	5	4	5
3.75	6.7	13.2	9.9	14.5	12.2	15.7	14.1	—	—	—	23	25	11	15	8	10	6	—	—	—
4	7.7	12.1	11.1	13.2	12.9	14.1	14.1	14.5	15.7	16.4	23	24	11	14	7	10	6	8	6	5
4.25	5.3	11.1	12.7	12.9	14.8	15.0	16.6	—	—	—	23	24	26	14	17	7	9	—	—	—
4.5	2.8	10.3	13.3	12.8	15.1	13.7	14.6	15.0	18.0	18.1	23	24	26	9	12	7	9	5	4	5
4.75	2.2	9.7	13.9	12.3	13.8	14.5	14.7	—	—	—	23	24	26	9	12	15	9	—	—	—
5	2.9	9.5	14.4	13.5	13.3	15.9	15.1	15.0	15.8	18.2	25	23	18	9	12	14	6	8	6	4
5.5	—	10.3	12.3	14.2	14.4	14.1	18.2	17.2	18.0	17.2	24	17	18	21	8	10	6	5	4	5
6	—	11.7	10.9	16.2	16.2	13.5	15.7	18.1	16.0	16.6	24	16	18	14	8	10	9	5	6	5
6.5	—	7.8	10.2	13.8	15.1	16.4	13.7	17.9	14.9	22.9	24	17	18	14	17	7	9	8	6	4
7	—	5.3	10.2	12.1	17.6	19.1	13.8	14.5	20.7	16.5	24	17	18	14	11	7	9	8	6	5
7.5	—	—	11.0	11.0	14.8	15.9	16.7	13.4	17.6	14.5	24	17	18	14	11	15	9	8	9	5
8	—	—	12.2	10.3	13.0	18.7	22.4	14.0	16.9	16.4	24	17	18	14	11	9	6	8	6	5
8.5	—	—	10.2	10.2	11.8	15.6	15.4	17.1	14.2	26.5	23	17	13	14	11	9	16	8	6	5
9	—	—	7.9	10.6	10.9	13.7	17.2	14.8	13.1	21.2	24	17	13	14	11	9	14	14	6	5
9.5	—	—	8.5	11.2	10.4	12.4	16.0	15.5	13.2	15.9	23	17	13	15	12	10	8	14	6	5
10	—	—	—	12.1	10.1	11.4	14.1	16.4	14.7	13.7	23	17	13	15	12	10	8	14	6	5

suppression and angle location. B/A and B/λ were chosen as variables because they are dimensionless quantities and hence apply to all reflectors regardless of physical size. The beamwidth calculated is the width in degrees of the main beam of the reflector radiation pattern at the points where the pressure is 3 dB less than the peak pressure and the power is 1/2 the peak power. The first-minor-lobe amplitude level is the ratio (in dB) of the maximum pressure of the first side lobe to the axial peak pressure. B/λ values of 10, 12, and 14 are omitted from Fig. E1 because the plot would be overcrowded, and portions of the curves for B/λ values of 2, 3, and 4 are omitted because the model is inadequate in these regions.

As an example of the use of these data, assume a designer wants a reflector pattern at 500 Hz which has a 10-degree beamwidth and maximum minor-lobe suppression. From Fig. E1 the beamwidth is 10 degrees at both B/A = 3.3 and B/A = 4.4 for B/λ = 3. From Table E1 at B/λ = 3 and B/A = 3.3 the minor lobe amplitude suppression is approximately -12 dB, with the minor lobe at 35 degrees off axis. At B/λ = 3 and B/A = 4.4 the minor lobe amplitude suppression is approximately -10.6 dB, with the minor lobe at 24 degrees off axis. Therefore the designer chooses B/A = 3.3 and B/λ = 3 for the reflector variables in order to meet the specifications of the reflector pattern. At 500 Hz, for a velocity of sound in water of 5000 feet per second, λ = 10 feet, $B = 3\lambda$ = 30 feet, and $A = B/3.4$ = 9.1

feet. Therefore the reflector dimensions are 9.1 feet for the focal length and 60 feet for the aperture width.

As another example of the use of these data, assume a designer wants a reflector pattern which has minor-lobe suppression of at least 15 dB and the first minor lobes at least 15 degrees off axis. From Table E1 these requirements are met for three possible combinations of B/A and B/λ: $B/\lambda = 6$ and $B/A = 6.5$, $B/\lambda = 7$ and $B/A = 7.5$, and $B/\lambda = 8$ and $B/A = 8.5$. From Fig. E1 the respective beamwidth are 5.3, 4.6, and 4.1 degrees. The dimensions of the reflector are then determined depending on the designer's preferences for beamwidth and frequency.

Security Classification

DOCUMENT CONTROL DATA - R & D

(Security classification of title, body of abstract and indexing annotation must be entered when the overall report is classified)

1. ORIGINATING ACTIVITY (Corporate author)	2a. REPORT SECURITY CLASSIFICATION
Naval Research Laboratory Washington, D.C. 20390	Unclassified
	2b. GROUP

3. REPORT TITLE

An Experimental Study of the Acoustic Field of a Line Source Coincident with the Focal Line of a Parabolic-Cylinder Reflector

4. DESCRIPTIVE NOTES (Type of report and inclusive dates)

An interim report on a continuing NRL Problem

5. AUTHOR(S) (First name, middle initial, last name)

J. A. Sinsky, Peter H. Rogers, and A. V. Bozzi

6. REPORT DATE	7a. TOTAL NO. OF PAGES	7b. NO. OF REFS
December 20, 1972	76	5

8a. CONTRACT OR GRANT NO.	9a. ORIGINATOR'S REPORT NUMBER(S)
NRL Problem S02-19	
b. PROJECT NO.	NRL Report 7486
RF 05-121-402-6200	
c.	9b. OTHER REPORT NO(S) (Any other numbers that may be assigned this report)
d.	

10. DISTRIBUTION STATEMENT

Approved for public release; distribution unlimited

11. SUPPLEMENTARY NOTES	12. SPONSORING MILITARY ACTIVITY
	Department of the Navy Office of Naval Research Arlington, Va. 22217

13. ABSTRACT

The acoustic radiation patterns from acoustically soft parabolic reflectors driven by a line source coincident with the focal lines of the reflectors were measured in the NRL Acoustic Research Tank Facility to verify a mathematical model of an ideal parabolic-cylinder reflector. Data taken in the near and far fields of the reflectors at various frequencies between 10 kHz and 40 kHz were plotted together with the theoretically prediced radiation patterns. Agreement is good between theory and experiment. The experiment was performed with a shallow reflector (4.0-inch focal length and 28.3-inch aperture) and with a deep reflector (2.0-inch focal length and 28.4-inch aperture), and all measurements were made in the median planes of the reflectors. Emphasis was placed on careful construction of the parabolic reflectors and precision alignment of the line source. Error analyses were performed to determine the parabolicness of the reflectors and the effect on the radiation pattern of a slight misalignment of the line source. To illustrate the use of the mathematical model as a design tool, curves were plotted showing the reflector performance characteristics as a function of the reflector parameters.

14. KEY WORDS	LINK A		LINK B		LINK C	
	ROLE	WT	ROLE	WT	ROLE	WT
Acoustic fields						
Underwater sound sources						
Parabolic-cylinder reflectors						
Near fields						
Far fields						
Mathematical models						
Design						